



**UNIVERSIDADE ESTADUAL DE CAMPINAS**  
Faculdade de Engenharia Mecânica

**CLAUDIA MARCELA PEREZ MADRID**

**Bi-directional Evolutionary Topology  
Optimization of Compliant Mechanisms Design  
using a Multi-criteria Approach**

**Otimização Topológica Bidirecional  
Evolucionária para o Projeto de Mecanismos  
Flexíveis usando um Enfoque Multi-critério**

CAMPINAS  
2016

CLAUDIA MARCELA PEREZ MADRID

## **Bi-directional Evolutionary Topology Optimization of Compliant Mechanisms Design using a Multi-criteria Approach**

### **Otimização Topológica Bidirecional Evolucionária para o Projeto de Mecanismos Flexíveis usando um Enfoque Multi-critério**

Thesis presented to the School of Mechanical Engineering of the University of Campinas in partial fulfillment of the requirements for the degree of Master in Mechanical Engineering in the area of Solid Mechanics and Mechanical Design.

Tese de Mestrado apresentada à Faculdade de Engenharia Mecânica da Universidade Estadual de Campinas como parte dos requisitos exigidos para obtenção do título de Mestra em Engenharia Mecânica na área de Mecânica dos Sólidos e Projeto Mecânico.

Orientador: Prof. Dr. Renato Pavanello

ESTE EXEMPLAR CORRESPONDE À VERSÃO FINAL DA DISSERTAÇÃO DEFENDIDA PELA ALUNA CLAUDIA MARCELA PEREZ MADRID E ORIENTADA PELO PROF. DR. RENATO PAVANELLO.



.....  
ASSINATURA DO ORIENTADOR

CAMPINAS  
2016

**Agência(s) de fomento e nº(s) de processo(s):** CAPES, 33003017

Ficha catalográfica  
Universidade Estadual de Campinas  
Biblioteca da Área de Engenharia e Arquitetura  
Luciana Pietrosanto Milla - CRB 8/8129

P415b Perez Madrid, Claudia Marcela, 1988-  
Bi-directional evolutionary topology optimization of compliant mechanisms design using a multi-criteria approach / Claudia Marcela Perez Madrid. – Campinas, SP : [s.n.], 2016.

Orientador: Renato Pavanello.  
Dissertação (mestrado) – Universidade Estadual de Campinas, Faculdade de Engenharia Mecânica.

1. Otimização topológica. 2. Otimização estrutural. 3. Análise multicritério. I. Pavanello, Renato, 1959-. II. Universidade Estadual de Campinas. Faculdade de Engenharia Mecânica. III. Título.

Informações para Biblioteca Digital

**Título em outro idioma:** Otimização topológica bidiecional evolucionária para o projeto de mecanismos flexíveis usando um enfoque multi-critério

**Palavras-chave em inglês:**

Topology optimization

Structural optimization

Multi-criteria analysis

**Área de concentração:** Mecânica dos Sólidos e Projeto Mecânico

**Titulação:** Mestra em Engenharia Mecânica

**Banca examinadora:**

Renato Pavanello [Orientador]

Alberto Luiz Serpa

Marcelo Areias Trindade

**Data de defesa:** 27-07-2016

**Programa de Pós-Graduação:** Engenharia Mecânica

UNIVERSIDADE ESTADUAL DE CAMPINAS  
FACULDADE DE ENGENHARIA MECÂNICA  
COMISSÃO DE PÓS-GRADUAÇÃO EM ENGENHARIA MECÂNICA  
DEPARTAMENTO DE MECÂNICA COMPUTACIONAL

DISSERTAÇÃO DE MESTRADO ACADEMICO

**Bi-directional Evolutionary Topology Optimization of  
Compliant Mechanisms Design using a Multi-criteria  
Approach**

**Otimização Topológica Bidirecional Evolucionária  
para o Projeto de Mecanismos Flexíveis usando um  
Enfoque Multi-critério**

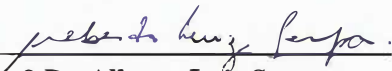
Autor: Claudia Marcela Perez Madrid  
Orientador: Prof. Dr. Renato Pavanello

A Banca Examinadora composta pelos membros abaixo aprovou esta Dissertação:



---

**Prof. Dr. Renato Pavanello**  
DMC/FEM/UNICAMP



---

**Prof. Dr. Alberto Luiz Serpa**  
DMC/FEM/UNICAMP



---

**Prof. Dr. Marcelo Areias Trindade**  
SEM/EESC/USP

Campinas, de 2016.

## **Dedicatória**

Para mi mamá, la persona más maravillosa que conozco. Y para mi papá, que donde sea que esté, sé que me mira y sonrío.

## **Agradecimentos**

Para minha querida família por todo o apoio e ajuda no desenvolvimento deste projeto pessoal. Especialmente para a minha mãe que no início não queria que eu fosse embora, mas como sempre, ajudo-me em tudo momento. Ela é a melhor pessoa que eu conheço e o melhor exemplo de viver uma vida sem medo e com um bom coração.

Para o professor Renato Pavanello por esta oportunidade incrível e todas as lições que ele me deu de forma desinteressada neste processo. Seu conselho foi sempre mais do que as palavras de um tutor e sua experiência e profissionalismo será sempre um exemplo para meus anos vindouros.

Para os meus amigos na Colômbia, que sempre ficaram comigo durante esta viagem, eu nunca vou esquecer os momentos em que um simples sorriso e a palavra certa me ajudaram a continuar. Especialmente para duas pessoas especiais: Juliana minha amiga mais antiga e a pessoa que sempre me incentivou a ser exatamente como eu sou, e para Sofia que ajudo-me nos momentos em que ninguém mais poderia, mesmo na distância. Ela definitivamente tornou minha vida mais feliz.

Para meus amigos da UNICAMP, especialmente para os meus parceiros de laboratório que me receberam com tanto amor e alegria: Renato, Sérgio, Tainan, Jaime, Felipe, Marcela, Vinícius e William. Obrigado por todos os momentos compartilhados, eles representam uma boa parte da minha viagem e eu vou sempre lembrar vocês com um sorriso.

Para todos os amigos que teve a sorte de fazer no Brasil, começando com os membros oficiais do clube do Ademir: Jorge, Mario, Diego, Hache, Carlos, e Zulma. Minha vida no Brasil não teria sido o mesmo sem vocês e definitivamente, não teria sido uma experiencia tão feliz. Para Carlos e Zulma: todo o café do mundo não é suficiente para tantas histórias, sonhos e risos, obrigada por cada momento. Finalmente, mas não menos importante, para Sonia a amiga mais querida que o Brasil me deu e que se tornou parte da minha família sem dúvida.

À Faculdade de Engenharia Mecânica da UNICAMP pela oportunidade de realizar este trabalho e à CAPES pelo suporte financeiro.

## Acknowledgements

To my dear family for all the support and help in the development of this personal project. Especially to my mom who at first didn't want me to go away, but as always, supported me anyway. She is the greatest person I know and the best example to live a life without fear and with a kind heart.

To professor Renato Pavanello for this incredible opportunity and all the lessons he gave me so disinterested through this process. His advice was always more than the words from a simple tutor and his experience and professionalism will always be an example to the years to come.

To my friends in Colombia, who always stay with me during this journey, I will never forget the moments when a simple smile and the right word help me to keep going. Especially to Juliana my oldest friend and the person who has only encouraged me to be exactly as I am and to Sofía who help me at times when nobody else could, even from the distance. She definitely has made my life more happy since she is in it.

To my friends from UNICAMP University, especially for my laboratory partners who receive me with such love and joy: Renato, Sergio, Tainan, Jaime, Felipe, Marcela, Vinicius and William. Thank you for all the shared moments, they represent a great part of my journey and I will always remember you with a smile.

To all the friends I have the fortune to made in Brazil, starting with the official members of the Ademir's Club: Jorge, Mario, Diego, Hache, Carlos, and Zulma. My life in Brazil wouldn't be the same without you and it wouldn't be such a happy experience. For Carlos and Zulma: all the coffee in the world is not enough for so many stories, dreams, and laughs, thank you for each moment. Finally but not least, to Sonia the dearest friend that Brazil gave me and who was my Brazilian family without a doubt.

To the Faculty of Mechanical Engineering at Unicamp for the opportunity to carry out this work and to CAPES for the financial support.

*"En un lejano país existió hace muchos años una Oveja negra. Fue fusilada. Un siglo después, el rebaño arrepentido le levantó una estatua ecuestre que quedó muy bien en el parque. Así, en lo sucesivo, cada vez que aparecían ovejas negras eran rápidamente pasadas por las armas para que las futuras generaciones de ovejas comunes y corrientes pudieran ejercitarse también en la escultura."*

---

Augusto Monterroso

## Resumo

MADRID, Claudia Marcela Perez. Otimização Topológica Bidirecional Evolucionária para o Projeto de Mecanismos Flexíveis usando um Enfoque Multi-critério. 2016. 98p. Dissertação (Mestrado). Faculdade de Engenharia Mecânica, Universidade Estadual de Campinas, Campinas, Brasil.

Os mecanismos flexíveis são dispositivos mecânicos que quando submetidos a determinados esforços, se deformam e por consequência geram o movimento desejado. A principal vantagem dos mecanismos flexíveis é a integração de diversas funções em uma única peça. Esta dissertação explora uma estratégia para projetar mecanismos flexíveis usando um método de Otimização Topológica. O método de otimização escolhido é o BESO (Bi-directional Evolutionary Structural Optimization) que requer uma função objetivo que considere simultaneamente os requisitos associados aos deslocamentos e as cargas do mecanismo. A formulação da função objetivo deve buscar a maximização do deslocamento desejado pelo mecanismo flexível e ao mesmo tempo a minimização dos efeitos de formação de rótulas muito delgadas que ocorrem em regiões com grandes gradientes do campo de deslocamentos. Os números de sensibilidade são definidos como a derivada da função objetivo com respeito às variáveis de projeto e são usados no método BESO para remover e adicionar material até atingir a topologia ótima. A implementação do algoritmo é validada comparando os resultados obtidos com topologias típicas de mecanismos flexíveis encontrados na literatura. Algumas considerações adicionais relacionadas com o método BESO são analisadas: a influência da rigidez da peça acionada sobre as topologias finais encontradas pelo algoritmo, a dependência dos resultados com respeito à malha de elementos finitos utilizada e a influência do domínio de projeto inicial sobre as topologias encontradas.

*Palavras-chave:* Otimização Topológica; Otimização Estrutural Evolucionária; Método BESO; Mecanismos Flexíveis; Otimização Multicritério.

## Abstract

MADRID, Claudia Marcela Perez. Bi-directional Evolutionary Topology Optimization of Compliant Mechanisms Design using a Multi-criteria Approach. 2016. 98p. Thesis (Mestrado). School of Mechanical Engineering, University of Campinas, Campinas, Brazil.

Compliant mechanisms are mechanical monolithic devices that deform under the action of a determined force and achieve the desired displacement as a consequence of this deformation. Their main advantages are related to the possibility of integrating different functions into one mechanical device. This thesis explores a strategy for compliant mechanisms design using the Bi-directional Evolutionary Structural Optimization (BESO) method. The studied BESO procedure requires an objective function that not only ensures the desired flexibility expected for a compliant mechanism but also enough stiffness to apply external loads. A multi-criteria approach was used to make both characteristics accountable by formulating the optimization problem to maximize the displacement ratio and minimize the structure compliance. This particular objective function improves the algorithm convergence and reduces the formation of hinges. Sensitivity numbers are found by the objective function variation with respect to the design variables, to be later used in the BESO method to add and remove material until an optimal topology is achieved. The implementation is validated by comparing the results with typical topologies found from the literature. Finally, some additional considerations related to the BESO method are analyzed: the influence of the stiffness workpiece over the final topologies found with the algorithm, the dependency of the finite element mesh over the results and the impact of the initial guess design domain.

*Keywords:* Topology Optimization; Evolutionary Structural Optimization; BESO Method; Compliant Mechanisms; Multi-criteria Optimization.

## List of Figures

1.1	Classification of compliant mechanisms (Li, 2014) . . . . .	18
1.2	Examples of compliant mechanisms (Howell, 2013). (a) An artificial spinal disc. (b) A compliant centrifugal clutch (c) A lamina emergent mechanism. . . . .	19
1.3	Classification of the different design methods for compliant mechanisms . . . . .	20
1.4	Compliant mechanisms topologies with different design approaches (Howell <i>et al.</i> , 2013). (a) Final topology obtained using ground structure approach; (b) Final topol- ogy obtained using the continuum approach . . . . .	21
2.1	(a) Checkboard pattern (Picelli, 2011); (b) Line segment with one node connections only (Picelli, 2011); (c) A typical checkerboard pattern in the BESO method. . . . .	35
2.2	(a) Nodes located inside the circular sub-domain are used in the filter scheme for the $eth$ element; (b) Nodal Sensibilities extrapolated into the element $eth$ that has been filtered. . . . .	36
2.3	Flowchart of the BESO method . . . . .	40
2.4	Dimensions of the design domain and boundary and loading conditions for a short cantilever . . . . .	41
2.5	Mean compliance and volume fraction evolution for a short cantilever . . . . .	42
2.6	Topology Optimization for a short Cantilever with different methods: (a) BESO method; (b) SIMP method (Huang and Xie, 2007); (c) BESO method with hexago- nal mesh (Picelli, 2011) . . . . .	43
2.7	Dimensions of the design domain, and boundary and loading conditions for a beam	43
2.8	Dimensions of the design domain, and boundary and loading conditions for a beam	44
2.9	Topology Optimization for a short Cantilever with different methods: (a) BESO method; (b) SIMP method (Huang and Xie, 2007); (c) BESO method with hexago- nal mesh (Picelli, 2011) . . . . .	44
2.10	Mean compliance and volume fraction evolution for a beam . . . . .	45
3.1	Topologies obtained for the inverter case using different objective functions: (a) Output displacement $u_{out}$ ; (b) Mechanical Advantage $GA$ ; (c) Objective function $GA/SE$ proposed by Li (2014) . . . . .	47
3.2	(a) Minimum compliance solution; (b) Maximum compliance solution composed of zero material. . . . .	47
3.3	General design model for hinge-free compliant mechanism (a) Mechanism design; (b) Structure design; . . . . .	49

3.4	Flowchart of the BESO method . . . . .	54
4.1	Design domain and boundary conditions for example 1 (inverter case). . . . .	57
4.2	Evolution of the volume fraction and objective function for example 1 (inverter case). . . . .	58
4.3	Optimal topologies comparison for the inverter case: (a) Topology found by Li <i>et al.</i> (2013) with $V_f = 40\%$ ; (b) Topology found by Li <i>et al.</i> (2013) with $V_f = 20\%$ ; (c) Topology found with BESO for $V_f = 40\%$ ; (d) Topology found with BESO for $V_f = 20\%$ . . . . .	58
4.4	Evolution of the mechanical advantage $GA$ and the Compliance $SE$ for example 1 (inverter case). . . . .	59
4.5	Optimal topologies for example 1 (inverter case): (a) Optimal topology deformed with a $V^* = 40\%$ ; (b) Optimal topology deformed with a $V^* = 20\%$ . . . . .	60
4.6	Design domain and boundary conditions or example 2 (gripper case): (a) Full design domain; (b) Symmetric part of the design domain. . . . .	61
4.7	Optimal topologies comparison for example 2 (gripper case): (a) Topology found by Li <i>et al.</i> (2013) with $V_f = 40\%$ ; (b) Topology found by Li <i>et al.</i> (2013) with $V_f = 20\%$ ; (c) Topology found with BESO for $V_f = 40\%$ ; (d) Topology found with BESO for $V_f = 20\%$ . . . . .	61
4.8	Evolution of the volume fraction and objective function for example 2 (gripper mechanism). . . . .	62
4.9	Evolution of the mechanical advantage $GA$ and the Compliance $SE$ for example 2 (gripper case). . . . .	63
4.10	Optimal topologies for the gripper case: (a) Optimal topology deformed with a $V^* = 40\%$ ; (b) Optimal topology deformed with a $V^* = 20\%$ . . . . .	64
4.11	Design domain and boundary conditions for example 3 (Inverse gripper): (a) Full design domain; (b) Simplified design domain. . . . .	65
4.12	Evolution of the volume fraction and objective function for example 3. . . . .	66
4.13	Optimal topologies for example 3 (gripper case): (a) Optimal topology deformed with a $V^* = 40\%$ ; (b) Optimal topology deformed with a $V^* = 20\%$ . . . . .	66
4.14	Design domain and boundary conditions for example 4 (crunching mechanism): (a) Full design domain; (b) Simplified design domain. . . . .	68
4.15	Evolution of the volume fraction and objective function for example 4 (crunching mechanism). . . . .	68
4.16	Evolution of the mechanical advantage $GA$ and the Compliance $SE$ for example 4 (crunch case). . . . .	69
4.17	Optimal topologies for example 4 (crunching mechanism): (a) Optimal topology deformed with a $V^* = 40\%$ ; (b) Optimal topology deformed with a $V^* = 20\%$ . . . . .	70

4.18	Design domain and boundary conditions for example 5: (a) Full design domain; (b) Simplified design domain. . . . .	71
4.19	Evolution of the volume fraction and objective function for example 5. . . . .	72
4.20	Optimal topologies for example 5: (a) Optimal topology deformed with a $V^* = 40\%$ ; (b) Optimal topology deformed with a $V^* = 20\%$ . . . . .	72
4.21	Optimal topologies for example 1 (inverter case) with different constant stiffness: (a) $k_{out} = 0$ N/m; (b) $k_{out} = 2 \times 10^6$ N/m; (c) $k_{out} = 2 \times 10^7$ N/m; (d) $k_{out} = 4.9 \times 10^8$ N/m. . . . .	73
4.22	Optimal topologies for example 2 (gripper case) with different constant stiffness: (a) $k_{out} = 0$ N/m; (b) $k_{out} = 7 \times 10^6$ N/m; (c) $k_{out} = 2 \times 10^7$ N/m; (d) $k_{out} = 2 \times 10^{10}$ N/m. . . . .	74
4.23	Optimal topologies for example 3 (inverse gripper case) with different constant stiffness: (a) $k_{out} = 0$ N/m; (b) $k_{out} = 5 \times 10^4$ N/m; (c) $k_{out} = 1 \times 10^8$ N/m. . . . .	75
4.24	Optimal topologies for example 4 (crunching mechanism) with different constant stiffness: (a) $k_{out} = 0$ N/m; (b) $k_{out} = 1 \times 10^5$ N/m; (c) $k_{out} = 1.5 \times 10^5$ N/m; (d) $2 \times 10^6$ N/m; (e) $k_{out} = 2 \times 10^{10}$ N/m. . . . .	75
4.25	Optimal topologies for example 5 (inverter with two output ports) with different constant stiffness: (a) $k_{out} = 0$ ; (b) $k_{out} = 100$ ; (c) $k_{out} = 150$ ; (d) $2 \times 10^3$ ; (e) $k_{out} = 2 \times 10^7$ . . . . .	76
4.26	Gripper stress distribution for the optimal topologies for $k_{out}$ extreme values: (a) $k_{out} = 0$ ; (b) $k_{out} = 2 \times 10^7$ . . . . .	77
4.27	Inverter optimal topologies for different mesh sizes: (a) $30 \times 30$ mesh; (b) $50 \times 50$ mesh; (c) $100 \times 100$ mesh; (d) $200 \times 200$ mesh. . . . .	78
4.28	Gripper optimal topologies for different mesh sizes: (a) $40 \times 40$ mesh; (b) $80 \times 80$ mesh; (c) $120 \times 120$ mesh; (d) $200 \times 200$ mesh. . . . .	79
4.29	Inverter stress distribution for the optimal topologies with $V_f = 40\%$ and for $k_{out}$ extreme values: (a) $k_{out} = 0$ ; (b) $k_{out} = 4.9 \times 10^5$ . . . . .	79
4.30	Inverter stress distribution for the optimal topologies with $V_f = 20\%$ and for $k_{out}$ extreme values: (a) $k_{out} = 0$ ; (b) $k_{out} = 4.9 \times 10^5$ . . . . .	80
4.31	Gripper stress distribution for the optimal topologies with $V_f = 40\%$ and for $k_{out}$ extreme values: (a) $k_{out} = 0$ ; (b) $k_{out} = 2 \times 10^7$ . . . . .	80
4.32	Gripper stress distribution for the optimal topologies with $V_f = 20\%$ and for $k_{out}$ extreme values: (a) $k_{out} = 0$ ; (b) $k_{out} = 2 \times 10^7$ . . . . .	81
4.33	Stress distribution for the optimal topologies: (a) Example 3: inverse gripper; (b) Example 4: crunch mechanism. . . . .	81
4.34	Checkerboard initial guess design domain: (a) Inverter; (b) Gripper. . . . .	82

4.35	Evolution of the volume fraction and objective function for the inverter mechanism with $V = 50\%$ and $V_f = 20\%$ . . . . .	84
4.36	Evolution of the volume fraction and objective function for the inverter mechanism with $V = 50\%$ and $V_f = 50\%$ . . . . .	85
4.37	Evolution of the volume fraction and objective function for the gripper mechanism with $V = 50\%$ and $V_f = 20\%$ . . . . .	86
4.38	Evolution of the volume fraction and objective function for the gripper mechanism with $V = 50\%$ and $V_f = 50\%$ . . . . .	87

## List of Tables

2.1	BESO Parameters for a short Cantilever . . . . .	42
2.2	BESO Parameters for a beam . . . . .	44
4.1	BESO parameters for the examples 1 and 2, the inverter and gripper design . . . . .	57
4.2	BESO parameters for the examples 1 and 2, the inverter and gripper design . . . . .	65
4.3	BESO parameters for the example 3 corresponding to the crunch mechanism . . . . .	67
4.4	BESO parameters for the example 3 corresponding to the crunch mechanism . . . . .	71
4.5	BESO parameters for the example 1 with a checkerboard initial design domain . . . . .	83
4.6	BESO parameters for the example 2 with a checkerboard initial design domain . . . . .	85

## Table of Contents

<b>List of Figures</b>		<b>xi</b>
<b>List of Tables</b>		<b>xv</b>
<b>Notations</b>		<b>xvi</b>
<b>Table of Contents</b>		<b>xvi</b>
<b>1 INTRODUCTION</b>		<b>18</b>
1.1 Motivation and general remarks . . . . .		18
1.2 Methods for Compliant Mechanism Design . . . . .		20
1.2.1 Ground Structure or Kinematic Approach . . . . .		21
1.2.2 Continuum Approach: Optimization-based Methods for Compliant Mechanisms Design . . . . .		22
1.2.2.1 Homogenization Method . . . . .		23
1.2.2.2 Level set-Method Method . . . . .		24
1.2.2.3 SIMP method . . . . .		25
1.2.2.4 BESO method . . . . .		25
1.3 Objectives and Contributions . . . . .		26
1.4 Work description . . . . .		27
<b>2 BIDIRECTIONAL EVOLUTIONARY TOPOLOGY OPTIMIZATION</b>		<b>29</b>
2.1 Introduction . . . . .		29
2.2 Problem Statement: BESO method to Stiffness Optimization . . . . .		30
2.3 Material Interpolation Scheme . . . . .		32
2.4 Sensitivity Calculation . . . . .		32
2.5 Filter Scheme and Stability Process . . . . .		34
2.6 Volume Constraint and Convergence Criterion . . . . .		37
2.7 Numerical Implementation and Iterative procedure . . . . .		39
2.8 BESO algorithm validation . . . . .		41
2.8.1 Topology Optimization of a Short Cantilever . . . . .		41
2.8.2 Topology Optimization of a Beam . . . . .		43

<b>3</b>	<b>BI-DIRECTIONAL TOPOLOGY OPTIMIZATION FOR COMPLIANT MECHANISMS DESIGN</b>	<b>46</b>
3.1	Selection of the Objective Function . . . . .	46
3.2	Problem formulation for the Objective function GA/SE . . . . .	48
3.3	Mechanical analysis using virtual load vectors . . . . .	50
3.3.1	Sensitivity Number using virtual load vectors . . . . .	51
3.4	Numerical Implementation and Iterative procedure . . . . .	53
<b>4</b>	<b>NUMERICAL EXAMPLES AND DISCUSSION</b>	<b>56</b>
4.1	Numerical Validation Examples . . . . .	56
4.1.1	Example 1: Inverter compliant mechanism . . . . .	56
4.1.2	Example 2: Gripper compliant mechanism . . . . .	60
4.2	Case studies: Gripper, Inverter and Crunch mechanisms . . . . .	64
4.2.1	Example 3: Inverted Gripper Mechanism . . . . .	64
4.2.2	Example 4: Crunching mechanism . . . . .	67
4.2.3	Example 5: Inverter with two output ports . . . . .	70
4.3	Influence of the Workpiece constraint . . . . .	73
4.4	Mesh-independence study . . . . .	78
4.5	Stress Analysis of compliant mechanisms . . . . .	79
4.6	Examples of compliant mechanisms from initial guess design . . . . .	82
4.6.1	Inverter case . . . . .	83
4.6.2	Gripper case . . . . .	84
<b>5</b>	<b>CONCLUSIONS AND SUGGESTED FUTURE WORKS</b>	<b>88</b>
5.1	Summary and Conclusions . . . . .	88
5.2	Suggestions for future research . . . . .	90
	<b>References</b>	<b>91</b>

# 1 INTRODUCTION

This chapter's objective is to present the principal investigation purposes and introduce some subjects related to compliant mechanism design. First, the motivations to conduct this research are discussed, followed by a brief bibliographic review. General and specific objectives are included and a description of each chapter goals in the overall work is presented.

## 1.1 Motivation and general remarks

A mechanism is defined as a mechanical device used to transmit motion, force or energy and is classified into two main groups: rigid-body and compliant mechanisms. The compliant or flexible mechanisms gain their mobility by transforming an input form of energy, either mechanical, electrical, thermal, or magnetic into output motion (Lobontiu, 2003). These devices can be fabricated from a single layer, do not require assembly or any lubrication and are commonly used for applications where high precision and reliability are needed (Howell, 2013).

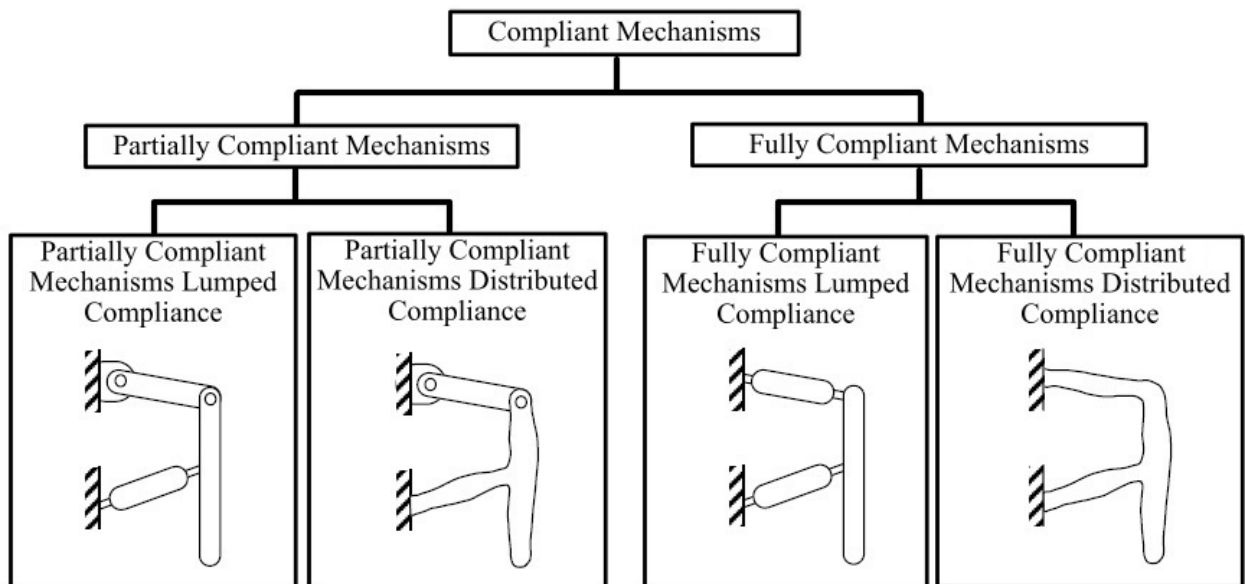


Figure 1.1: Classification of compliant mechanisms (Li, 2014)

The compliant mechanisms can also be divided into partially and fully compliant mechanisms according to the various rigid and flexural members composing the device (Midha *et al.*, 1994;

Cardoso *et al.*, 2003). Partially compliant mechanisms consist of some rigid members, traditional joints, and compliant members. Fully compliant mechanisms do not contain mechanical joints and their mobility is obtained from the elastic deformation of its members (Howell, 2002). The overall classification for compliant mechanisms can be seen in Figure 1.1.

The functions integration into fewer parts is one of the most compelling advantages of compliant mechanisms. Besides that, there is a potential for significantly lower costs. This comes from reduced assembly, fewer components to stock and the possibility of simplified manufacturing (mechanism fabrication from a single mold and additive manufacturing). Some of this applications can be seen in figure 1.2 such as an artificial spinal disc mechanism, a compliant centrifugal clutch or a laminar emergent mechanism. The compliant mechanisms expanded use can also be explained by an increased performance (high precision, low weight, low friction) (Howell *et al.*, 2013). However, because compliant mechanisms are relatively new compared to more traditional devices, it is difficult for designers to find examples and resources to guide them in their work. Many people are beginning to understand the advantages of compliant mechanisms but there is still a general lack of knowledge of how to implement them.

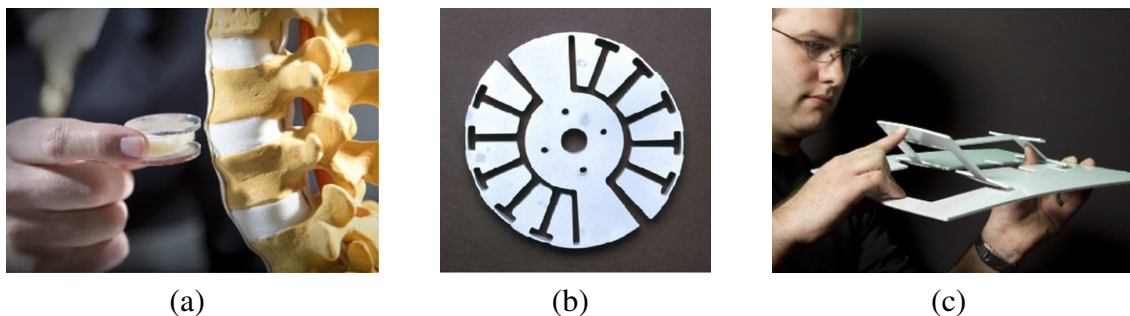


Figure 1.2: Examples of compliant mechanisms (Howell, 2013). (a) An artificial spinal disc. (b) A compliant centrifugal clutch (c) A lamina emergent mechanism.

While the advantages of compliant mechanisms already mentioned are outstanding, they also have some challenges that have to be carefully considered in their design. For example, integration of different functions into fewer parts offers advantages, but it also requires the design for motion and force behavior simultaneously. This difficulty increases by the fact that deflections often fall into the nonlinear range, making its design tough to address. The complexity of compliant mechanisms elastic behavior has done its design been typically accomplished by trial and error methods (Sigmund, 1997). However, over the past few decades the scientific community has advanced on this matter developing new materials and new approaches for a more systematic design using high-performance computing facilities.

The primary motivation of this dissertation is to explore the compliant mechanisms design using the bi-directional evolutionary topology optimization (BESO method). This particular interest is due the lack of works found related to compliant mechanisms design using BESO and the diversity of applications that could be addressed with this particular optimization method. Problems involving design dependent loads or fluid-structure interaction are just an example of interesting optimization problems in compliant mechanism design that have already been addressed using topology optimization (Yoon, 2014; Panganiban *et al.*, 2010). These subjects are also related to the research topics of our investigation group (Picelli, 2015; Picelli *et al.*, 2014; Calixto *et al.*, 2015), which makes it an excellent opportunity to explore the compliant mechanisms design for this kind of applications and this work is the first step in that direction. Studying the influence of the different BESO parameters into the final topologies is also necessary to achieve better results and to find the better model that describes the complaint mechanisms behavior.

## 1.2 Methods for Compliant Mechanism Design

There are two general approaches to parameterize the optimization problem for compliant mechanisms design, in other words, two different strategies to discretize and define the design domain: the ground structure approach and the continuum approach.

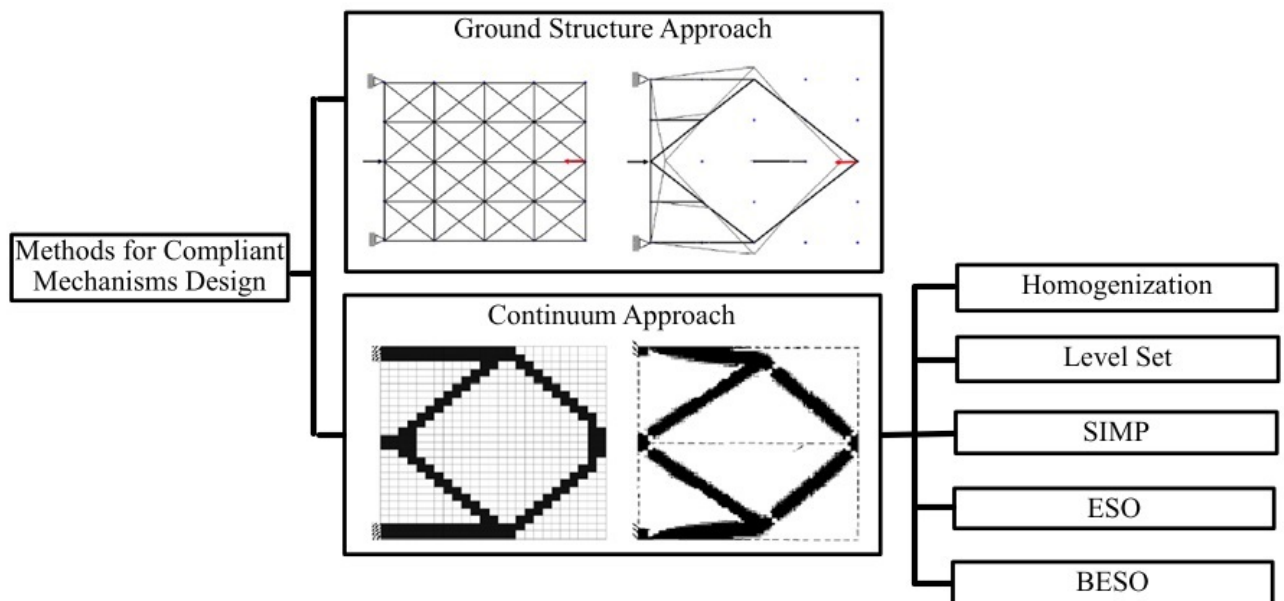


Figure 1.3: Classification of the different design methods for compliant mechanisms

Both methods have different advantages and challenges depending on the particular application. This section introduces these main approaches for compliant mechanisms design, specifically the ones related to topology optimization. Figure 1.3 illustrates the different methods for compliant mechanism design and its classification.

### 1.2.1 Ground Structure or Kinematic Approach

In the ground structure approach, a continuous design domain is approximated using a dense network of truss or beam elements. The largest number of elements would be contained in a full ground structure, where every node is connected to every other node by an element. (Howell *et al.*, 2013). Starting with a full ground structure, the optimization process performs an iterative elastic analysis after each iteration where bars with low cross sections (lower than an admissible threshold) are removed gradually until an optimal topology is achieved (Chen and Wang, 2006).

The design variables for this approach are the cross-sectional areas of the truss elements. The design variables threshold is set to a very small value, nearly zero. When the optimization process converges, elements that have a value close to this lower limit are considered to be void, and the remaining elements define the optimal topology (Howell *et al.*, 2013). Figure 1.4a shows an example of a compliant mechanism design problem solved using a ground structure, where the different truss elements remaining after the optimization process constitute the final topology.

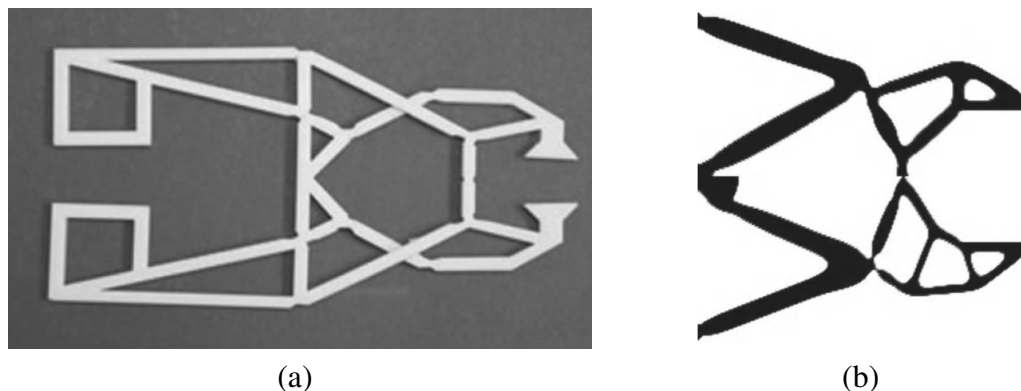


Figure 1.4: Compliant mechanisms topologies with different design approaches (Howell *et al.*, 2013). (a) Final topology obtained using ground structure approach; (b) Final topology obtained using the continuum approach

The ground structure approach was first proposed by Dorn *et al.* (1964), where the optimization problem was formulated as a linear programming problem to minimize weight and subjected

to stress constraints (Wang and Zhang, 2014). On the design of compliant mechanisms, ground structures of both truss and beam elements have been considered by several researchers, such as Frecker *et al.* (1997), who adopted a multi-criteria approach to compliant mechanism design using a truss ground structure. (Saxena and Ananthasuresh, 2000) also considered this approximation to analyze an optimal structural property for compliant mechanisms design and Zhan and Zhang (2010) used the ground structure approach for designing compliant mechanisms with multiple input forces and output displacements. Some other interesting applications can be seen in the investigations of Canfield and Frecker (2000) who addressed the design of compliant mechanical amplifiers for piezoelectric actuators and Wang and Zhang (2014) that proposed a multi-material approach for compliant mechanism design.

One of the advantages of using the ground structure approach is that commonly the stiffness matrix used in the elastic analysis is a linear function of the design variables, making the analytical sensitivity calculations very simple (Howell *et al.*, 2013). However, the kinematic-based design approach is still considered as a simplified method for the analysis and synthesis of compliant mechanisms, and this is precisely one of its biggest disadvantages. This strategy is limited to simple applications because the kinematic approximation could end up in a very simplified version of the optimal design (Li, 2014). The continuum approach is a more accurate strategy of designing compliant mechanisms, and there are several optimization-based methods to achieve that goal as explained below.

### **1.2.2 Continuum Approach: Optimization-based Methods for Compliant Mechanisms Design**

The second approach to synthesize compliant mechanisms is the continuum approach which includes different topology optimization methods. These techniques are especially useful, they are intended to predict the best topology or material connectivity in a compliant structure, for a particular design problem (Howell *et al.*, 2013). Several systematic methods have been developed to synthesize and design compliant mechanisms. Ananthasuresh and Kota (1995) originally developed a continuum-based approach which uses the techniques of structural optimization and the homogenization method. Sigmund (1997) developed the density method based on the continuum-type topology optimization technique for the optimal design of compliant mechanisms. Nishiwaki *et al.* (1998) adopted the homogenization method for solving optimization problems of compliant mechanisms by introducing a mutual energy concept and Saxena and Ananthasuresh (2001) generalized multi-criteria formulations in terms of monotonically increasing functions of the output

deformation and the strain energy.

One of the advantages of topology optimization is that with very little prior knowledge about the resulting compliant mechanism is needed and any prejudgment of the designer is reduced. Topology optimization is often integrated with finite element methods to consider many possible ways of distributing material with the design domain (Howell, 2013). Some of this interesting works have been developed in the Brazilian research community using topology optimization such as Cardoso and Fonseca (2006) who designed a strategy to optimize piezoelectric actuators considering geometric nonlinearities using the generalized method of moving asymptotes (GMMMA) or Lopes and Novotny (2015) who used the topological derivative to synthesize compliant mechanisms with stress restrictions. Some important works have also been addressed by Rubio *et al.* (2009); Carbonari *et al.* (2005); Silva *et al.* (2007) covering diverse topics from the design of compliant mechanisms considering thermal effect compensation to the study of graded elements for multiphysics applications. The majority of this works use one material interpolation method.

Some of the topology optimization techniques are discussed in this chapter such as the homogenization, level-set, SIMP, ESO and BESO method. Finally, this investigation focuses on the BESO method for compliant mechanisms design which will be addressed in detail in Chapter 2.

### 1.2.2.1 Homogenization Method

The homogenization method is based on the assumption of a microstructure in which the properties are homogenized. In the topology optimization area, the problem is posed as optimizing the material distribution in a perforated structure with infinite microscale voids. In the optimization process, the portions of the perforated structure that are filled with the material can be identified as a solid structure. On the other hand, the portions that are filled with voids can be identified as no structure (Nishiwaki *et al.*, 1998). There are three design variables associated with each finite element, two of them represent the dimensions of the rectangular hole in the element and the last one is for the orientation of the hole (Solehuddin *et al.*, 2007)

This method has been widely used to parameterize the topology design problem in a continuum approach. It was originally developed by Bendsoe and Kikuchi (1988) for minimum compliance design and was also the first continuum-based method used to optimize the distributed compliance of this kind of mechanisms (Li, 2014). Ananthasuresh (1994) originally developed the homogenization method as a structural optimization technique for the synthesis of compliant

mechanisms (Anantasuresh, 2003). Thereafter Frecker *et al.* (1997) introduced a multi-criteria optimization procedure to satisfy the flexibility and stiffness requirements for compliant mechanisms, formulation that was also adopted by Nishiwaki *et al.* (1998) to solve the optimization problem of compliant mechanisms using the homogenization method. Some of the recent works that use this method for this particular application address the problem of compliant mechanism design considering large displacements (Pedersen *et al.*, 2001) and different strategies to avoid numerical instabilities such as one node connections (Luo *et al.*, 2005). This instability refers to the appearance of elements connected only by one node to their neighboring elements as the arrangement in a checkerboard.

### 1.2.2.2 Level set-Method Method

Level-set methods have emerged recently as an attractive alternative to solve topology optimization problems without homogenization. The approach was initially proposed by Osher and Sethian (1988) on a physical base to solve the boundary-capturing problem in computational fluid dynamics. Most recently, the level-set method has been presented to perform shape and topology optimization of an elastic compliant mechanism and it is now widely used in various applications. For example, the method has been used for the topology and shape optimization field especially with the works of (Wang *et al.*, 2003) and (Allaire *et al.*, 2004). Wang and Chen (2005) also proposed the level-set method for the optimal design of monolithic compliant mechanisms with multiple materials.

A level-set representation can describe, concisely, the geometric and material boundaries of a structure and more importantly, it is capable of performing topological changes of geometric components, especially merging and splitting (Wang and Chen, 2005). The method has become very popular given some of his advantages: it has the ability to handle arbitrary objective functions and state equations, and for its great efficiency and versatility (Jouve and Mechkour, 2008). The method has been successfully applied to compliant mechanism design, since the works of Chen and Wang (2006) and more recently with the investigations of Luo and Wang (2011) and Zhu *et al.* (2014) to eliminate the presence of hinges in the final topologies, a recurrent problem in compliant mechanism design.

### 1.2.2.3 SIMP method

One of the most popular methods to parameterize the design domain in topology optimization problems is the Solid Isotropic Material with Penalization (SIMP) method. This method was developed for the first time by Bendsoe and Sigmund (2003), using a sequential linear programming approach that is introduced in the optimization algorithm. In this case, the objective was to maximize the mechanical advantage of a compliant mechanism subjected to a restriction in the structure final volume (Li, 2014). This method showed results with topologies more complex and elaborate than the ones found with the ground structure approach (see Figure 1.4b). The SIMP final topologies were better even comparing with density based optimization results such as the homogenization method (Nishiwaki *et al.*, 1998). The SIMP method also presents some undesired inconveniences such as topologies with checkerboard problems, one node connected hinges and in designs poorly defined caused by the presence of gray scales.

The original formulations for the SIMP method was the work of Sigmund (1997), who has been working intensely to expand the methods applications and to explain the SIMP method to the optimization community (Rozvany, 2009). Sigmund's versatile applications include compliant mechanisms (Sigmund, 1997), geometrically nonlinear structures (Buhl *et al.*, 2000) and multi-physics actuators (Sigmund, 2001). Most recently and together with his collaborators have developed a robust formulation for compliant mechanism design to ensure insensitivity to manufacturing variations (Schevenels *et al.*, 2011) and avoid large-displacement for compliant mechanisms (Lazarov *et al.*, 2011). Other compliant mechanism design issues that have been addressed while employing the SIMP method include control of the direction of the output control displacement, multiple outputs, and geometric nonlinearity (Bendsoe and Sigmund, 2003).

### 1.2.2.4 BESO method

The evolutionary topology optimization is another topology optimization method commonly used in structural optimization and is based on a simple concept that inefficient material is gradually removed from the design domain so that the resulting topology evolves towards an optimum. The later version of the BESO method, namely the bi-directional evolutionary topology optimization (BESO), allows not only to remove material but also to add material near the most efficient regions simultaneously (Li *et al.*, 2013). The BESO method could be used in several applications, such as problems with fluid-structure interaction (Vicente *et al.*, 2015), design dependent loads

(Picelli *et al.*, 2014) or porous-acoustic absorbing systems (Silva and Pavanello, 2010). The traditional BESO method is used in this work for the compliant mechanism design using a multi-criteria objective function. For this purpose, the structure strain energy is introduced into the optimization problem formulation as was already made by Li *et al.* (2013). The work of Li (2014) is one of the few found investigations that used the BESO method for compliant mechanism design and was a very important reference for the development of this investigation. After the BESO method is implemented and the results validated with previous topologies found in the literature, the workpiece constraint ( $k_{out}$ ) influence was studied, as well as its importance into the problem formulation is verified.

It is important to mention that choosing the best method to parameterize the design domain and solve the optimization problem will depend on the designer, taking into consideration the computation time, the software availability, and the requirements of the particular application. The ground structure method may be preferred when computation time is important because a relatively small number of elements can be used and it is relatively easy to implement. The homogenization method is more complicated and requires more computation time and their formulas may not be available to the average designer trying to implement his own code (Howell *et al.*, 2013). The SIMP or BESO method are convenient for many optimization problems, especially where more complex topologies are desired.

### 1.3 Objectives and Contributions

The main purpose of this investigation is to implement and explore a structural topology optimization algorithm using the BESO method for the compliant mechanism design. Considering that a multiobjective function needs to be considered in the problem formulation, a simple strategy to calculate both objective functions and sensitivity numbers is proposed. The influence of certain optimization parameters over the final topologies was also part of this investigation concerns. In terms of the specific objectives, these are summarized in the list below:

- Analysis of the structural behavior of compliant mechanisms to formulate the optimization problem of maximizing its output displacement.
- Propose a strategy to calculate the objective functions and the sensitivity number in order to simplify the problem formulation and the numerical implementation;
- Implement an algorithm for compliant mechanism design.

- Validate the code accuracy using typical examples of compliant mechanisms and comparing results already found from a literature review.
- Analyze the BESO parameters influence over the final topologies and its importance in the overall optimization process.

The most important contribution of this investigation will be the analysis of the BESO parameters influence over the final topologies, especially given the limited published information about designing compliant mechanisms using the BESO method. This study could also help to a better understanding of the optimization problem and the general compliant mechanisms structural behavior.

## 1.4 Work description

This dissertation is divided into five chapters. This first chapter presents a general view about compliant mechanisms, including the advantages and challenges related to its design. The general and specific objectives are also explained in detail and the main contributions and motivations for the development of this investigation is discussed.

Chapter 2 explains the basic concepts of the BESO method and all the different aspects related to its numerical implementation. The topology optimization often searches for the stiffest structure with a given volume of material, whereby the problem formulation is chosen to minimize the structure compliance with satisfying a particular volume constraint. A short cantilever and a beam are used as examples for the BESO method validation and compared with the results already found by Huang and Xie (2010).

The evolutionary BESO method applied for compliant mechanism design is described in Chapter 3, specifically, the problem formulation to maximize the output displacement. A multicriteria objective function is used in order to fulfill the kinematic and structural requirements, and the overall structural analysis required is addressed. Once the optimization problem is formulated, a new strategy is proposed to calculate the objective functions for both loading conditions and its respective sensitivity numbers. Finally, the algorithm for compliant mechanism design using the BESO method is presented.

Chapter 4 shows the numerical results obtained for the compliant mechanism design, where

two different examples are proposed to validate the algorithm by comparing the results with topologies found from previous works . The chapter also includes the study of certain parameters related to the optimization process and its influence over the final topologies for both cases.

Finally, Chapter 5 presents the conclusions from the results obtained in previous sections, as well as the suggested future works.

## 2 BIDIRECTIONAL EVOLUTIONARY TOPOLOGY OPTIMIZATION

This chapter explains in detail the basic concepts related to the BESO (Bi-directional Evolutionary Structural Optimization) method. This includes studying its different stages: problem statement, finite element analysis, sensitivity number calculation, filter scheme, element removal/addition and convergence criteria. The method is discussed as a general approach, analyzing the parameters used through the optimization process and the numerical implementation. Finally, two examples are employed to validate the code implemented in this work by simple comparison with typical results from previous works.

### 2.1 Introduction

The Evolutionary Structural Optimization approach was first proposed by Xie and Steven in the early 1990s. The ESO method is based on the simple concept of gradually removing inefficient material from a structure. Through this process, the resulting structure will evolve towards its optimal shape and topology (Huang and Xie, 2010). Some of the original work on ESO, which was carried out by Xie and Steven (1993) and Chu *et al.* (1996, 1997), was complemented by Xie and Steven (1996) and has undergone a continuous development since it was proposed in 1992. Its use has been extended to topology optimization of structures with all kind of constraints such as buckling load (Manickarajah *et al.*, 1998), frequency (Xie and Steven, 1996), or temperature (Li *et al.*, 2001).

Despite that the ESO method seems to follow a logical procedure to reduce the structural weight (or volume) of the structure, this first approach had significant problems. It is possible that material removed in an early iteration might be required later to be part of the optimal design and the ESO algorithm is unable to recover this material once it has been prematurely or wrongly deleted from the structure. Hence, while the ESO method is capable of producing an upgraded solution over an initial guess design in most cases, the result may not necessarily be the best solution. To overcome these deficiencies, an improved algorithm known as the bi-directional evolutionary structural optimization (BESO) was developed by (Huang and Xie 2007).

The early BESO method not only eliminates inefficient elements from the structure but also recovers the erased elements, allowing material to be removed and added throughout the optimization process. Initial research on BESO was conducted by Yang and Xie (1999b) for stiffness

optimization. In their study, the sensitivity numbers of the void elements are estimated through a linear extrapolation of the displacement field after the finite element analysis. Then, the solid elements showing the lowest sensitivity numbers are removed from the structure, and the void elements with the highest sensitivity numbers are changed into solid elements (Huang and Xie, 2010). The method is also more flexible in choosing the initial design and recovering the inappropriately removed element than the previous ESO method (Yang and Xie, 1999a).

For the current BESO method, some techniques are introduced into the optimization procedure to improve its performance. For example, the material can be removed and added simultaneously in the design domain using the material interpolation scheme (Huang and Xie, 2009) where void elements are replaced by soft elements. A filter scheme is also used in this technique to prevent unstable phenomena such as checkerboard and mesh-dependency in structural topology optimization (Huang and Xie, 2007). This is an effective mechanism for modifying the element density to become a function of its neighboring design variables. Finally, given that elements may frequently switch between void (or soft) and solid status between iterations, the BESO method averages the element sensitivity historical information to avoid an unstable evolution process.

## 2.2 Problem Statement: BESO method to Stiffness Optimization

To seek for an optimal topology given a determined volume of material, the BESO method formulates the general optimization problem as follows:

$$\begin{aligned} \text{Minimize:} \quad & h(x_e) = \mathbf{H}(x_1, x_2, x_3, \dots, x_N) \\ \text{constrained to:} \quad & V^* - \sum_{e=1}^N V_e x_e = 0 \end{aligned} \tag{2.1}$$

where  $h(x_e)$  denotes the objective function of the optimization problem and  $\mathbf{H}$  is defined as an  $n$ -dimensional function. In addition,  $V_e$  and  $V^*$  represent respectively the volumes for an individual element and the prescribed volume structure. The binary design variable  $x_e$  declares the absence (0) or presence (1) of an element.

Stiffness has been widely used as criteria for classic engineering problems such as buildings or bridges design. But the mean compliance  $C$ , the inverse measure of the overall stiffness of a structure, is commonly considered as an objective function. This work uses this criterion for the BESO method validation and to be later extended to compliance mechanism design. The mean

compliance  $C$  can be defined by the structure's total strain energy or the external work done by applied loads as in Equation 2.2, with  $\mathbf{f}$  being the force vector and  $\mathbf{u}$  the nodal displacement vector.

$$C = \frac{1}{2} \mathbf{f}^T \mathbf{u} \quad (2.2)$$

Now we can reformulate the optimization problem in Equation 2.1 by making  $h(x) = C$  and considering that the element itself as the design variable, rather than its associated physical or material parameters (Huang and Xie, 2010). Under this assumptions, the optimization problem for mean compliance is stated as:

$$\begin{aligned} \text{Minimize:} \quad & C = \frac{1}{2} \mathbf{f}^T \mathbf{u} \\ \text{constrained to:} \quad & V^* - \sum_{e=1}^N V_e x_e = 0 \end{aligned} \quad (2.3)$$

$$\mathbf{K} \mathbf{u} = \mathbf{f}$$

$$x_e = x_{min} \text{ or } 1$$

In Equation 2.3,  $N$  is the total number of elements in the system. The variable  $x_e$  can be equal to 1 for solid elements and 0 for void ones. This approach is called hard-kill BESO method, and establish a solid-void scheme where the removed elements are completely erased from the design. However, this complete removal of a solid element could result in numerical difficulties for the topology optimization. To avoid this, a solid-soft design named soft-kill BESO method presents an alternative way of removing an element by reducing its elastic modulus to a small value.

The soft-kill BESO method is used in this work, which means that no element is allowed to be completely removed from the design domain. Under this approach a small value  $x_{min} = (0.0001)$  is adopted into Equation 2.3. The design variable  $x_{min}$  is penalized using the material interpolation scheme to minimize the elastic modulus of removed elements.

### 2.3 Material Interpolation Scheme

Material interpolation schemes with penalization have been widely used in the classical SIMP (Simple Interpolation Material Problem) method for implementing the solution to nearly solid-void designs (Bendsoe, 1989; Zhou and Rozvany, 1991). In the BESO method it is used to achieve a nearly solid-void design by interpolating the Young modulus of the intermediate material as a function of the element density:

$$E(x_e) = E^0 x_e^p \quad (2.4)$$

with  $E^0$  as the Young's modulus of the solid material and  $p$  being the penalty exponent. It is assumed that the Poisson's ratio is independent of the design variables and the global stiffness matrix  $\mathbf{K}$  can be expressed by the elemental stiffness matrix and design variable  $x_e$  as in Equation 2.5, where  $\mathbf{K}_e^0$  denotes the elemental stiffness matrix of the solid element,  $\mathbf{K}$  is the global stiffness matrix of the system and  $\sum_e$  is the assembly operator (Bathe, 1996).

$$\mathbf{K} = \sum_e x_e^p \mathbf{K}_e^0 \quad (2.5)$$

### 2.4 Sensitivity Calculation

The element sensitivity denotes the objective function gradient. It intends to measure the variation tendency due a small change in the design variable when the whole design domain is discretized into finite elements. Generally the calculation can be written as Equation 2.6 by differentiating the objective function  $h(x)$ :

$$\alpha_e = \frac{\partial h(x)}{\partial x_e} = \frac{\partial \mathbf{H}(x_1, x_2, x_3, \dots, x_n)}{\partial x_e} \quad (2.6)$$

In our case, the mean Compliance  $C$  was chosen as the objective function and assumed that the design variable  $x_e$  continuously changes from 1 to  $x_{min}$ . The objective function sensitivity with respect to the change in the design variable can be found by deriving Equation 2.2.

$$\frac{\partial C}{\partial x_e} = \frac{1}{2} \frac{\partial \mathbf{f}^T}{\partial x_e} \mathbf{u} + \frac{1}{2} \mathbf{f}^T \frac{\partial \mathbf{u}}{\partial x_e} \quad (2.7)$$

In finite element analysis, the equilibrium equation of a static structure can be expressed as in Equation 2.8:

$$\mathbf{K}\mathbf{u} = \mathbf{f} \quad (2.8)$$

By introducing a vector of Lagrangian multiplier  $\lambda$ , an extra term  $\lambda^T(\mathbf{f} - \mathbf{K}\mathbf{u})$  can be added to the objective function without changing anything due to the equilibrium Equation 2.8. This is called the adjoint method and will be used to determinate the displacement vector sensitivity. Once the Lagrangian multiplier is added to the compliance, the expression in Equation 2.2 becomes:

$$C = \frac{1}{2} \mathbf{f}^T \mathbf{u} + \lambda^T (\mathbf{f} - \mathbf{K}\mathbf{u}) \quad (2.9)$$

The sensitivity of this new objective function can be written as:

$$\frac{\partial C}{\partial x_e} = \frac{1}{2} \frac{\partial \mathbf{f}^T}{\partial x_e} \mathbf{u} + \frac{1}{2} \mathbf{f}^T \frac{\partial \mathbf{u}}{\partial x_e} + \frac{\partial \lambda^T}{\partial x_e} (\mathbf{f} - \mathbf{K}\mathbf{u}) + \lambda^T \left( \frac{\partial \mathbf{f}}{\partial x_e} - \frac{\partial \mathbf{K}}{\partial x_e} \mathbf{u} - \mathbf{K} \frac{\partial \mathbf{u}}{\partial x_e} \right) \quad (2.10)$$

The third term in Equation 2.10 becomes zero due to the equilibrium equation. Also, given that the applied load does not change with element variations,  $\partial \mathbf{f} / \partial x_e = 0$ , the objective function sensitivity can be expressed as:

$$\frac{\partial C}{\partial x_e} = \left( \frac{1}{2} \mathbf{f}^T - \lambda^T \mathbf{K} \right) \frac{\partial \mathbf{u}}{\partial x_e} - \lambda^T \frac{\partial \mathbf{K}}{\partial x_e} \mathbf{u} \quad (2.11)$$

Equation 2.10 show that the Lagrangian multiplier vector  $\lambda$  could be chosen freely given that  $(\mathbf{f} - \mathbf{K}\mathbf{u})$  is equal to zero from equilibrium Equation 2.8. To eliminate the unknown  $\partial \mathbf{u} / \partial x_e$  from the sensitivity expression in Equation 2.11,  $\lambda$  is chosen such that:

$$\frac{1}{2}\mathbf{f}^T - \lambda^T \mathbf{K} = 0 \quad (2.12)$$

Comparing the expression above to the equilibrium Equation 2.8, the solution for the Lagrangian multiplier vector  $\lambda$  is:

$$\lambda = \frac{1}{2}\mathbf{u} \quad (2.13)$$

Replacing  $\lambda$  into Equation 2.11, the mean compliance sensitivity stays:

$$\frac{\partial C}{\partial x_e} = -\frac{1}{2}\mathbf{u}^T \frac{\partial \mathbf{K}}{\partial x_e} \mathbf{u} \quad (2.14)$$

By substituting the material interpolation scheme (Equation 2.5) into Equation 2.14, the objective function sensitivity with regards to the change in the  $e$ th element can be found as:

$$\frac{\partial C}{\partial x_e} = -\frac{1}{2}p x_e^{p-1} \mathbf{u}_e^T \mathbf{K}_e^0 \mathbf{u}_e \quad (2.15)$$

Finally, considering that the BESO method uses discrete design variables, we can express the sensitivity number to only the two materials allowed in the design solid and soft. Therefore, the sensitivity of the mean compliance is expressed at all elemental level as:

$$\alpha_i = -\frac{1}{p} \frac{\partial C}{\partial x_e} = \begin{cases} \frac{1}{2} \mathbf{u}_e^T \mathbf{K}_e^0 \mathbf{u}_e & \text{when: } x_e = 1 \\ \frac{x_{min}^{p-1}}{2} \mathbf{u}_e^T \mathbf{K}_e^0 \mathbf{u}_e & \text{when: } x_e = x_{min} \end{cases} \quad (2.16)$$

## 2.5 Filter Scheme and Stability Process

Some unstable phenomena could be present in the topology optimization methods, such as checkerboard patterns and mesh-dependency problems. These difficulties are related to the use of

low order bilinear finite elements and how their sensitivity numbers could become discontinuous across element boundaries (Jog and Haber, 1996). The checkerboard pattern is the area where the density jumps frequently from  $x_{min}$  to 1 between neighboring elements in a resulting topology (see Figure 2.1) and its presence causes difficulty in interpreting and manufacturing the optimal structure. On the other hand, mesh dependency is related to the problem of obtaining different topologies from using different finite element meshes. When a fine mesh is used, the numerical process of structural optimization will produce a topology that contains more members of smaller sizes in the final design. Ideally, mesh-refinement should result in a better finite element modeling of the same structure and a better description of boundaries, not in a more detailed or qualitatively different structure (Huang and Xie, 2010).

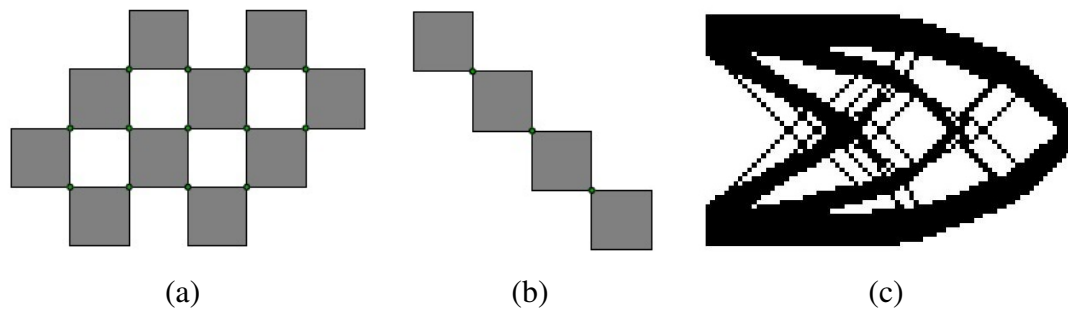


Figure 2.1: (a) Checkerboard pattern (Picelli, 2011); (b) Line segment with one node connections only (Picelli, 2011); (c) A typical checkerboard pattern in the BESO method.

To suppress checkerboard patterns formation and prevent mesh dependency at the same time, a filtering scheme is introduced into the BESO method. The procedure consists of two basic steps: calculate sensitivity numbers at each node and transform this sensitivity nodal numbers into smoothed elemental sensitivities. The nodal sensitivity numbers  $\alpha^n$  have no real physical meaning and can be found by averaging the sensitivity numbers of elements connected to one node through Equation 2.17.

$$\alpha_d^n = \frac{\sum_{e=1}^M V_e \alpha_e}{\sum_{e=1}^M V_e} \quad (2.17)$$

where  $M$  is the total number of nodes connected to the  $d$ th node. To identify the quantity of elements that will influence the sensitivity number of a certain  $e$ th element, a circular sub-domain of ratio  $r_{min}$  is projected from the center of the  $e$ th element as can be seen in Figure 2.17a, where  $r_{ed}$  denotes the distance between the center of the element  $e$  and node  $d$ . The nodal sensitivities of

every element inside the circular domain will be considered into the filter scheme.

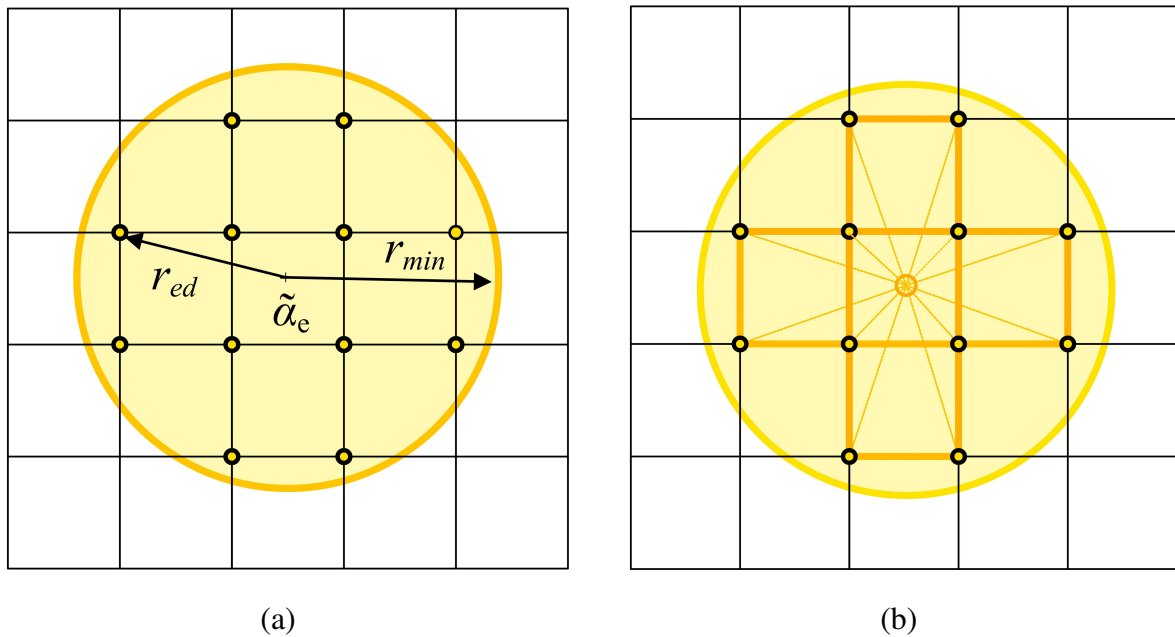


Figure 2.2: (a) Nodes located inside the circular sub-domain are used in the filter scheme for the  $eth$  element; (b) Nodal Sensibilities extrapolated into the element  $eth$  that has been filtered.

The smoothed sensitivity numbers for an element are calculated by averaging all nodal sensitivities already found by Equation 2.17, related to this element. The approximation is made based on the distance  $r_e$  between each node in the circular sub-domain and the center of the element  $eth$  under consideration. This can be seen in Figure 2.2b, where all nodal sensitivity numbers within the sub-domain contribute to the element sensitivity. The weight of a node  $d$ th related to an element  $eth$  is called  $w_{ed}$  and can be defined by Equation 2.18

$$w_{ed} = \begin{cases} \frac{r_{ed}}{\sum_{k=1}^L r_{ek}}; & r_{ed} \leq r_{min} \\ 0; & r_{ed} > r_{min} \end{cases} \quad (2.18)$$

where  $L$  is the number of elements inside the circular sub-domain of ratio  $r_{min}$ . A matrix  $\mathbf{A}$  that contains all the weights of all nodes with respect to each element, will be used as an artifact to facilitate the numerical implementation of the filter and can be calculated as:

$$[\mathbf{A}] = \begin{matrix} & 1 & \left[ \begin{array}{cccccc} w_{11} & w_{21} & w_{31} & \dots & w_{no1} \\ w_{12} & w_{22} & w_{32} & \dots & w_{no2} \\ w_{13} & w_{23} & w_{33} & \dots & w_{no3} \\ \vdots & \vdots & \vdots & \ddots & \vdots \\ w_{1N} & w_{2N} & w_{3N} & \dots & w_{Nno} \end{array} \right. \\ & 2 & \\ & 3 & \\ & \vdots & \\ & N & \end{matrix} \quad (2.19)$$

As in previous sections,  $N$  represents the total number of finite elements and  $no$  is the total number of nodes in the design domain. The next step is to convert the sensitivity numbers  $\alpha^n$  into smoothed elemental sensitivity numbers  $\tilde{\alpha}_e$  by Equation 2.20.

$$\{\tilde{\alpha}_e\}_N = [\mathbf{A}]_{N \times no} \{\alpha_e^n\}_{no \times 1} \quad (2.20)$$

The filter scheme adoption can effectively address the mesh dependency problem, however, the objective function and the corresponding topology could still not be convergent. The reason for this behavior is that sensitivity numbers of solid and soft elements are based on discrete design variables, making the objective function difficult to converge. To solve this problem, the element sensitivities will be modified by averaging their historical information, using Equation 2.21 to stabilize the evolution process (Huang and Xie, 2007).

$$\tilde{\alpha}_e = \frac{\tilde{\alpha}_{e,k} + \tilde{\alpha}_{e,k-1}}{2} \quad (2.21)$$

where  $k$  is the current iteration number. Then, we let  $\tilde{\alpha}_{e,k} = \tilde{\alpha}_e$ , to consider the sensitivity information in previous iterations for the actual sensitivity number.

## 2.6 Volume Constraint and Convergence Criterion

The BESO method is an iterative approach where the structure volume changes continuously through iterations before it reaches the prescribed volume  $V^*$ . But for the evolutionary procedure to consider adding or removing an element in the current iteration, the target volume for the next iteration  $V_{k+1}$  should be determined in advance. This target volume  $V_{k+1}$  is formulated as:

$$V_{k+1} = \begin{cases} V_k \times (1 + ER) & \text{when not satisfying } V^* \text{ but } V_{k+1} > V_k \\ V_k \times (1 - ER) & \text{when not satisfying } V^* \text{ but } V_{k+1} < V_k \\ V^* & \text{when satisfying } V^* \end{cases} \quad (2.22)$$

where  $ER$  is the evolutionary ratio and  $V_k$  means the current material volume of the  $k$ th iteration. Meanwhile, Equation 2.22 implies that the volume constraint can be larger or smaller than the volume of the initial guess design. The prescribed volume can be achieved by increasing or decreasing material step by step before the volume of the structure reaches the requirement ( $V_{k+1} = V^*$ ).

To address material removal or addition, all elements including soft and solid elements will be arranged in descending order according to the values of their sensitivity numbers. For solid elements, the element density is switched from 1 to  $x_{min}$  if the criterion  $\alpha_e \leq \alpha_{del}^{th}$ , is satisfied. As for soft elements, the element density is changed from  $x_{min}$  to 1 if the criterion  $\alpha_e > \alpha_{add}^{th}$ , is satisfied. The reference variables  $\alpha_{del}^{th}$  and  $\alpha_{add}^{th}$  represent the threshold sensitivity numbers for removing and adding elements, which can be easily determined by the following three simple steps:

1. Let  $\alpha_{add}^{th} = \alpha_{del}^{th} = \alpha^{th}$ , thus  $\alpha^{th}$  can be easily determined by  $V_{k+1}$ . For example if they are  $N$  elements in the design domain and  $V_{k+1}$  corresponds to a design with  $n$  elements then  $\alpha^{th} = \alpha_n$ .
2. Calculate the volume addition ratio  $AR$ , which is defined as the number of added elements divided by the total number of elements in the design domain. If  $AR \leq AR_{max}$ , where  $AR_{max}$  is a prescribed maximum volume addition ratio, skip step 3. Otherwise recalculate  $\alpha_{del}^{th}$  and  $\alpha_{add}^{th}$  as in step 3.
3. Calculate  $\alpha_{add}^{th}$  by first sorting the sensitivity number of soft elements ( $x_e = x_{min}$ ). The number of elements to be switched from  $x_{min}$  to 1 will be equal to  $AR_{max}$  multiplied by the total number of elements in the design domain.  $\alpha_{add}^{th}$  is the sensitivity number of the element ranked just below the last added element.  $\alpha_{del}^{th}$  is then determined so that the removed volume is equal to  $(V_k - V_{k+1} + \text{the volume of the added elements})$ .

The cycle of finite element analysis and element removal/addition continues until the objective volume  $V^*$  is reached and the convergence criterion is satisfied. The method employs Equa-

tion 2.23 as the convergence criterion and is defined in terms of how much the objective function changes between iterations.

$$\frac{|\sum_{i=1}^N C_{k-e+1} - \sum_{i=1}^N C_{k-N-e+1}|}{\sum_{i=1}^N C_{k-e+1}} \leq \tau \quad (2.23)$$

where  $k$  is the current iteration number,  $\tau$  is an allowable convergence tolerance and  $N$  is an integer number. Normally,  $N$  is selected to be 5 which implies that the change in the mean compliance over the last 10 iterations is acceptably small.

## 2.7 Numerical Implementation and Iterative procedure

The evolutionary iteration procedure of the BESO method can be divided into different steps:

1. Discretize the whole design domain using a finite element mesh with given boundary and loading conditions.
2. Define parameters relative to the BESO method such as elemental densities  $x_e$ , penalty exponent  $p$  and filter radius  $r_{min}$ .
3. Perform finite element analysis and then calculate the elemental sensitivity number according to equation 2.16, then, update sensitivity numbers using equation 2.20.
4. Average the sensitivity number with its historical information using equation 2.21 and then, save it for next iteration.
5. Determine the target volume for the next iteration using equation 2.22
6. Add and delete elements according to the procedure described in Section 2.6.
7. Repeat steps 2-5 until the constraint volume ( $V^*$ ) is achieved and the convergence criterion (equation 2.23) is satisfied.

Figure 2.3 illustrates the BESO method flowchart, where each step has a different function in the overall algorithm. The BESO method and the finite element analysis were programmed using MATLAB.

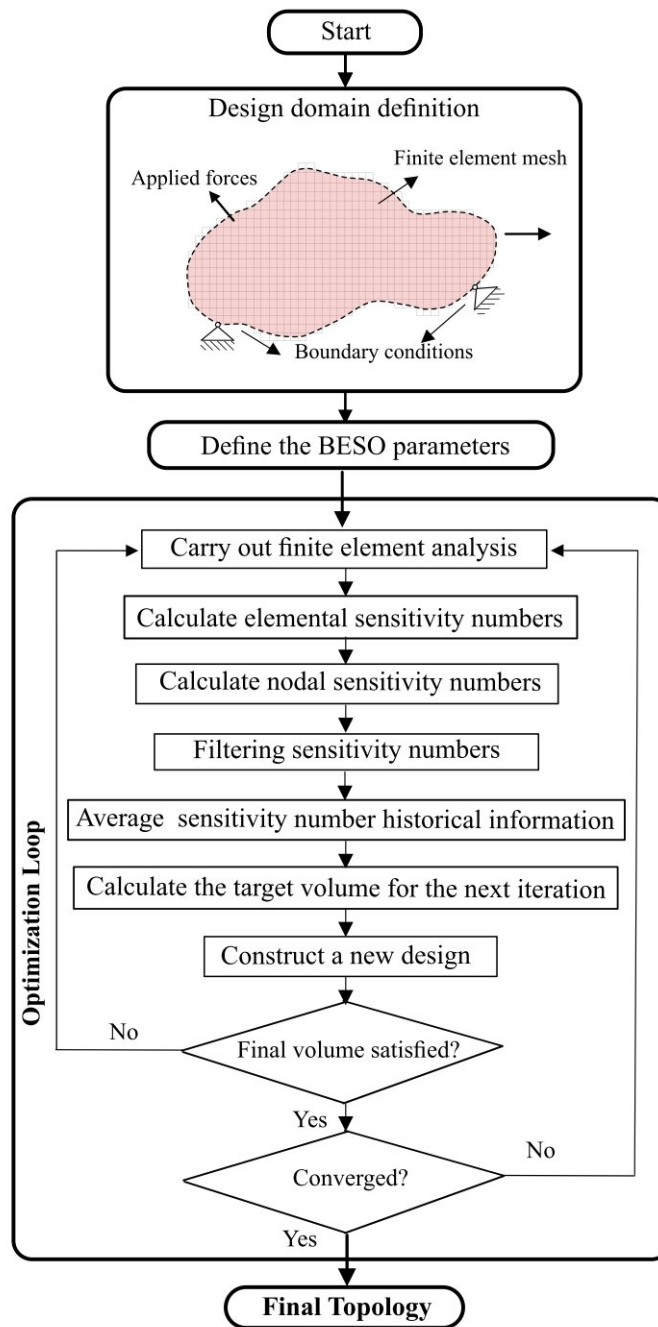


Figure 2.3: Flowchart of the BESO method

## 2.8 BESO algorithm validation

This section resumes the BESO algorithm validation using two classical problems broadly studied in topology optimization: a short cantilever and a beam. Once again, the objective function will minimize the structure compliance and the results are compared with the topologies found by Huang and Xie (2010).

### 2.8.1 Topology Optimization of a Short Cantilever

The first example considers the stiffness optimization of a short cantilever shown in Figure 2.4. The design domain is 80 mm in length, 55 mm in height and 1 mm in thickness. A 100 N downward force is applied at the center of the free end. Young's modulus of 100 GPa and Poisson's ratio of 0.3 are assumed. The BESO method starts from the full design which is subdivided using a mesh of  $160 \times 80$  four node plane stress elements. The remaining BESO parameters considered for this first example can be seen in Table 2.1.

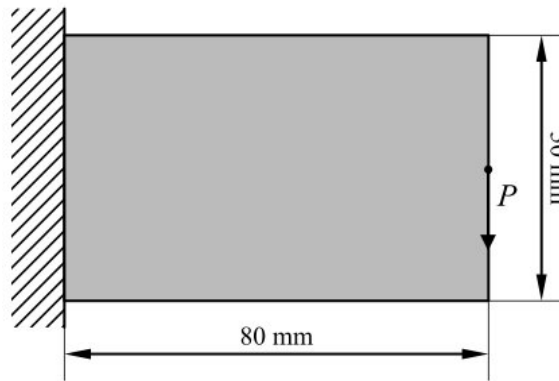


Figure 2.4: Dimensions of the design domain and boundary and loading conditions for a short cantilever

The evolution histories of the mean compliance and the volume fraction are shown in Figure 2.5. We can see how the mean compliance increase as the material is gradually removed from the structure until approximately the 70 iteration where the volume requirement is reached and the mean compliance converges to an almost constant value. Some of the occasional jumps in the mean compliance are caused by a significant change of topology, resulting from the elimination of one or more bars that may appear in the structure between iterations. For example, in the cantilever

Table 2.1: BESO Parameters for a short Cantilever

Variable	Description	Value
$V_f$	Final volume fraction	0,5
$ER$	Evolutionary volume ratio	1%
$AR_{\max}$	Maximum addition ratio	5%
$r_{\min}$	Filter ratio	3mm
$\tau$	Convergence tolerance	0.1%
$N$	Convergence parameter	5

seen in Figure 2.5, the topology suffers 3 important jumps. After these abrupt changes, the mean compliance quickly recovers and continues a smooth ascent until convergence is achieved. It is important to consider that to find the stiffest structure for a given volume, the increase in the mean compliance should be kept as small as possible.

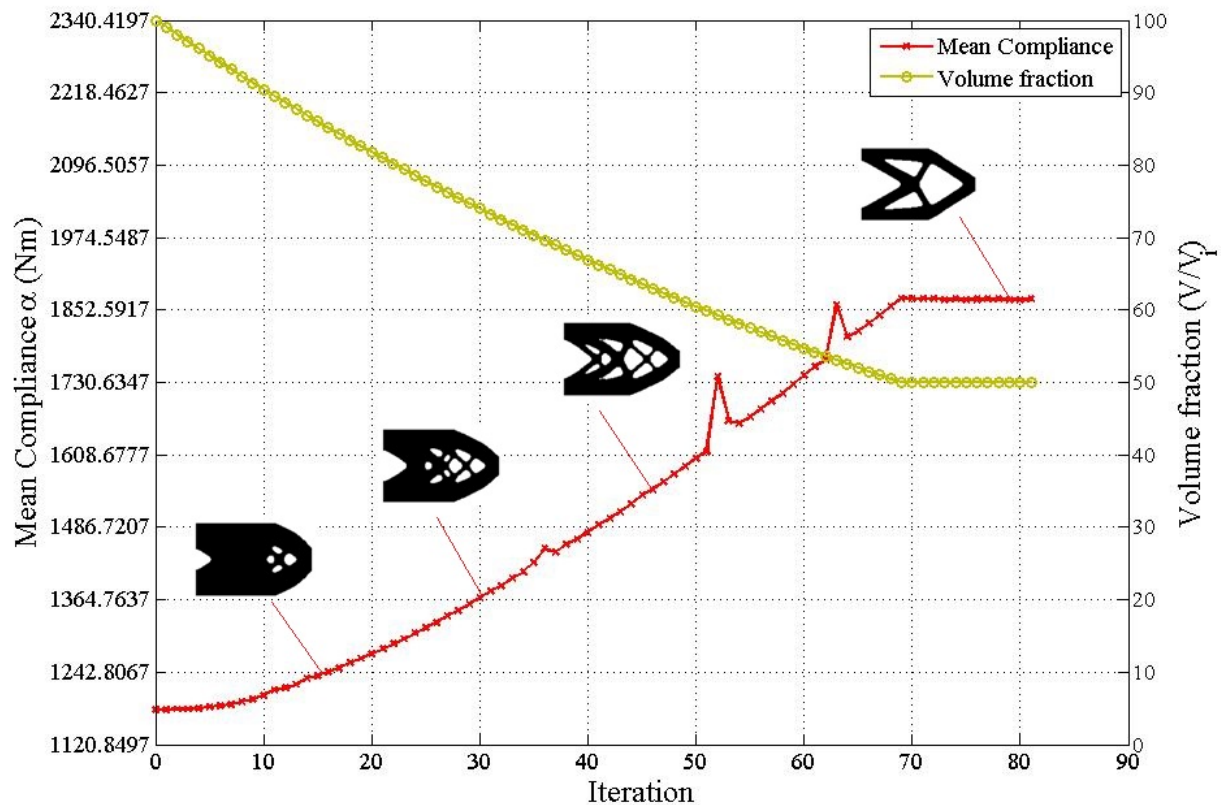


Figure 2.5: Mean compliance and volume fraction evolution for a short cantilever

The cantilever final topology was also compared with results obtained by Huang and Xie (2007) for the SIMP method and Picelli (2011) for the BESO method using a hexagonal mesh.

Figure 2.6 illustrates three different topologies showing that each case throws out the same result. This correspondence between the final results and the topologies from references found in the literature, validate the BESO method for compliance minimization of bidimensional structures. In the next chapter this implementation will be extended to a different objective function and different boundary conditions.

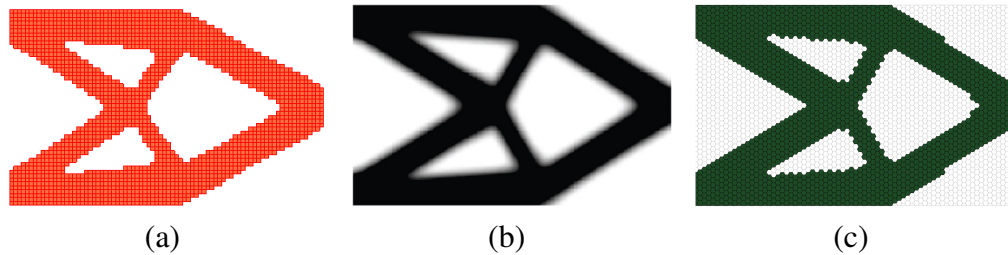


Figure 2.6: Topology Optimization for a short Cantilever with different methods: (a) BESO method; (b) SIMP method (Huang and Xie, 2007); (c) BESO method with hexagonal mesh (Picelli, 2011)

## 2.8.2 Topology Optimization of a Beam

A second example is included to validate the BESO method implementation. In this case, we will consider the beam showed in Figure 2.7.

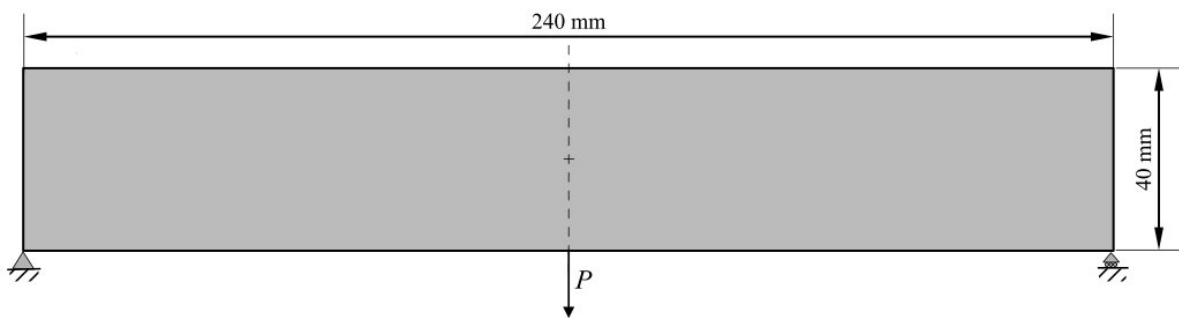


Figure 2.7: Dimensions of the design domain, and boundary and loading conditions for a beam

To facilitate the algorithm implementation, the symmetric right half of the  $120 \text{ mm} \times 40 \text{ mm}$  domain (with  $1 \text{ mm}$  thickness) is discretized using a  $120 \times 40$  mesh with four node plane stress elements (see Figure 2.8). Only 50% of the design domain volume is available for constructing the final structure and the material has Young's modulus  $E = 200 \text{ GPa}$  and Poisson's ratio  $\nu = 0.3$ . Initially, the material occupies the entire design domain. The BESO parameters used for this second example are resumed in Table 2.2.

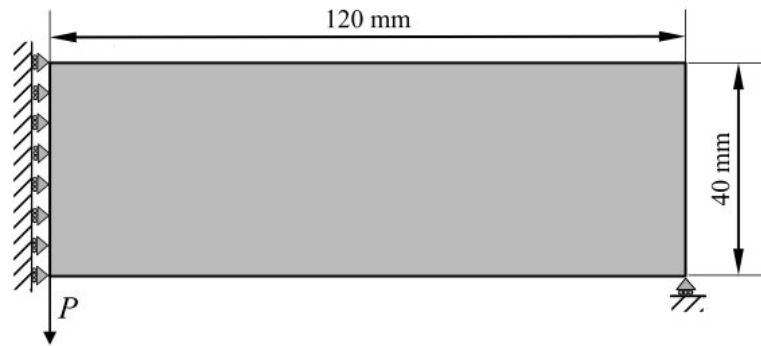


Figure 2.8: Dimensions of the design domain, and boundary and loading conditions for a beam

Table 2.2: BESO Parameters for a beam

Variable	Description	Value
$V_f$	Final volume fraction	0.5
$ER$	Evolutionary volume ratio	5%
$AR_{\max}$	Maximum addition ratio	5%
$r_{\min}$	Filter ratio	6mm
$\tau$	Convergence tolerance	0.1%
$N$	Convergence parameter	5

Figure 2.10 shows the evolution histories of the beam compliance and volume fraction for the beam. The mean compliance converges to a stable value at the final stage, after 80 iterations. We can also observe how the topology changes throughout this process, adding or removing elements in the same proportion until convergence is achieved. The volume restriction is satisfied approximately at iteration 23, from which the objective function decreases and the topology suffer very little variations.

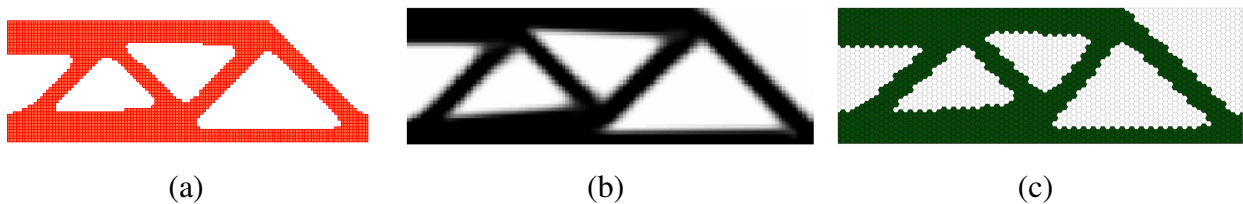


Figure 2.9: Topology Optimization for a short Cantilever with different methods: (a) BESO method; (b) SIMP method (Huang and Xie, 2007); (c) BESO method with hexagonal mesh (Picelli, 2011)

For this example, we compared the final topologies to the results found by (Huang and Xie, 2007) using the SIMP method and for (Picelli, 2011) using the BESO with a hexagonal mesh, in the same way it was made in the last section. It can be seen from Figure 2.9 that the BESO method

results match the topologies found using other optimization methods, which once again proves the method functionality.

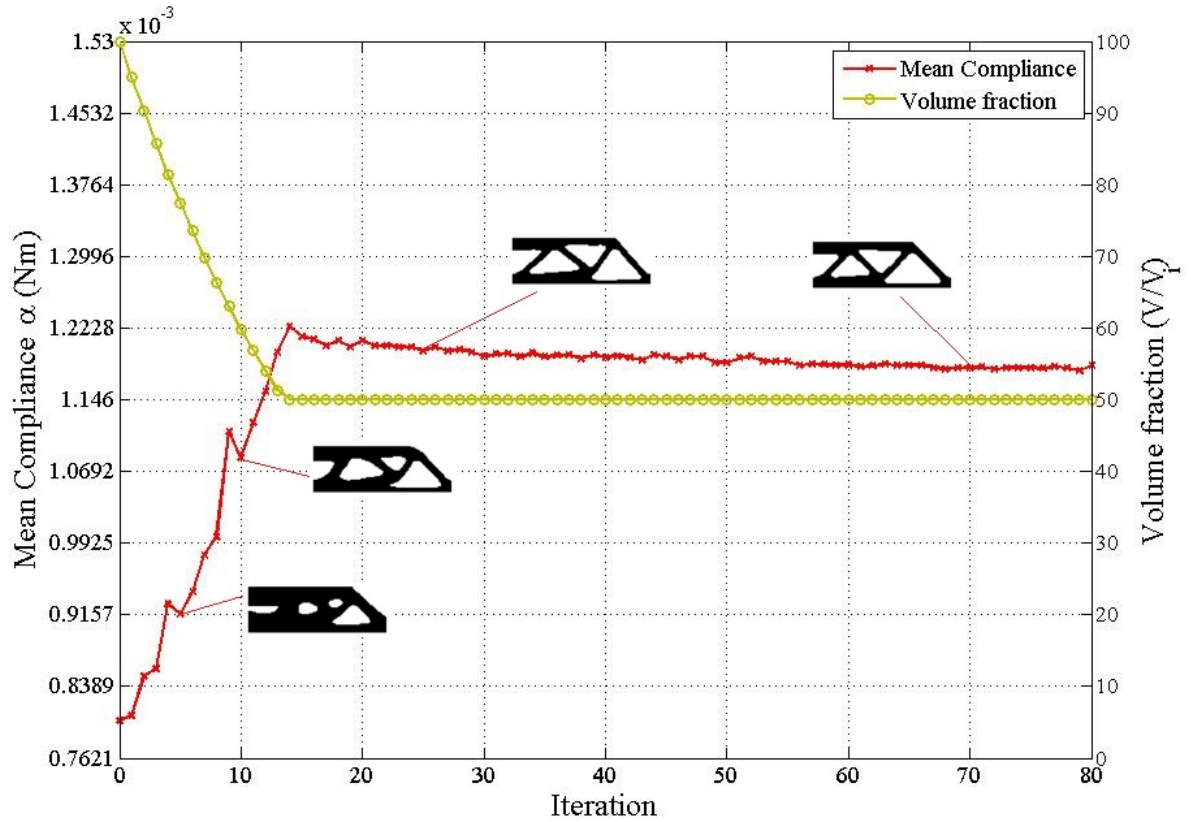


Figure 2.10: Mean compliance and volume fraction evolution for a beam

### 3 BI-DIRECTIONAL TOPOLOGY OPTIMIZATION FOR COMPLIANT MECHANISMS DESIGN

This chapter develops the necessary concepts to apply the BESO method for compliant mechanisms design. The objective function choice is discussed and a multi-criteria approach already addressed in previous works is used in this investigation to maximize the desired displacement and simultaneously minimize the structure compliance. A different approach to the superposition principle is explored to calculate the output displacements using virtual load vectors and is adopted given its simplicity. A sensitivity analysis for both cases is also made to find the objective function variation with respect to the design variable.

#### 3.1 Selection of the Objective Function

The BESO method formulates the general optimization problem through Equation 2.1, with  $h(x)$  being any particular objective function. In the case of compliant mechanisms design, a variety of objective functions  $h(x)$  has been considered in previous works (Sigmund, 1997; Saxena and Ananthasuresh, 2001; Ansola *et al.*, 2007; Luo *et al.*, 2007; Lin *et al.*, 2010; Frecker *et al.*, 1997) such as the output displacement  $u_{out}$ , mechanical advantage  $MA$ , geometric advantage  $GA$  and mechanical efficiency  $ME$ . Determining the correct objective function for the optimization of compliant mechanisms using the BESO method was an important issue to attend through this investigation and the process had several stages before understanding the problem's nature and the limitations of the chosen optimization method.

The first choice for the objective function using the BESO method was the output displacement. The results end up in disconnected topologies and convergence problems as can be seen in Figure 3.1a. This result was obtained for an inverter design, one of the typical examples of compliant mechanisms. The expected topology for this optimization case can be seen in Figure 3.1c, the result found by Li *et al.* (2013) who also used the BESO method for this particular application. A second objective function was also tested during the objective function selection: the geometric advantage  $GA$  defined as the ratio between the output and input displacement ( $u_{out}/u_{in}$ ). This objective function was tested for the same example and the results can be seen in Figure 3.1b. In this case, the algorithm still did not converge showing disconnected topologies at any iteration.

After a more careful literature review, it was found that for compliant mechanisms design,

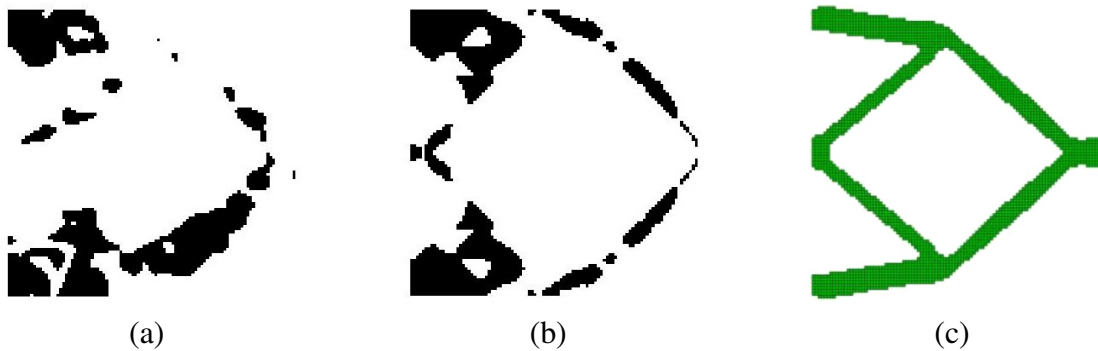


Figure 3.1: Topologies obtained for the inverter case using different objective functions: (a) Output displacement  $u_{out}$ ; (b) Mechanical Advantage  $GA$ ; (c) Objective function  $GA/SE$  proposed by Li (2014)

the objective function must account for two different conditions simultaneously: the kinematic (motion) and the structural (loading) requirements (Frecker *et al.*, 1997). This means that contrary to the first objective functions choices where only the mechanisms flexibility was desired, a compromise between this characteristic and the structure stiffness needs to be established to correctly address the problem of designing compliant mechanisms. The same example already used for the different objective functions  $u_{out}$  and  $GA$ , the inverter mechanism, can be used to a better explanation of this phenomenon. If a solution with only the maximum stiffness where considered for the inverter, the result will be the topology shown in Figure 3.2b and the structure will exhibit very little displacement in response to the input load (Howell *et al.*, 2013). The opposite solution, maximizing compliance instead of minimizing it may appear as the easier approach, but the most flexible solution will be the one with actually no material (Figure 3.2c). This alternative is not practical and in fact, the best approach is to find an objective function that reconciles these two properties.

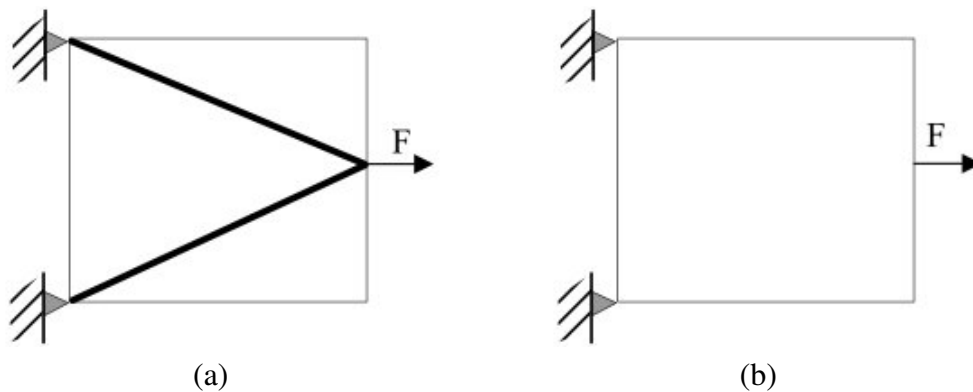


Figure 3.2: (a) Minimum compliance solution; (b) Maximum compliance solution composed of zero material.

Under this considerations, a more suitable objective function was found to ensure not only the structure flexibility but the necessary stiffness to apply external loads. Li (2014) investigation also tested different objective functions to understand which one delivered a better result. Some of his conclusions show that the traditional BESO algorithm leads to the introduction of *de facto* hinges into the final topologies and several convergence problems. He even modified the original BESO method to solved this problem by including intermediate densities into the problem formulation. This inconveniences for obtaining final topologies with hinges were solved by establishing a new objective function to maximize the desired displacement and prevent its formation (Li, 2014). Given the advantages, this new objective function is adopted and the formulation presented by Li (2014) is set up in this work as the basis for designing compliant mechanisms using the traditional BESO method.

### 3.2 Problem formulation for the Objective function GA/SE

Because required flexibility and stiffness are conflicting design objectives, incorporating both into a single design problem requires two different loading conditions and a multi-criteria optimization strategy (Frecker *et al.*, 1997). The first condition is called "mechanism design" where maximum flexibility is needed. The objective function to accomplish maximum flexibility can be established by maximizing the displacement ratio between input and output ports, or as was called earlier the geometric advantage  $GA = u_{out}/u_{in}$ . The mechanism design can be seen in Figure 3.3a, where a general design domain  $\Omega$  under given loading and boundary conditions is shown. The applied force at the input port  $i$  is  $F_{in}$  and the reaction force at the output  $j$  is  $F_{out}$  representing the workpiece resistance.  $F_{out}$  is modeled by adding a spring with constant stiffness  $k_{out}$  at the output port.

To formulate the objective function correctly the second loading condition needs to be considered. This new design domain is called "structure design" where the structural requirements are met by maximizing the stiffness (Frecker *et al.*, 1997). The compliant mechanism becomes a structure as shown in Figure 3.3b when the input port is fixed and a "dummy load"  $F_2$  is applied to the output port, accounting for the workpiece resistance. The boundary conditions stay invariable and the dummy load has the opposite direction to the desired displacement  $u_{out}$ . Maximizing the stiffness is equivalent to minimizing the structure compliance, so the second objective function will be  $SE = \frac{1}{2}\mathbf{u}^T\mathbf{K}\mathbf{u}$  where  $\mathbf{u}$  is the displacement vector for the second loading condition. Maximizing the structural stiffness or minimizing the total strain energy has the advantage that can also preclude the formation of hinges in the compliant mechanism design (Rahmatall and Swan, 2005).

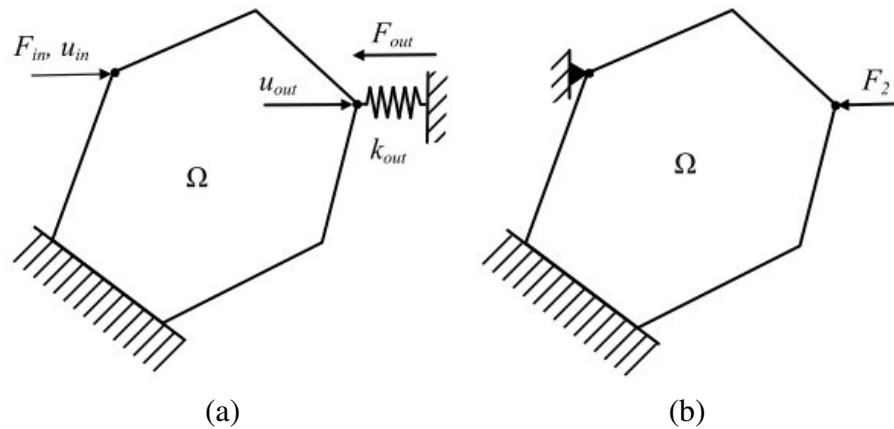


Figure 3.3: General design model for hinge-free compliant mechanism (a) Mechanism design; (b) Structure design;

Now that the two loading conditions and the two objective functions  $GA$  and  $SE$  are modeled, they need to be combined somehow. The usual multi-criteria approach uses a weighted linear combination, but it's not practical for this particular case: values for both objectives often differ by several orders of magnitude depending on the problem specifications and when this happens, the larger one will dominate (Frecker *et al.*, 1997). An easy way to avoid this problem is the use of a ratio. Since the mutual energy needs to be maximized and the strain energy minimized, the objective function can be formulated as in Equation 3.1:

$$\begin{aligned}
 &\text{Maximize: } h(x_e) = GA/SE \\
 &\text{sujeito a: } V^* - \sum_{e=1}^N V_e x_e = 0 \\
 &\quad \quad \quad x_e = x_{min} \text{ or } 1
 \end{aligned} \tag{3.1}$$

The problem for compliant mechanisms design has already been formulated by Equation 3.1, which involves two different objectives functions:  $GA$  and  $SE$ . To obtain the input and output displacements in order to find  $GA$ , the classical approach uses a mechanical analysis where this values can be found by solving equations for two load cases that are later added by the superposition principle (Sigmund, 1997). This work proposes a little different strategy to facilitate the algorithm calculation, especially for the sensitivity numbers. This new strategy will be explained in the last section of this chapter, but first, the mechanical analysis using the superposition principle is addressed.

### 3.3 Mechanical analysis using virtual load vectors

The same objective function established in Equation 3.1 is also used for this new mechanical analysis for the compliant mechanism case. The difference for this approach lies in the calculation of output/input displacements and sensitivity numbers. But first, we will define only two cases for the finite element analysis, that refer to the two structures shown in Figure 3.3.

The first case is related to the first loading condition or "mechanism design" explained in Section 2.2 and illustrated in Figure 3.3a. In this case, the superposition principle is not used for the output and input displacement calculation as was made for the classical approach. Instead, the spring constant stiffness  $k_{out}$  is added to the global stiffness matrix  $\mathbf{K}$  at the degree of freedom  $i_{out}$  corresponding to the output displacement, as shown in Equation 3.2.

$$\mathbf{K}_s(i_{out}, i_{out}) = \mathbf{K}(i_{out}, i_{out}) + k_{out} \quad (3.2)$$

where  $\mathbf{K}_s$  is the new global stiffness matrix that includes the workpiece constraint influence. The next step is to solve the equilibrium problem  $\mathbf{K}_s \mathbf{U}_1 = \mathbf{F}$  to find the displacement vector  $\mathbf{U}_1$ , with  $\mathbf{F}$  being the load vector containing the input force  $F_{in}$ . An usual approach to dealing with individual displacements using a virtual load vector is considered to calculate the displacements  $u_{in}$  and  $u_{out}$ . This load vector has all its components being equal to zero except the one corresponding to the constrained displacement component. The non-zero component is given a unit value at the same direction as the displacement constraint (Yang and Xie, 1999a). To facilitate the numerical implementation, two virtual load vectors  $\mathbf{L}_{in}$  and  $\mathbf{L}_{out}$  are created and the individual displacements can be calculated as:

$$\begin{aligned} u_{in} &= \mathbf{L}_{in} \mathbf{U}_1 \\ u_{out} &= \mathbf{L}_{out} \mathbf{U}_1 \end{aligned} \quad (3.3)$$

The second case or second loading condition from section 2.2 is calculated by simply solving the equilibrium equation  $\mathbf{K} \mathbf{U}_2 = \mathbf{F}_2$  for the structure in Figure 3.3b, with  $\mathbf{U}_2$  being the displacement vector for the stiff structure and  $\mathbf{F}_2$  the force vector with the dummy load  $F_2 = 1$  as the only non-zero component. The displacement vector  $\mathbf{U}_2$  found after the finite element analysis is used to calculate the compliance  $SE$  for the second loading condition by the expression  $SE = \frac{1}{2} \mathbf{U}_2^T \mathbf{K} \mathbf{U}_2$ .

Once both loading conditions are solved, the output and input displacements found by Equation 3.3 are used to calculate the geometric advantage defined as  $GA = u_{out}/u_{in}$ . With values for  $GA$  and  $SE$ , and the help of Equation 3.1, the objective function now can be estimated. It is important to observe that this way, only two equilibrium equations need to be solved to find the objective function and the sensitivity numbers.

### 3.3.1 Sensitivity Number using virtual load vectors

To find the elemental sensitivity number, the objective function variation with respect to the design variable is needed and can be calculated as was made in the previous section. In this case, the sensitivity numbers are determined by deriving Equation 3.1:

$$\alpha_e = \left( SE \times \frac{\partial GA}{\partial x_e} - GA \times \frac{\partial SE}{\partial x_e} \right) / SE^2 \quad (3.4)$$

The sensitivity numbers for the geometric advantage  $\partial GA/\partial x_e$  and the compliance  $\partial SE/\partial x_e$  are calculated separately to be later included in Equation 3.4. We start calculating  $\partial GA/\partial x_e$  by deriving equation  $GA = u_{out}/u_{in}$

$$\frac{\partial GA}{\partial x_e} = \left( \frac{\partial u_{out}}{\partial x_e} u_{in} - \frac{\partial u_{in}}{\partial x_e} u_{out} \right) / u_{in}^2 \quad (3.5)$$

The next step in order to find an expression for the sensitivity number of the geometric advantage is to calculate both sensitivities  $\partial u_{out}/\partial x_e$  and  $\partial u_{in}/\partial x_e$ . To calculate this values, the expressions for  $u_{out}$  and  $u_{in}$  from Equation 3.3 are derived as follows:

$$\frac{\partial u_{out}}{\partial x_e} = \frac{\partial(\mathbf{L}_{out}\mathbf{U}_1)}{\partial x_e} = \mathbf{L}_{out} \frac{\partial \mathbf{U}_1}{\partial x_e} \quad (3.6)$$

$$\frac{\partial u_{in}}{\partial x_e} = \frac{\partial(\mathbf{L}_{in}\mathbf{U}_1)}{\partial x_e} = \mathbf{L}_{in} \frac{\partial \mathbf{U}_1}{\partial x_e}$$

Deriving the equilibrium equation  $\mathbf{K}_s\mathbf{U}_1 = \mathbf{F}$  and reorganizing the terms, the displacement

sensitivity  $\partial \mathbf{U}_1 / \partial x_e$  can be found as shown in Equation 3.7.

$$\begin{aligned} \mathbf{K}_s \mathbf{U}_1 &= \mathbf{F} \\ \frac{\partial \mathbf{K}_s \mathbf{U}_1}{\partial x_e} &= \frac{\partial \mathbf{F}}{\partial x_e} \\ \frac{\partial \mathbf{K}_s}{\partial x_e} \mathbf{U}_1 + \mathbf{K}_s \frac{\partial \mathbf{U}_1}{\partial x_e} &= \frac{\partial \mathbf{F}}{\partial x_e} \end{aligned} \quad (3.7)$$

Considering that the vector  $\mathbf{F}$  only contains the load conditions related to the problem design and that those loads do not change with  $x_e$  variations,  $\partial \mathbf{F} / \partial x_e$  is equal to zero and the expression for  $\partial \mathbf{U}_1 / \partial x_e$  becomes:

$$\frac{\partial \mathbf{U}_1}{\partial x_e} = -\mathbf{K}_s^{-1} \frac{\partial \mathbf{K}_s}{\partial x_e} \mathbf{U}_1 \quad (3.8)$$

With the expression found in Equation 3.8 for  $\partial \mathbf{U}_1 / \partial x_e$  we can rewrite the expressions for  $\partial u_{out} / \partial x_e$  and  $\partial u_{in} / \partial x_e$  using Equation 3.6.

$$\begin{aligned} \frac{\partial u_{in}}{\partial x_e} &= -\mathbf{L}_{in} \mathbf{K}_s^{-1} \frac{\partial \mathbf{K}_s}{\partial x_e} \mathbf{U}_1 = -\mathbf{\Lambda}_{in} \frac{\partial \mathbf{K}_s}{\partial x_e} \mathbf{U}_1 \\ \frac{\partial u_{out}}{\partial x_e} &= -\mathbf{L}_{out} \mathbf{K}_s^{-1} \frac{\partial \mathbf{K}_s}{\partial x_e} \mathbf{U}_1 = -\mathbf{\Lambda}_{out} \frac{\partial \mathbf{K}_s}{\partial x_e} \mathbf{U}_1 \end{aligned} \quad (3.9)$$

Where the vectors  $\mathbf{\Lambda}_{out}$  and  $\mathbf{\Lambda}_{in}$  represent the displacement response to the virtual load vectors  $\mathbf{L}_{out}$  and  $\mathbf{L}_{in}$ . Finally, using Equation 2.5 the stiffness matrix derivative  $\partial \mathbf{K}_s / \partial x_e$  can be calculated by Equation 2.5 similarly as was estimated in Chapter 2. This way we obtained all the values needed to calculate the first objective function derivative  $\partial GA / \partial x_e$ .

$$\begin{aligned} \frac{\partial u_{in}}{\partial x_e} &= -p x_e^{(p-1)} \mathbf{\Lambda}_{in,e} \mathbf{K}_e^0 \mathbf{U}_{1,e} \\ \frac{\partial u_{out}}{\partial x_e} &= -p x_e^{(p-1)} \mathbf{\Lambda}_{out,e} \mathbf{K}_e^0 \mathbf{U}_{1,e} \end{aligned} \quad (3.10)$$

Output and input displacements sensitivities  $\partial u_{out} / \partial x_e$  and  $\partial u_{in} / \partial x_e$  can be expressed at elemental levels for solid and soft elements, as two discrete design variables  $x_e = 1$  (for solid

elements) and  $x_e = x_{min}$  (for soft elements), as was employed in the soft kill BESO method (Huang and Xie, 2010).

$$\frac{\partial u_{in}}{\partial x_e} = \begin{cases} -p\Lambda_{in,e}\mathbf{K}_e^0\mathbf{U}_e & \text{when: } x_e = 1 \\ -px_{min}^{(p-1)}\Lambda_{in,e}\mathbf{K}_e^0\mathbf{U}_e & \text{when: } x_e = x_{min} \end{cases} \quad (3.11)$$

$$\frac{\partial u_{out}}{\partial x_e} = \begin{cases} -p\Lambda_{out,e}\mathbf{K}_e^0\mathbf{U}_e & \text{when: } x_e = 1 \\ -px_{min}^{(p-1)}\Lambda_{out,e}\mathbf{K}_e^0\mathbf{U}_e & \text{when: } x_e = x_{min} \end{cases} \quad (3.12)$$

Replacing this new expressions for  $\partial u_{in}/\partial x_e$  and  $\partial u_{out}/\partial x_e$  into Equation 3.5, the sensitivity number for  $GA$  at the elemental level is determined. There is only one step left to find the overall sensitivity number and is to obtain the compliance sensitivity number  $\partial SE/\partial x_e$ , from the second load case in the structure showed in Figure 3.3b. For this propose, Equation 2.16 is used as follows:

$$\frac{\partial SE}{\partial x_e} = -\frac{1}{2}\mathbf{U}_2^T \frac{\partial \mathbf{K}}{\partial x_e} \mathbf{U}_2 = -\frac{1}{2}px_e^{(p-1)}\mathbf{U}_{2,e}^T \mathbf{K}_e^0 \mathbf{U}_{2,e} \quad (3.13)$$

The total strain sensitivity can also be expressed for solid and void elements for the BESO Method accordingly with the material interpolation as was made in Section 2 for the compliance minimization. With this considerations Equation 3.13 stays:

$$\frac{\partial SE}{\partial x_e} = \begin{cases} -\frac{1}{2}p\mathbf{U}_{2,e}^T \mathbf{K}_e^0 \mathbf{U}_{2,e} & \text{when: } x_e = 1 \\ -\frac{1}{2}px_{min}^{(p-1)}\mathbf{U}_{2,e}^T \mathbf{K}_e^0 \mathbf{U}_{2,e} & \text{when: } x_e = x_{min} \end{cases} \quad (3.14)$$

### 3.4 Numerical Implementation and Iterative procedure

The traditional BESO method described in chapter two is now implemented for compliant mechanisms design with a few variations in the iterative procedure. The flowchart for this new procedure is shown in Figure 3.4.

The finite element analysis is carried out to find the nodal displacements, but this time, the

problem is divided and two different load conditions are established to satisfy the kinematic and structural requirements. This two analysis are made separately to estimate the nodal displacements  $U_1$  and  $U_2$  for each case. The sensitivity numbers calculation also changes given that derivatives for both objective functions  $\partial GA/\partial x_e$  and  $\partial SE/\partial x_e$  need to be computed separately to be later included in Equation 3.4 to obtain the overall sensitivity numbers. Once calculated, they are also updated with the filter scheme using Equation 2.20 and averaged with their historical information by Equation 2.21.

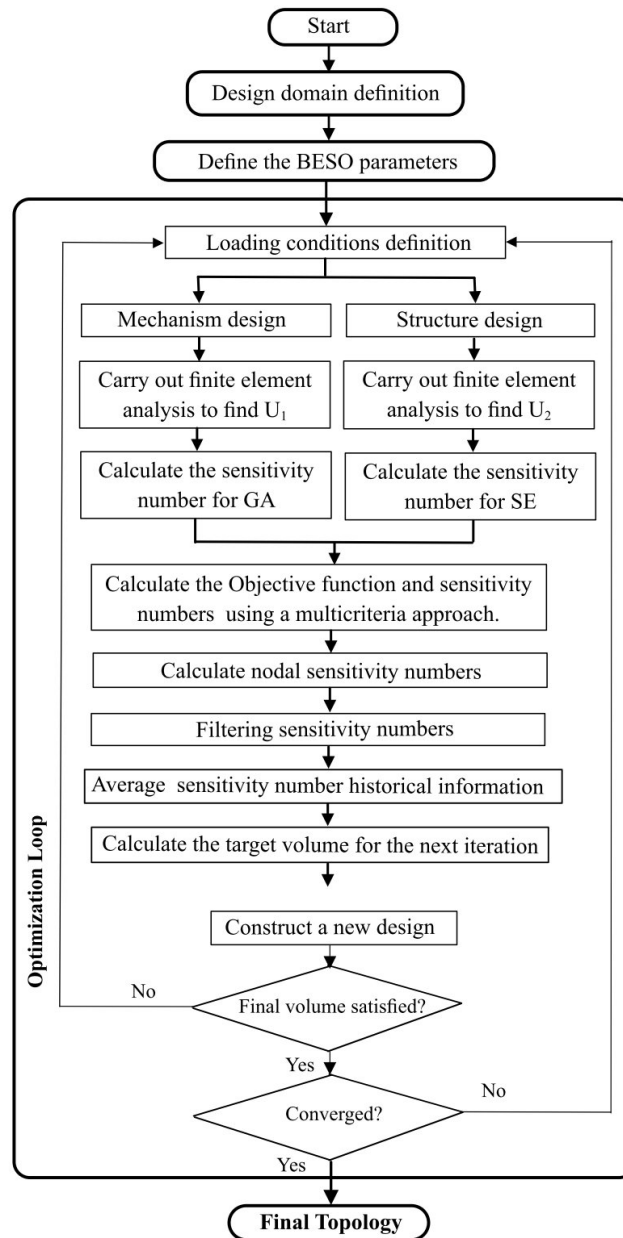


Figure 3.4: Flowchart of the BESO method

The next steps are the same as in Chapter 2: Calculate and satisfy the volume constraint, remove or add elements according to the sensitivity numbers for each element and repeat the process until two conditions are accomplished: the volume fraction reaches target volume and the performance of objective function satisfies the convergence criteria.

## 4 NUMERICAL EXAMPLES AND DISCUSSION

This chapter presents the main results obtained in this research for the compliant mechanisms design problem. The studied Bi-directional Evolutionary Structural Optimization (BESO) method is used for this purpose, and the results are compared with classical problems found in the literature to validate the algorithm. The influence of the BESO parameters was also studied and its importance in the compliant mechanism design is showed.

### 4.1 Numerical Validation Examples

The BESO algorithm for compliant mechanism design already addressed in the previous chapter was implemented using MATLAB and validated by comparing the results with topologies found from previous works. For this verification stage, the results from Li (2014) and Li *et al.* (2013) research are used as reference for the first two examples. Once again, it is important to note that few articles were found that implement the BESO method for compliant mechanisms design and much less that discussed the objective function formulation.

#### 4.1.1 Example 1: Inverter compliant mechanism

The first validation example is an inverter mechanism with a design domain that can be shown in Figure 4.1. This particular mechanisms is called inverter because the desired direction for the output displacement is in the opposite direction of the input force. The design domain is  $200\text{ mm} \times 200\text{ mm}$  and is discretized with a  $100 \times 100$  four-node quadrilateral element mesh. The structure is supported at the top and bottom corners of the left edge and an input force  $F_{in} = 1N$  is applied at the input port in the horizontal direction. The output port is located at the center of the right edge and is expected to produce a horizontal displacement  $u_{out}$  to the right. The material properties are Young's modulus  $E = 200GPa$  and Poisson's ratio  $\nu = 0.3$ . The BESO parameters for this simulation are resumed in Table 4.1.

The evolution of the objective function and the volume fraction can be seen in Figure 4.2. The BESO algorithm starts with a full design domain and gradually decreases the volume fraction until it satisfies the  $V_f = 20\%$  constraint value at the 80 *th* iteration. It can also be seen the way the topology evolves during the optimization, with significant changes until the volume constraint is

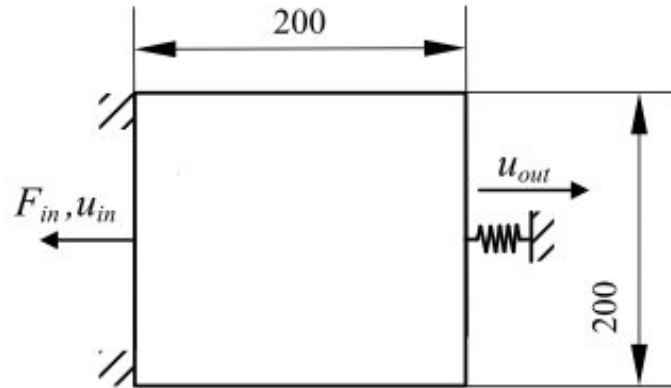


Figure 4.1: Design domain and boundary conditions for example 1 (inverter case).

Table 4.1: BESO parameters for the examples 1 and 2, the inverter and gripper design

Variable	Description	Value
$V$	Initial volume	100%
$V_f$	Final volume fraction	20%
$ER$	Evolutionary volume ratio	2%
$AR_{\max}$	Maximum addition ratio	1%
$r_{\min}$	Filter ratio	6 mm
$\tau$	Stopping criteria tolerance	$1 \times 10^{-3}$
$N$	Stopping criteria parameter	5
$k_{out}$	Workpiece resistance	0 N/m

achieved. Beyond this point, the topology remains almost invariable, only reorganizing the elements to fulfill the convergence criterion.

The same example was tested with a 40% final volume and the result can be seen in Figure 4.3c. This result and the final topology already found for a 20% final volume is presented in Figure 4.2d and compared with the outcome from Li *et al.* (2013), as can be seen in Figure 4.3a and 4.3b. The comparison verifies the algorithm validity for the compliance mechanism design considering that the final results were the same as the ones found by Li *et al.* (2013). The final topologies for the inverter case were also very similar to those obtained using the density-based optimization approach (Sigmund, 1997).

Some jumps in the objective function curve between iterations 20 and 30 are shown in Figure

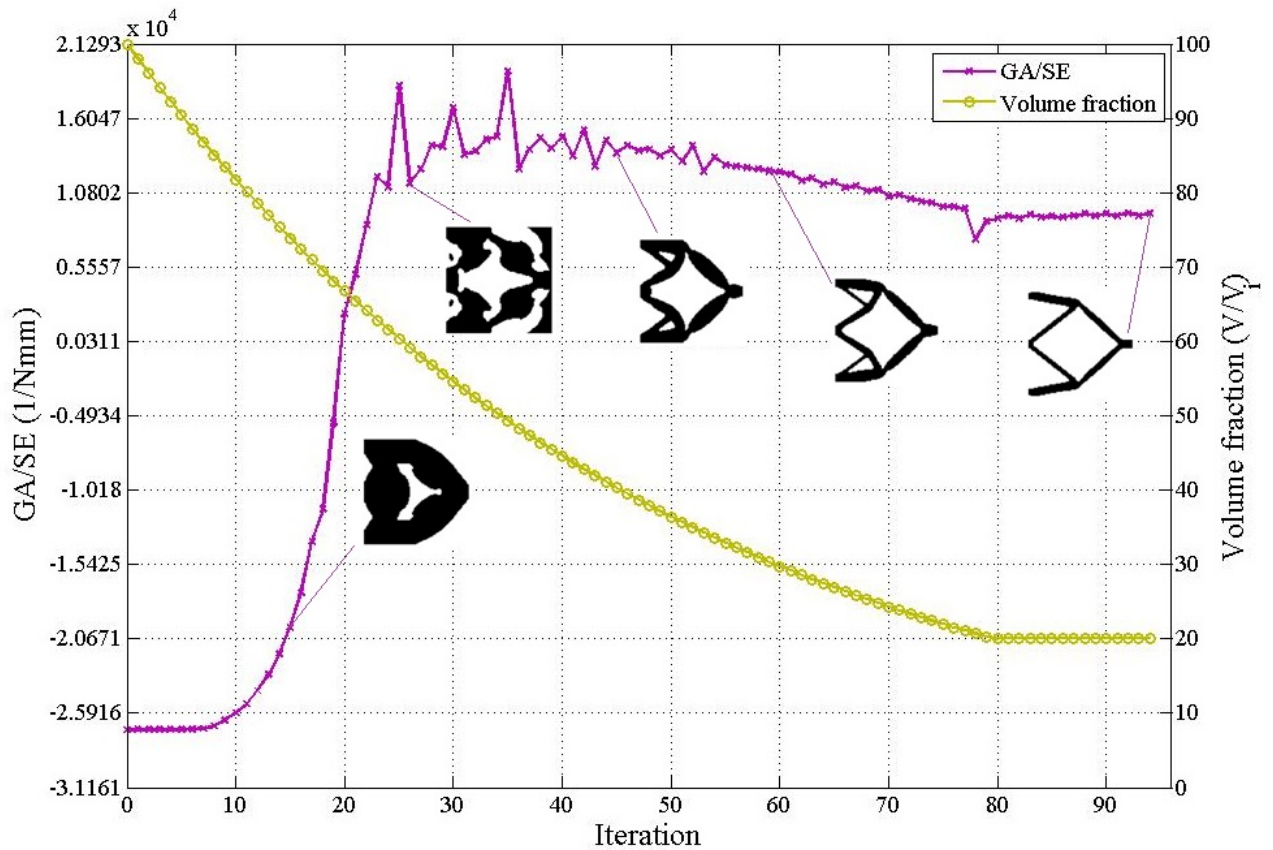


Figure 4.2: Evolution of the volume fraction and objective function for example 1 (inverter case).

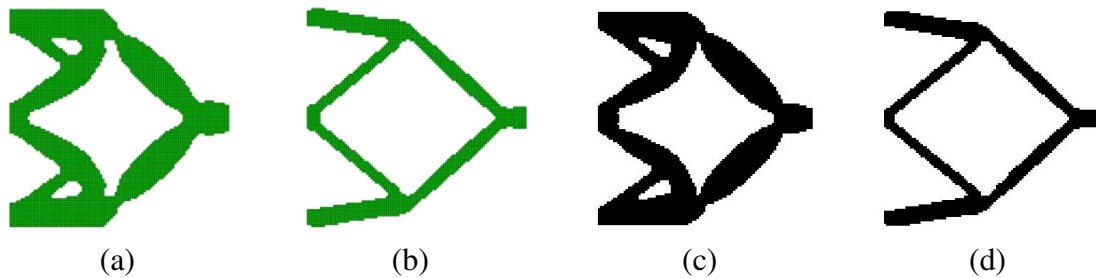


Figure 4.3: Optimal topologies comparison for the inverter case: (a) Topology found by Li *et al.* (2013) with  $V_f = 40\%$ ; (b) Topology found by Li *et al.* (2013) with  $V_f = 20\%$ ; (c) Topology found with BESO for  $V_f = 40\%$ ; (d) Topology found with BESO for  $V_f = 20\%$ .

4.2. Within this range, the topology suffers drastic changes as can be appreciated in Figure 4.2 for the 25<sup>th</sup> iteration. The jumps in the convergence function are related to these changes, and those variations can be associated to *GA* and *SE* individual evolution as shown in Figure 4.4. At the beginning, both objective functions increase almost at the same rate, but from iteration 20, the compliance *SE* changes this pattern, starting to decrease. The mechanical advantage *GA* continues

constantly increasing, while the compliance  $SE$  has an oscillatory behavior. This conduct continues as far as the 30<sup>th</sup> or 32<sup>th</sup> iteration, where the compliance  $SE$  begins its recovery, with a steady increase. Comparing Figure 4.2 and 4.4, it can be verified that the topology erratic behavior matches the sections where the Compliance  $SE$  also fluctuates, showing a strong influence of this variable on the overall objective function.

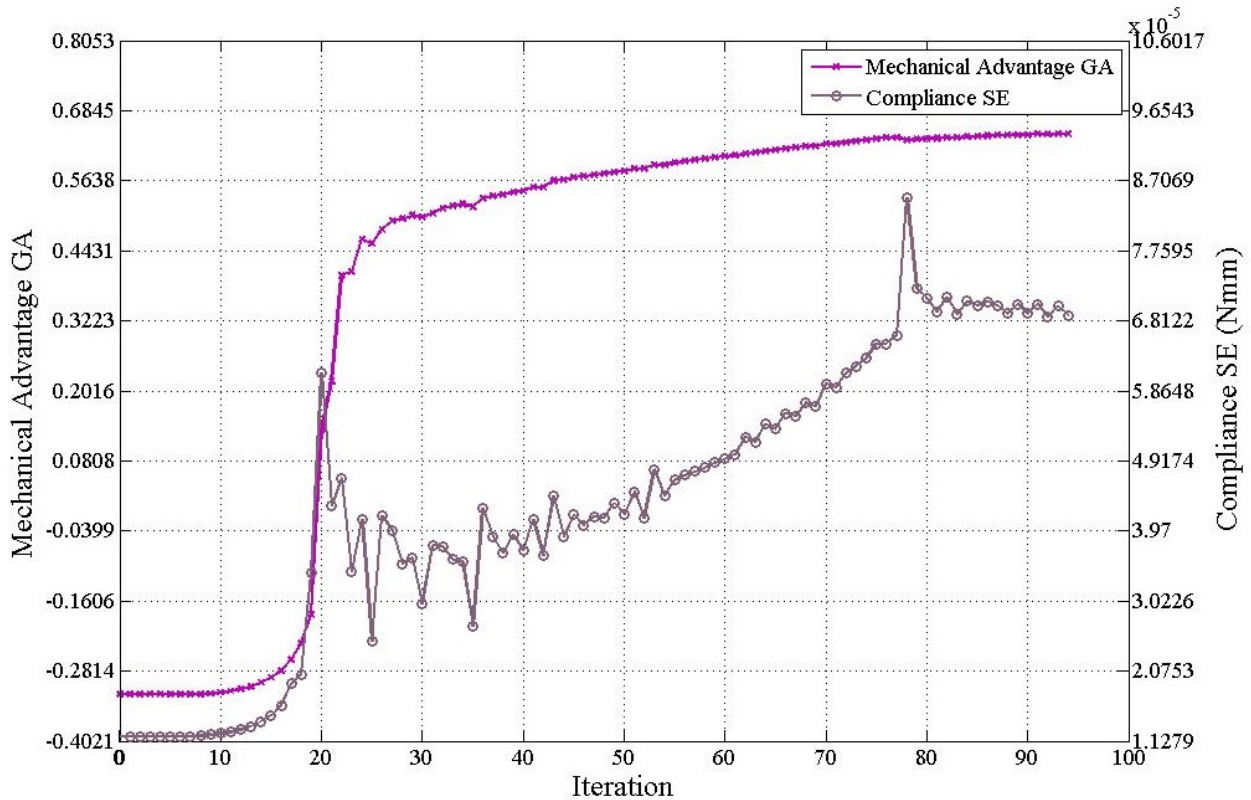


Figure 4.4: Evolution of the mechanical advantage  $GA$  and the Compliance  $SE$  for example 1 (inverter case).

Finally, Figure 4.5 illustrates the deformed shape of the inverter subject to the external force  $F_{in}$ , demonstrating that in fact, the topology obtained from the algorithm generates a displacement at the output port to the right, as expected. It is important to mention that the displacements were enlarged in a scale of  $1 \times 10^9$ , to make them visible in Figure 4.5 and to verify the output displacement direction.

The results for volume fractions  $V_f = 40\%$  and  $V_f = 20\%$  in Figure 4.5a and 4.5b show that the structures behave as expected, considering that the output displacement is maximized in both cases and matches the desired direction. Under this considerations, the algorithm implemented can be used for compliant mechanisms design given that the results match the imposed conditions and

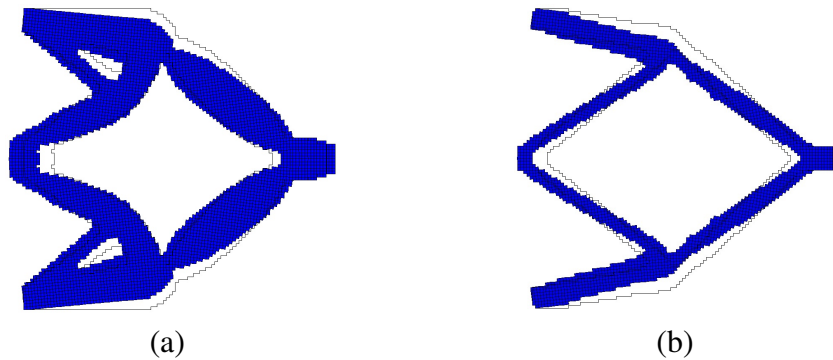


Figure 4.5: Optimal topologies for example 1 (inverter case): (a) Optimal topology deformed with a  $V^* = 40\%$ ; (b) Optimal topology deformed with a  $V^* = 20\%$ .

we can consider that the algorithm is validated for the case of an inverter compliant mechanism.

#### 4.1.2 Example 2: Gripper compliant mechanism

The second example involves the design of a gripper compliant mechanism. The design domain is shown in Figure 4.6a, as a  $200\text{ mm} \times 400\text{ mm}$  rectangle with a  $50\text{ mm} \times 100\text{ mm}$  notch which allows the workpiece to be gripped. For this case, the displacement at the input port is orthogonal to the output displacement  $u_{out}$ .

Considering that the problem is symmetrical in both geometry, material behavior, boundary and loading conditions, it is possible to simplify the problem and reduce computational time by taking into account only half of the design domain, as can be seen in Figure 4.6b. With this variation, the new design domain stays as a  $200\text{ mm} \times 200\text{ mm}$  rectangle with a  $50\text{ mm} \times 50\text{ mm}$  gap. The lower edge is vertically restricted and the problem goes from having multiple output displacements into only one.

The whole design domain is discretized with 7500 four node quadrilateral elements. A linear spring with stiffness constant  $k = 200\text{ N/m}$  is included to simulate the workpiece stiffness. The structure is supported at the top and bottom corners of the left edge as shown in Figure 4.6a. The input load  $F_{in} = 1\text{ N}$  is applied at the center of the left edge. The gripper objective is to produce efficiently a gripping force  $F_{out}$  and an output displacement  $u_{out}$  on the workpiece under the action of the input force  $F_{in}$ . The material properties are Young's modulus  $E = 200\text{ GPa}$  and Poisson's ratio  $\nu = 0.3$ . The BESO parameters for this example were the same as the ones used for the

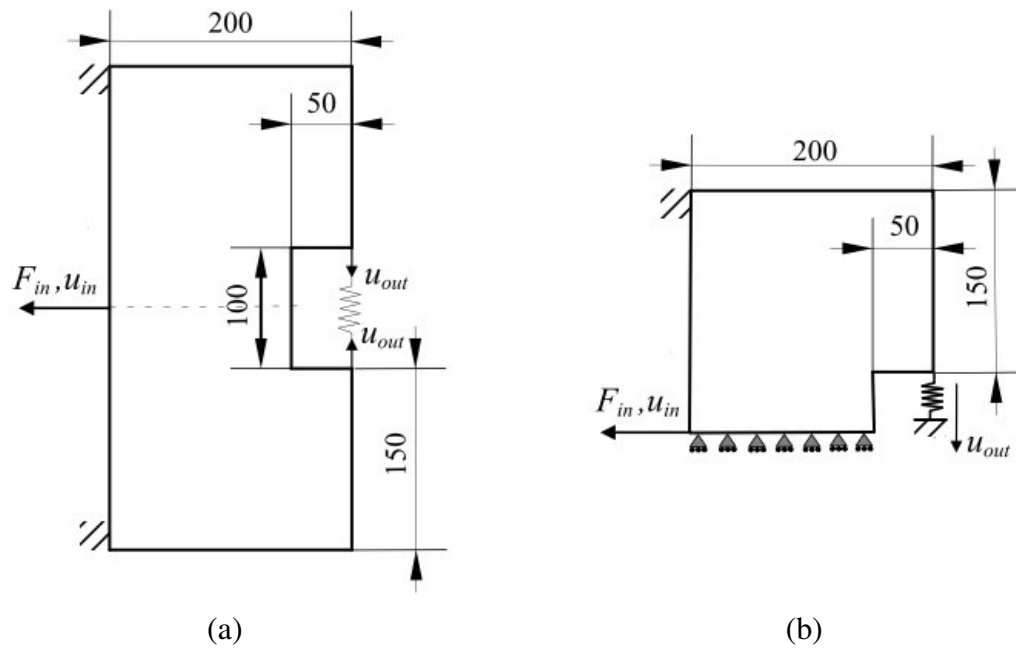


Figure 4.6: Design domain and boundary conditions for example 2 (gripper case): (a) Full design domain; (b) Symmetric part of the design domain.

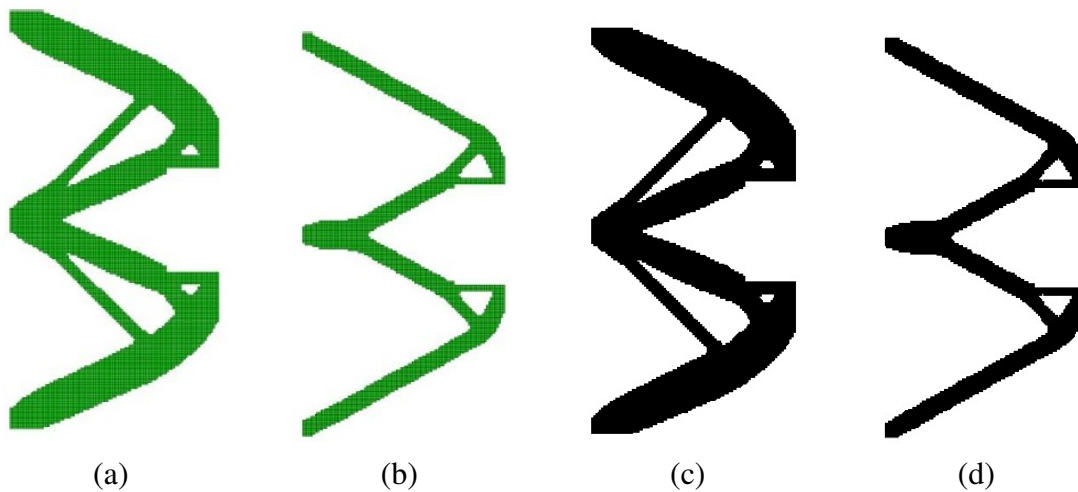


Figure 4.7: Optimal topologies comparison for example 2 (gripper case): (a) Topology found by Li *et al.* (2013) with  $V_f = 40\%$ ; (b) Topology found by Li *et al.* (2013) with  $V_f = 20\%$ ; (c) Topology found with BESO for  $V_f = 40\%$ ; (d) Topology found with BESO for  $V_f = 20\%$ .

inverter case in Table 4.1.

Once the parameters and initial conditions are all set, the BESO method is carried out until convergence for the objective function and the final volume is achieved. Figure 4.8 illustrates the

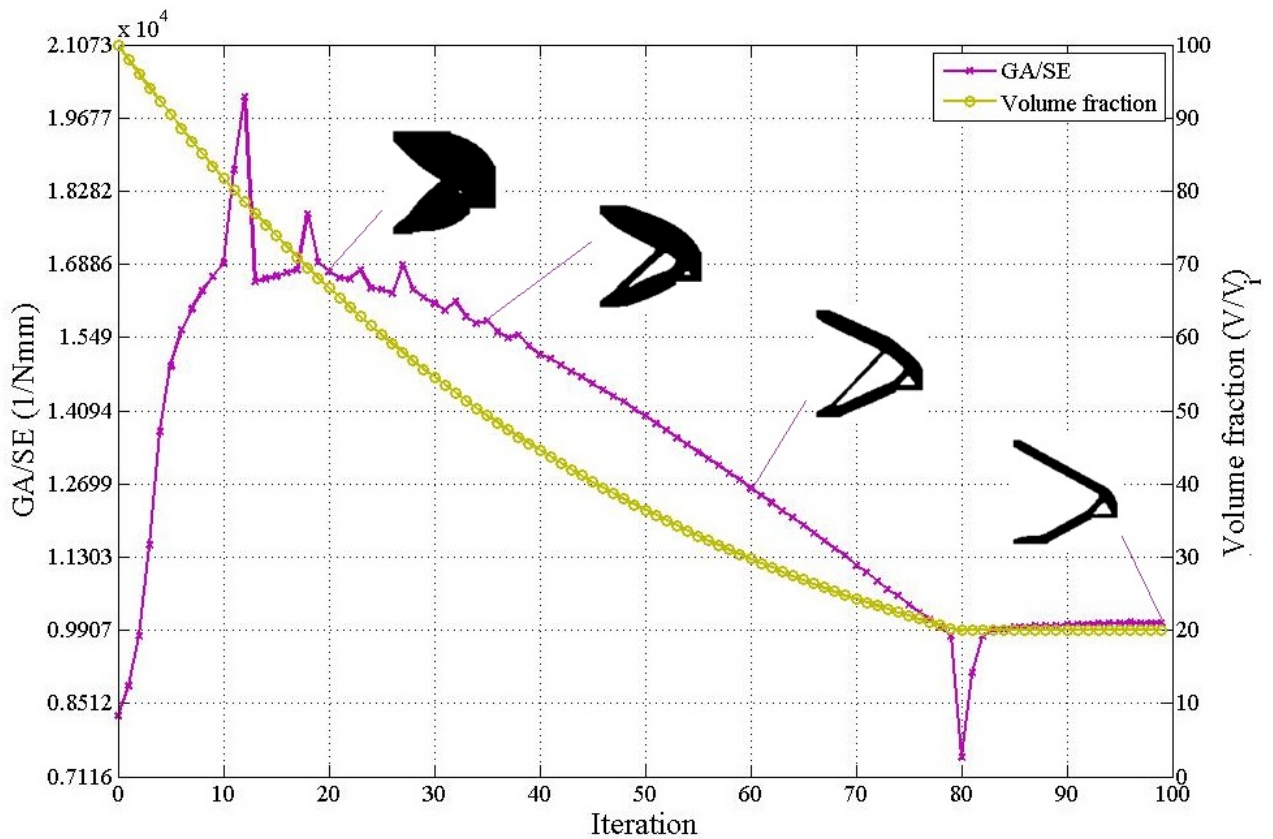


Figure 4.8: Evolution of the volume fraction and objective function for example 2 (gripper mechanism).

evolution of these two variables and how the topology changes throughout the iterations. In this case, the final volume is reached approximately after 80 iterations, and the algorithm continues until the objective function variation is lower than the tolerance value  $\tau$ .

A few jumps in the objective function curve were noticed in the gripper convergence, very similar to the fluctuations already found for the inverter mechanism showed in item 4.1.1. In the previous section, this tendency was explained by drastic changes in the topology and once again the behavior of the objective functions  $GA$  and  $SE$  acting separately was considered as part of the analysis. Figure 4.9 resumes the objective functions progression, exhibiting some leaps at iterations 12, 18, 23 and 80 approximately. These are the same iterations where the general objective functions vary, especially when the compliance  $SE$  decreases. Once more it becomes evident the strong influence of compliance  $SE$  over the optimization process to ensure convergence.

The topologies obtained for the gripper are also compared with the results found from Li

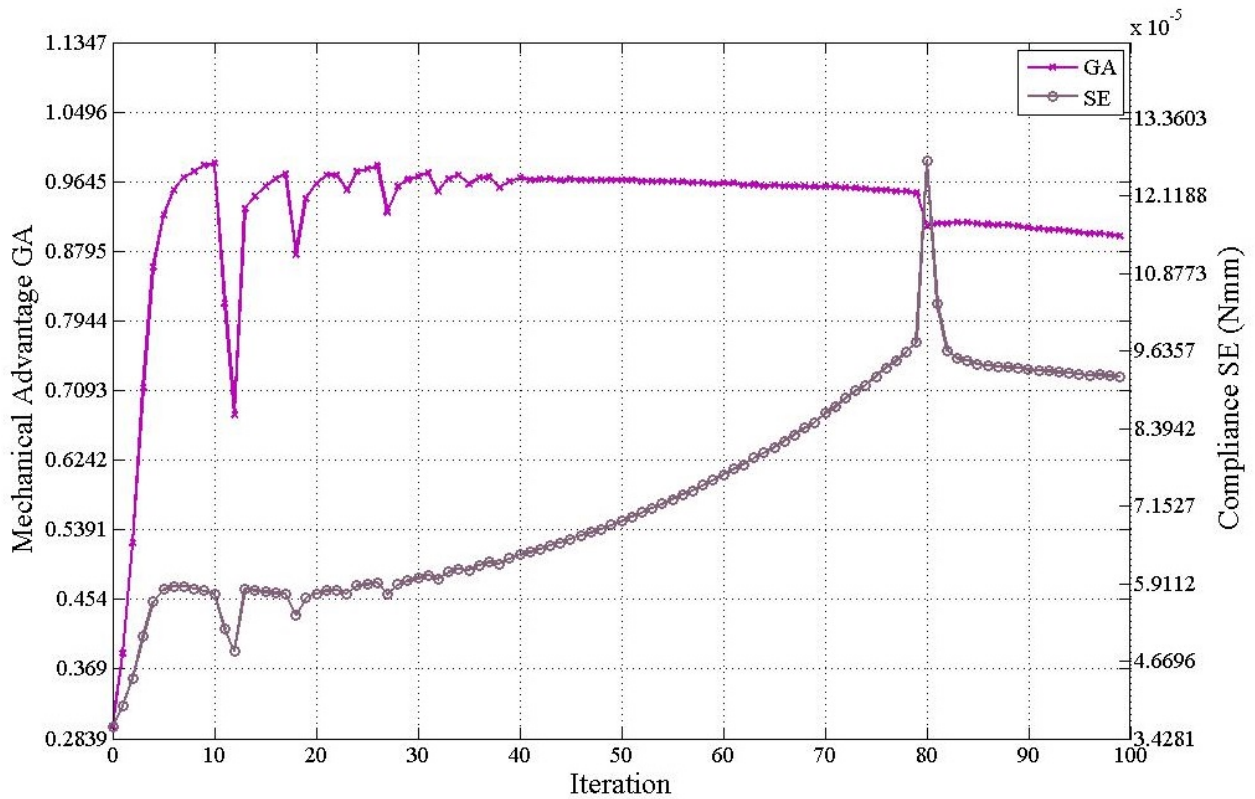


Figure 4.9: Evolution of the mechanical advantage  $GA$  and the Compliance  $SE$  for example 2 (gripper case).

(2014) as can be observed in Figure 4.7. Topologies with a  $V_f = 40\%$  and  $V_f = 20\%$  final volume ratio are almost identical to the results found in Li (2014) investigation, which verifies the algorithm validity. Finally, Figure 4.10 shows the mechanism behavior under the applied initial force  $F_{in}$ , proving that the output displacement is maximized in the desired direction.

The two previous examples corresponding to the inverter and gripper mechanisms were used to corroborate the method validity and the BESO parameters were maintained invariable to compare with Li *et al.* (2013) work who also uses the BESO method for compliant mechanisms design. The following examples are included to study some interesting subjects about the method, especially the influence of the workpiece resistance  $k_{out}$  over the final topologies.

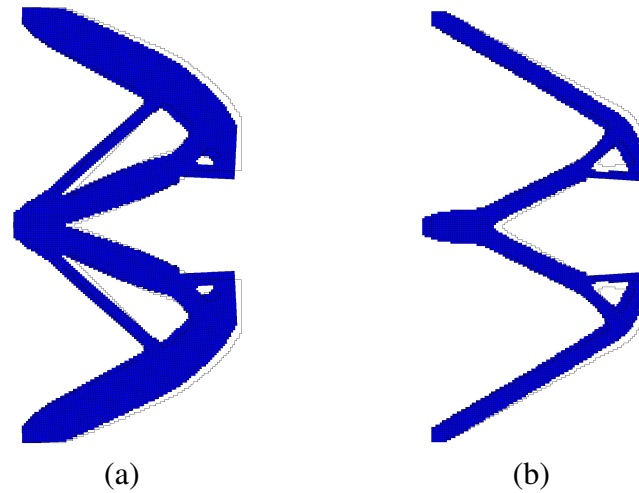


Figure 4.10: Optimal topologies for the gripper case: (a) Optimal topology deformed with a  $V^* = 40\%$ ; (b) Optimal topology deformed with a  $V^* = 20\%$ .

## 4.2 Case studies: Gripper, Inverter and Crunch mechanisms

The algorithm is also applied to three additional examples to have a greater view of the influence of the workpiece restriction  $k_{out}$  over the final topologies.

### 4.2.1 Example 3: Inverted Gripper Mechanism

The third example represents an interesting case of study because has similar boundary conditions to the gripper mechanism studied in example 2 but with an initial force  $F_{in}$  actuating in the opposite direction. This means that while the gripper mechanism in example 2 closes under the action of an input force to the left, the current example seeks this same behavior but with an initial force to the right. The new design domain can be seen in Figure 4.11, set as a  $120 \mu\text{m} \times 120 \mu\text{m}$  square with a  $30 \mu\text{m} \times 24 \mu\text{m}$  gap which allows the workpiece to be gripped. The design domain is meshed with 4-node quadrilateral elements with uniform sizes  $1 \mu\text{m} \times 1 \mu\text{m}$ . An input force  $F_{in} = 1\text{N}$  to the right is applied at the center point of the left edge. The material properties are assumed to be Young's modulus  $E = 1\text{GPa}$  and Poisson ratio  $\nu = 0.3$ . An artificial spring with stiffness  $k_{out} = 1 \times 10^3 \text{N/m}$  is attached at the output port to simulate the workpiece resistance. The vertical displacement  $u_{out}$  at the output port will be maximized to grip the workpiece, as was already made by the gripper case.

Table 4.2: BESO parameters for the examples 1 and 2, the inverter and gripper design

Variable	Description	Value
$V$	Initial volume	100%
$V_f$	Final volume fraction	30%
$ER$	Evolutionary volume ratio	1%
$AR_{\max}$	Maximum addition ratio	2%
$r_{\min}$	Filter ratio	$3 \mu\text{m}$
$\tau$	Stopping criteria tolerance	$1 \times 10^{-3}$
$N$	Stopping criteria parameter	5
$k_{out}$	Workpiece resistance	$1 \times 10^3 \text{ N/m}$

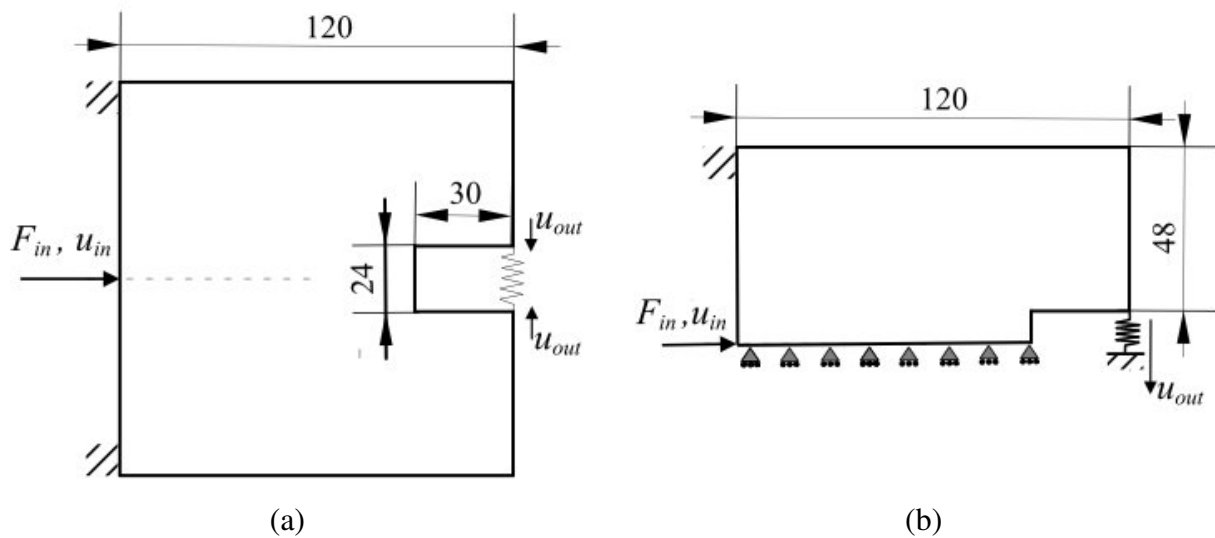


Figure 4.11: Design domain and boundary conditions for example 3 (Inverse gripper): (a) Full design domain; (b) Simplified design domain.

The BESO parameters used in this example are the evolution rate  $ER = 1\%$ , filter radius  $r_{\min} = 3\mu\text{m}$ , maximum addition ratio  $2\%$ . The objective volume fraction is set to be  $30\%$  of the full design domain starting from an initial volume of  $V = 100\%$ . Once again only half of the design domain (Figure 4.11b) will be considered to simplify the problem, save computational time and work only with one output displacement.

The evolution of the volume fraction and the objective function for the example 3 corresponding to the inverse gripper can be seen in Figure 4.12, showing a similar behavior to the previous examples, with few jumps due to the abrupt changes in the topology. These variations are more significant in the first iterations, given that the algorithm is finding the evolution path that could meet the stiffness and flexibility requirements at the same time. This range of iterations were the

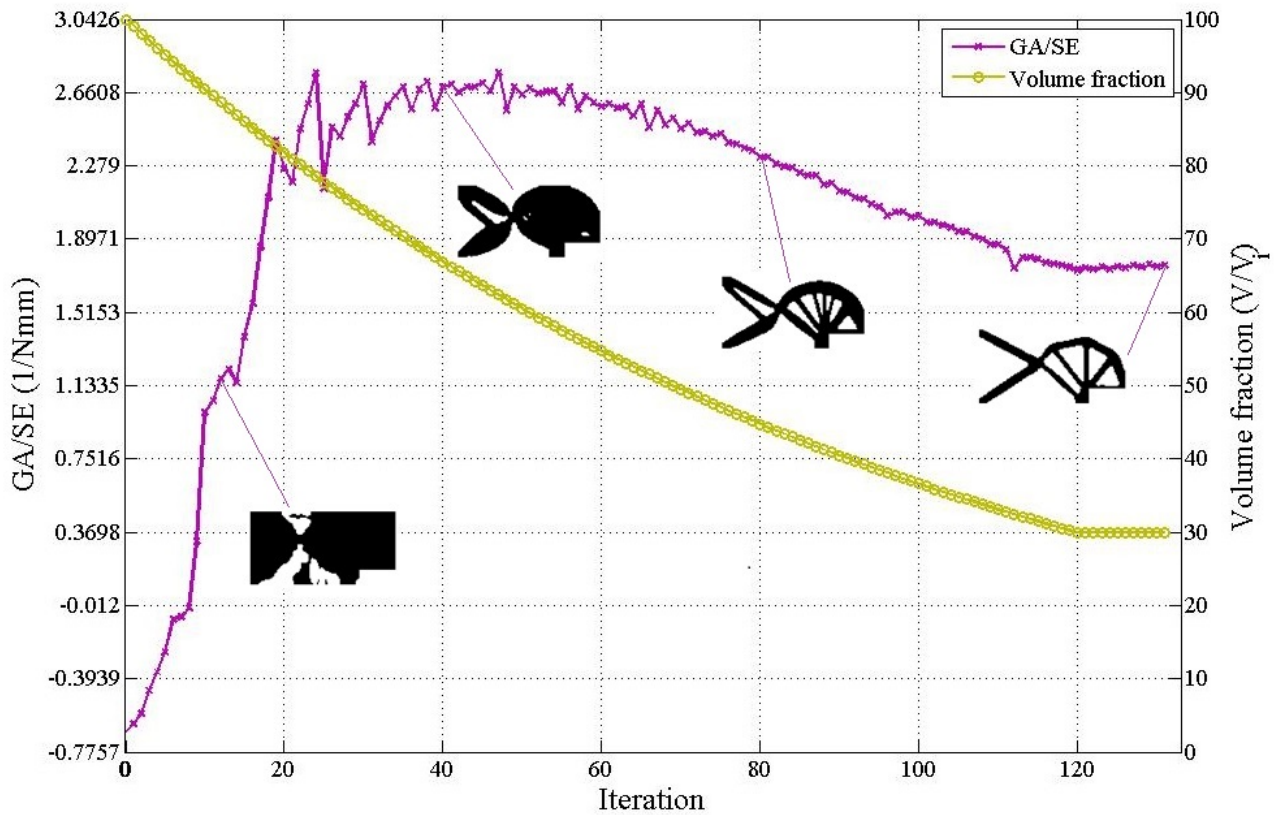


Figure 4.12: Evolution of the volume fraction and objective function for example 3.

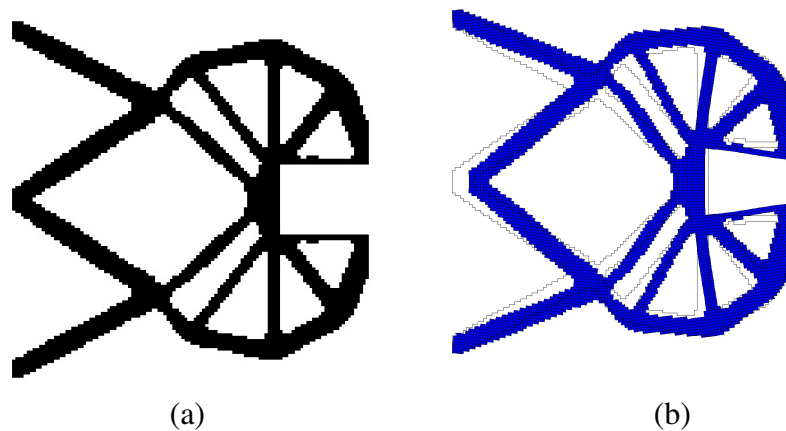


Figure 4.13: Optimal topologies for example 3 (gripper case): (a) Optimal topology deformed with a  $V^* = 40\%$ ; (b) Optimal topology deformed with a  $V^* = 20\%$ .

structures suffers radical changes will depend on the particular optimization problem and boundary conditions. The topology evolution can also be seen in Figure 4.12 for the iterations 15th, 40th, 80th until achieves a final topology at the iteration 132.

Figure 4.13a and 4.13b presented the final topology obtained for the inverse gripper and the deformed shape under the initial force  $F_{in}$ . It can be observed that the output displacement is, in fact, maximized in the desired direction, under the input force. It's interesting noting that only by changing the direction of the input force, the final topology obtained changes radically, given that the displacement field affects directly the objective function values and correspondingly the sensitivity numbers. The final topology obtained is hinge free with internal bars uniformly distributed and similar sizes, however, the intermediate solutions for example 3 can present internal hinges as can be observed in Figure 4.12 for the 40th iteration.

#### 4.2.2 Example 4: Crunching mechanism

The objective of this example is to show one application considering multiple inputs forces with a single orthogonal output displacement.

Table 4.3: BESO parameters for the example 3 corresponding to the crunch mechanism

Variable	Description	Value
$V$	Initial volume	100%
$V_f$	Final volume fraction	30%
$ER$	Evolutionary volume ratio	2%
$AR_{max}$	Maximum addition ratio	2%
$r_{min}$	Filter ratio	12 mm
$\tau$	Stopping criteria tolerance	$1 \times 10^{-3}$
$N$	Stopping criteria parameter	5
$k_{out}$	Workpiece resistance	$1 \times 10^7$ N/m

The design domain for example 4 corresponding to a crunching mechanism can be seen in Figure 4.14, a quadratic region of 200 mm  $\times$  200 mm, supported at the upper and lower right corners. The objective, once again, is to maximize the displacement at the output port by distributing material in the design domain area. In this case, two simultaneous forces are considered in the design domain.

The mechanism material has Young's modulus 200 GPa and Poisson's ratio  $\nu = 0.3$ . The allowable amount of material is 30% of the full design domain, using a mesh of 200  $\times$  200 quadrilateral elements. Two input forces  $F_{in}$  are applied at the upper and lower corners of the right side of the design domain and the objective is to generate an output displacement at the center of the left edge also to the left. The BESO parameters to this case are resumed in Figure 4.16.

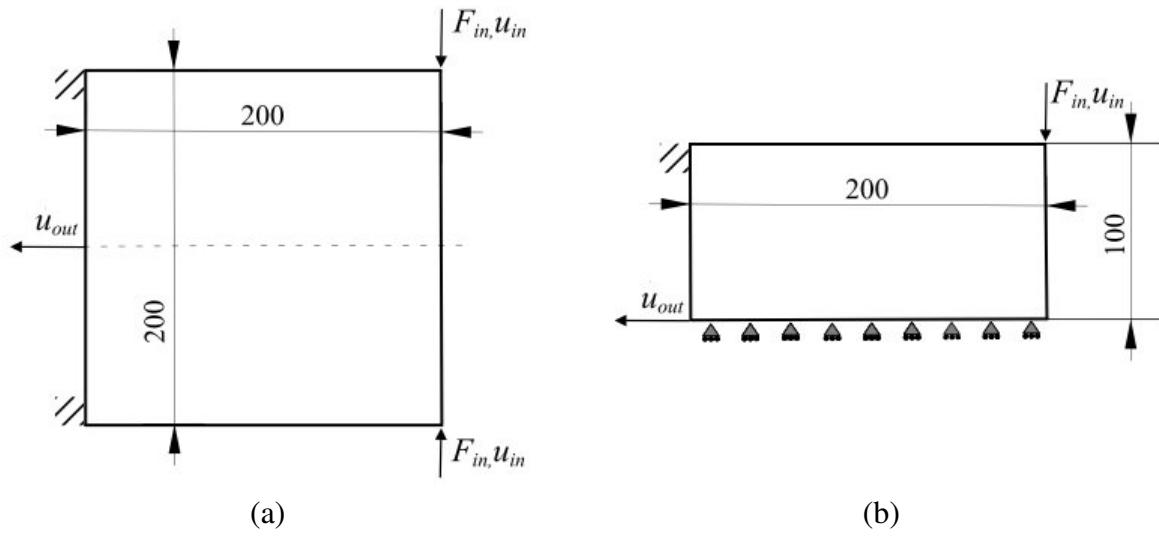


Figure 4.14: Design domain and boundary conditions for example 4 (crunching mechanism): (a) Full design domain; (b) Simplified design domain.

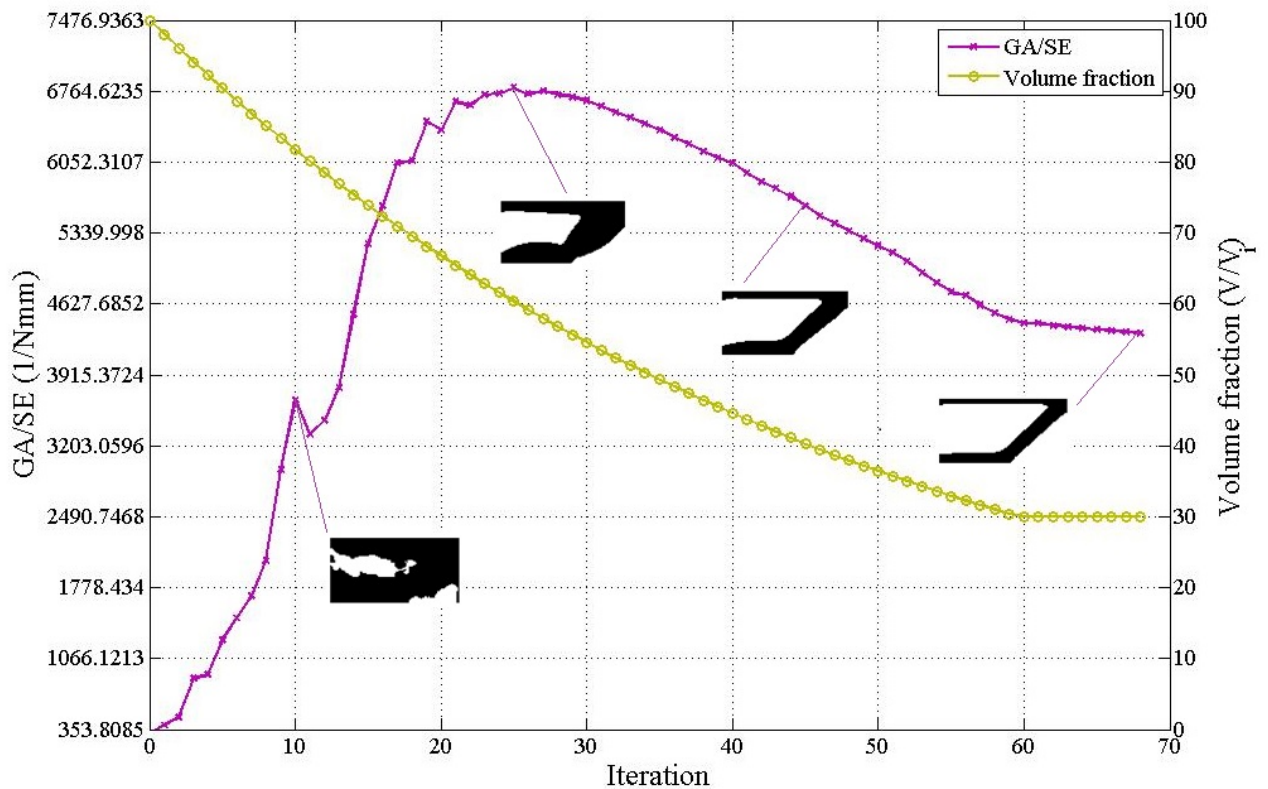


Figure 4.15: Evolution of the volume fraction and objective function for example 4 (crunching mechanism).

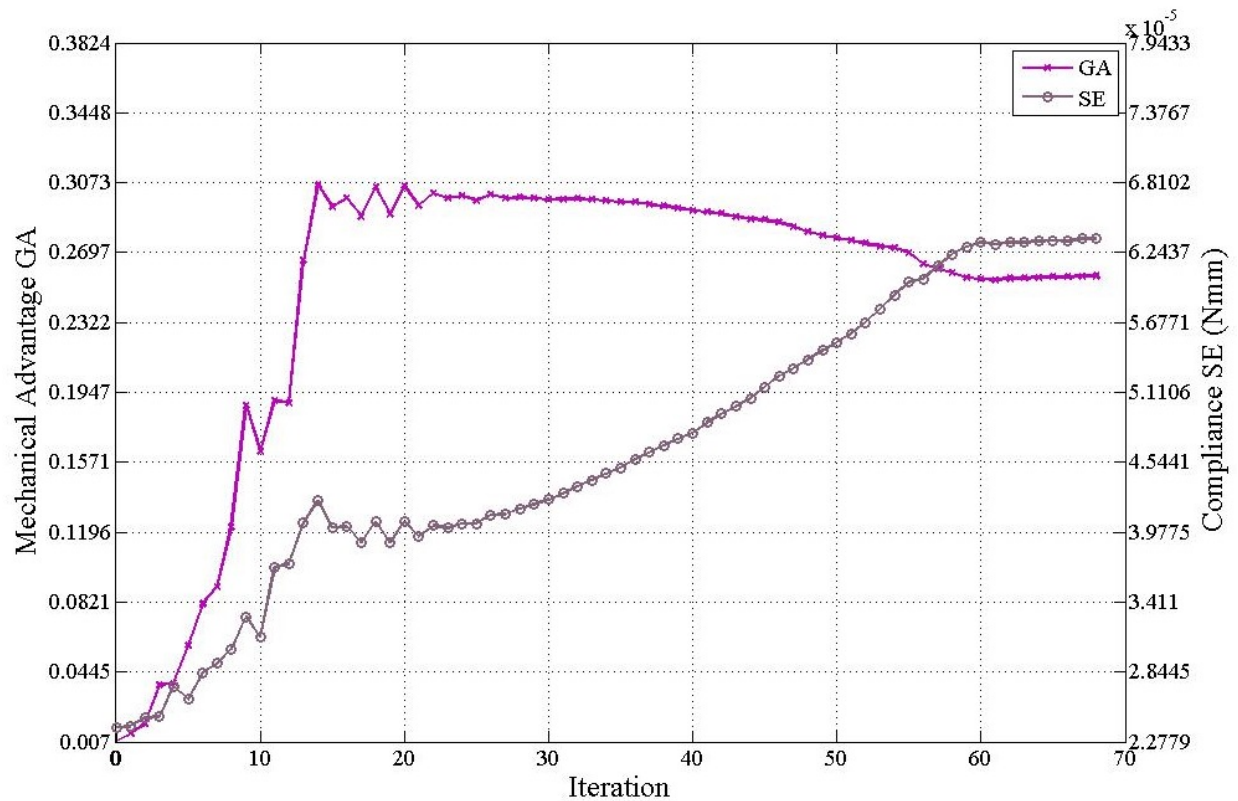


Figure 4.16: Evolution of the mechanical advantage  $GA$  and the Compliance  $SE$  for example 4 (crunch case).

The historical evolution of the objective function can be seen in Figure 4.15, with a similar behavior to the examples presented in previous sections. The topology evolves throughout the iterations until it reaches the final topology at iteration 69. The volume convergence is reached at the 60<sup>th</sup> iteration, value after which the topology keeps readjusting to meet the stopping criteria. In this case, the drastic changes observed in the other examples are only present for the first iterations, rapidly reaching the desired topology.

The evolution of functions  $GA$  and  $SE$  acting separately for example 4 can be seen in Figure 4.16. In this case the few jumps observed for the objective function convergence in Figure 4.15 between iterations 10 and 25 match the variations present in both objective functions  $GA$  and  $SE$  (Figure 4.16), especially for iterations 10 and 15. Both functions follow a steady evolution after the 21<sup>th</sup> iteration reflected in a smooth behavior for the objective function  $GA/SE$ . The high value of  $k_{out}$  assumed for this case, could also explain this soft evolution given that the same behavior was observed for the other numerical examples a subject that will be addressed in Section 4.3.

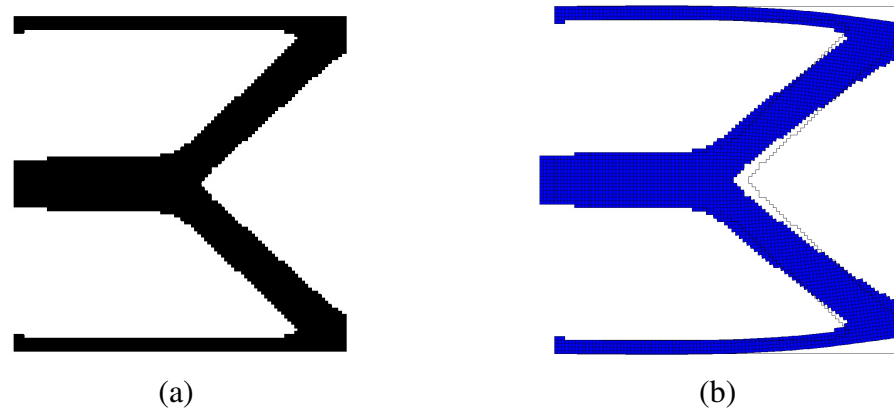


Figure 4.17: Optimal topologies for example 4 (crunching mechanism): (a) Optimal topology deformed with a  $V^* = 40\%$ ; (b) Optimal topology deformed with a  $V^* = 20\%$ .

Figure 4.17a and Figure 4.17b shows the final topology and its deformation under the input force  $F_{in}$  respectively. From the dislocated topology can be seen that the output displacement is indeed maximized in the desired direction. This example was also addressed by Ansola *et al.* (2007) and Sigmund (1997), showing very similar results to the ones found in this work by using the BESO method. The final topology obtained is smoothed and "internal hinge free" showing the capacity of the present algorithm to solve cases of mechanisms with multiples input forces and a single output displacement.

### 4.2.3 Example 5: Inverter with two output ports

Finally, the last example is an inverter with a single input and multiple output ports, also an interesting case of study given that there is not an obvious structure that could generate the desired displacements under the design requirements. The general boundary conditions to the overall problem and the simplified design domain can be seen in Figure 4.18a and 4.18b respectively.

For this case, the design domain is defined as a rectangle with  $100 \text{ mm} \times 60 \text{ mm}$  size and meshed with  $100 \times 60$  4-node quadrilateral elements. It's supported at the top and the bottom corners of the left edge. An input force  $F_{in} = 1\text{N}$  is applied at the center of the left edge in the horizontal direction to the right. Two output ports placed at the top and the bottom corners of the left edge are expected to produce horizontal displacements  $u_{out}$ . The workpiece stiffness for this example is  $k_{out} = 1 \times 10^7$  and represents the workpiece resistance as an artificial spring attached to each output port. The volume constraint is 25% of the design domain during the whole evolutionary

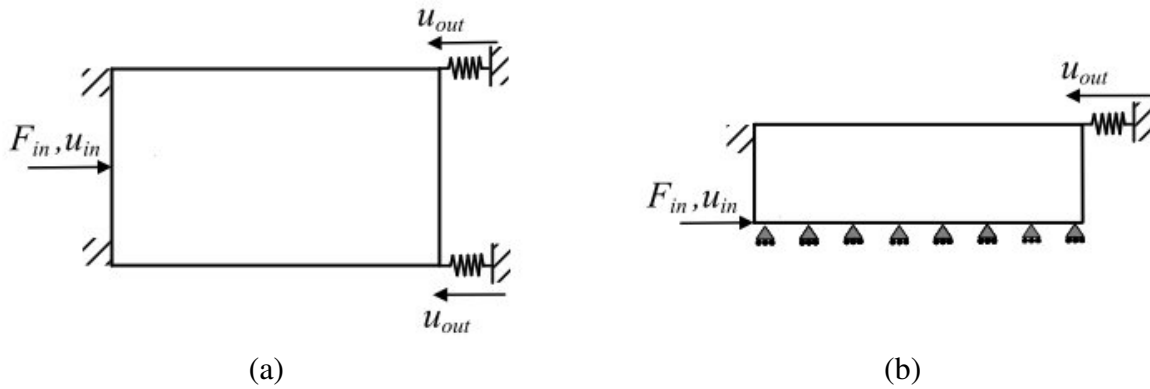


Figure 4.18: Design domain and boundary conditions for example 5: (a) Full design domain; (b) Simplified design domain.

Table 4.4: BESO parameters for the example 3 corresponding to the crunch mechanism

Variable	Description	Value
$V$	Initial volume	100%
$V_f$	Final volume fraction	25%
$ER$	Evolutionary volume ratio	2%
$AR_{max}$	Maximum addition ratio	2%
$r_{min}$	Filter ratio	3 mm
$\tau$	Stopping criteria tolerance	$1 \times 10^{-3}$
$N$	Stopping criteria parameter	5
$k_{out}$	Workpiece resistance	$1 \times 10^7$ N/m

process. The material properties are Young's modulus  $E = 100$  GPa and Poisson's ratio  $\nu = 0.3$ . The BESO parameters are the filter radius  $r_{min} = 3$  mm, penalty exponent  $p = 3$  and  $x_{min} = 0.001$ . The Evolutionary volume ratio will be  $ER = 2\%$  and the volume addition ratio  $AR_{max} = 2\%$ , the precision on the stop criterion will be  $\tau = 1 \times 10^{-3}$ .

The evolution of the volume fraction and objective function for example 5 can be observed in Figure 4.19. The stopping criteria is reached after 75 iterations and the volume fraction achieved at iteration 69. The objective function evolution is also smoother than the curves obtained for examples 1, 2 and 3 and the workpiece resistance was set at  $k_{out} = 1 \times 10^7$  N/m. This case shows a similar behavior than example 4, where high values of the workpiece restriction  $k_{out}$  turn out to improve the objective function convergence and avoid the drastic changes in the topology between iterations.

Figure 4.20 shows the final topology and its behavior under the action of an initial force

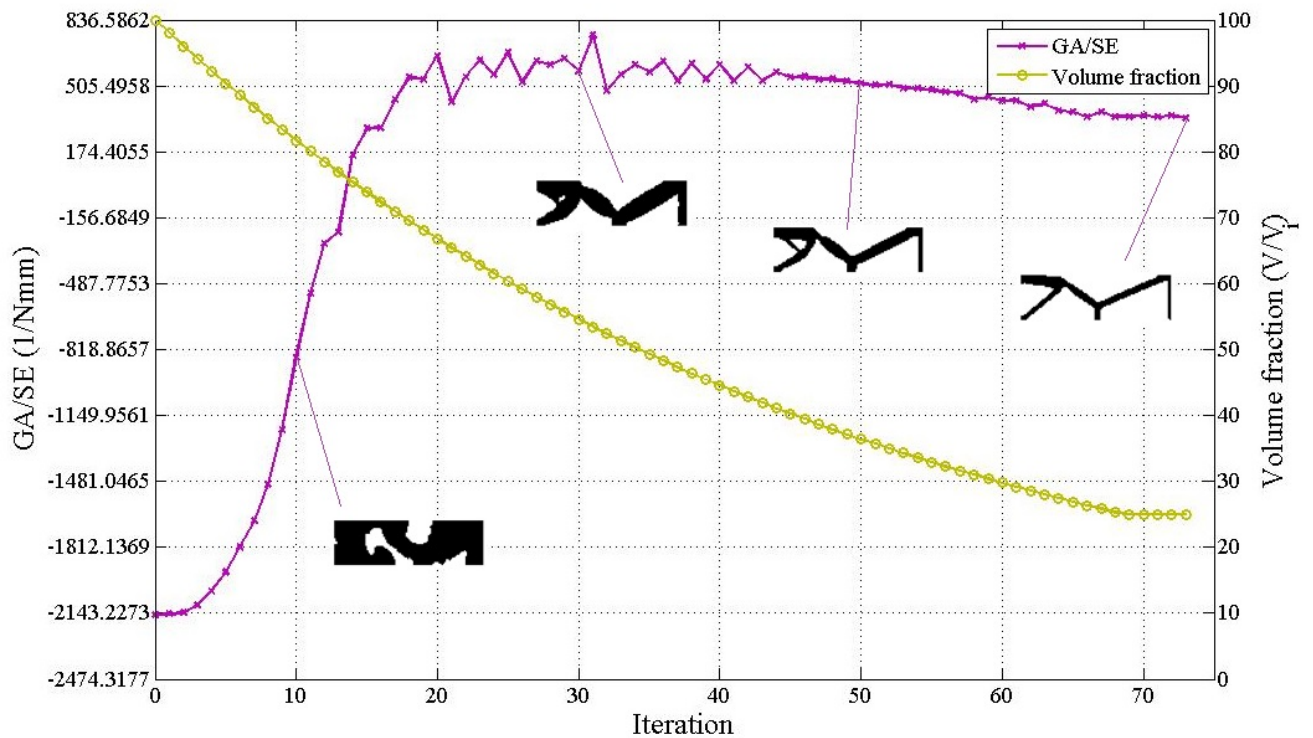


Figure 4.19: Evolution of the volume fraction and objective function for example 5.

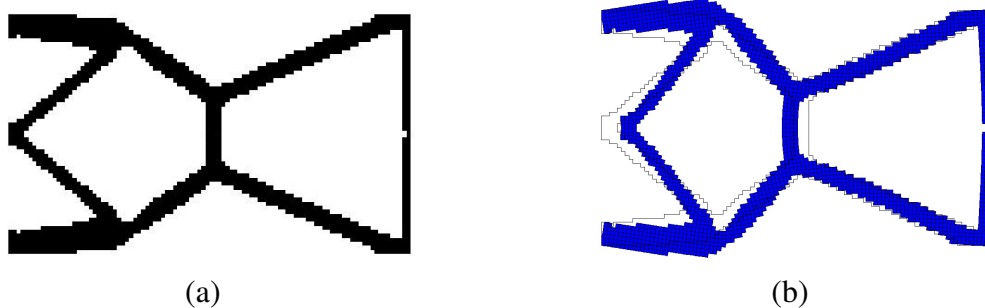


Figure 4.20: Optimal topologies for example 5: (a) Optimal topology deformed with a  $V^* = 40\%$ ; (b) Optimal topology deformed with a  $V^* = 20\%$ .

$F_{in}$  This particular example involves an interesting boundary condition where the final topology obtained is not expected and could not be easily achieved by trial and error methods. However, the final topology accomplishes to maximize the output displacement in the desired direction as can be seen in Figure 4.20b. Under the applied force at the center of the left edge, the structure moves to the right at the output ports, as expected. This design case is also an inverter mechanism which minds that the input force generates an output displacement in the opposite direction as desired.

The results were also very similar to the results found by Li (2014) using a modified version of the BESO method with intermediary densities.

### 4.3 Influence of the Workpiece constraint

Besides the common BESO parameters involved in the evolutionary topology optimization such as initial guess design domain, mesh density,  $ER$ ,  $AR_{max}$  or  $r_{min}$ , there is a new parameter included in the formulation problem for compliant mechanism design: the workpiece constraint  $k_{out}$ . This parameter allows to incorporate a restriction at the output port to simulate the workpiece resistance and its estimation depends on the particular application. This section analyzes the influence of the workpiece stiffness on the obtained results.

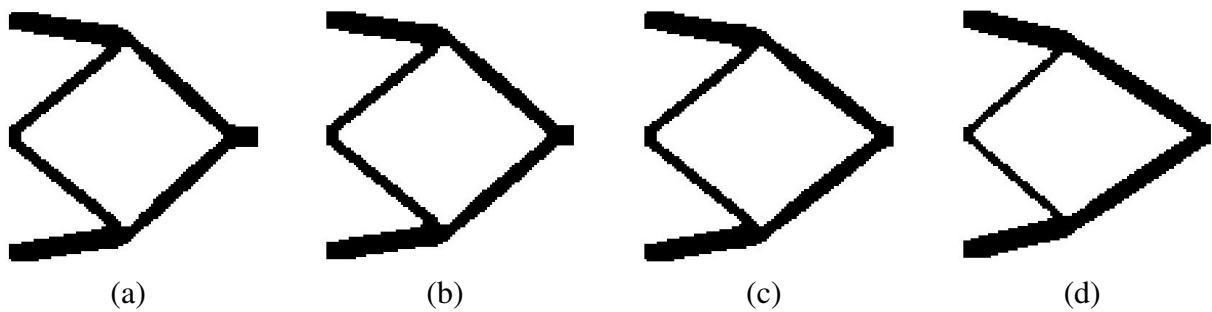


Figure 4.21: Optimal topologies for example 1 (inverter case) with different constant stiffness: (a)  $k_{out} = 0$  N/m; (b)  $k_{out} = 2 \times 10^6$  N/m; (c)  $k_{out} = 2 \times 10^7$  N/m; (d)  $k_{out} = 4.9 \times 10^8$  N/m.

The analysis starts with example 1 or the inverter case, where the algorithm was tested by varying  $k_{out}$  from 0 to the maximum possible value. This upper limit was reached at  $k_{out} = 4.9 \times 10^8$  N/m, beyond this point the structure no longer supports the loading conditions and delivers a disconnected topology. Figure 4.21 gather the topologies for  $k_{out}$  values that had important variations between  $k_{out}$  extreme values.

From the different topologies found in Figure 4.21, there are some important remarks related to the  $k_{out}$  variation. First, small alterations in the topology are only noticed after  $k_{out} = 2 \times 10^6$  N/m, which can be appreciated by comparing Figure 4.21a and 4.21b, showing that the topology for  $k_{out} = 20$  N/mm is almost identical to the topology without any workpiece constraint. Also, the variations occur for high values of  $k_{out}$  and close to the Young modulus magnitude level. Figures 4.21c and 4.21d are also similar, showing a slight reinforcement at the output port with the increase of  $k_{out}$ .

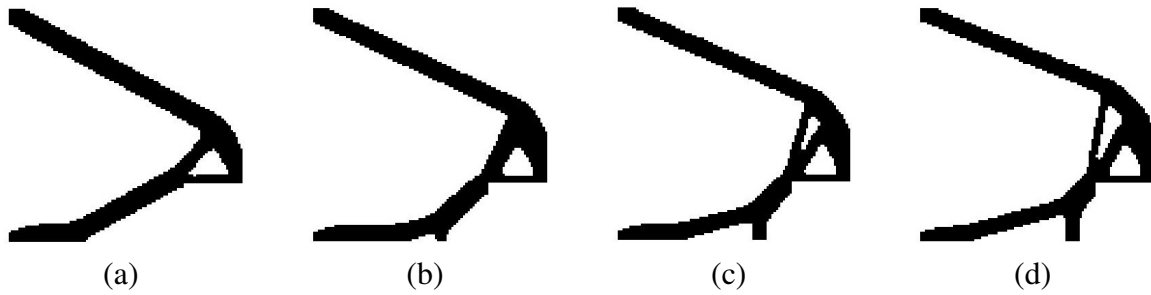


Figure 4.22: Optimal topologies for example 2 (gripper case) with different constant stiffness: (a)  $k_{out} = 0$  N/m; (b)  $k_{out} = 7 \times 10^6$  N/m; (c)  $k_{out} = 2 \times 10^7$  N/m; (d)  $k_{out} = 2 \times 10^{10}$  N/m.

After examining the different topologies in Figure 4.21, it could be concluded for this particular case that  $k_{out}$  does not radically affect the final topology and the variations are observed only for large increases in  $k_{out}$ . The biggest change is observed at the output port, showing a representative reinforcement to obtain a stiffer structure that tends to behave as a truss when the  $k_{out}$  value continue to rise.

For the inverter case all the structures obtained fulfilled the stiffness requirement even when the workpiece resistance was set as  $k_{out} = 0$ . This could be explained by including the compliance  $SE$  in the optimization problem, making the structure already strong enough to support any external load. This way  $k_{out}$  is not the only parameter that considers the workpiece resistance, preventing its direct influence over the final topology. Without the  $SE$  condition, the variable  $k_{out}$  will be necessarily different from zero to account for the workpiece resistance and to ensure a well-conditioned problem.

The same analysis is now made for the gripper mechanism by changing the  $k_{out}$  values to analyze the topology response. However, in this case, an increase in  $k_{out}$  does produce important changes in the final topology. The first remarkable alteration take place at  $k_{out} = 7 \times 10^6$  N/m as can be seen in Figure 4.22b; before this value, the topology variations are perceptible, but still small, as observed in Figure 4.22a and 4.22b. On the other hand, beyond this value the topology suffers the most severe alteration for  $k_{out} = 2 \times 10^7$  N/m (see Figure 4.22c), but does not vary drastically if  $k_{out}$  continue increasing as in Figure 4.22d.

Once again the  $k_{out}$  value could be equal to zero, given the restriction impose by including  $SE$  into the optimization problem. For example 2, the workpiece restriction does influence the final topology unlike example 1 where those changes were not representative, indicating that such influence may or may not be important depending on the boundary and loading conditions.

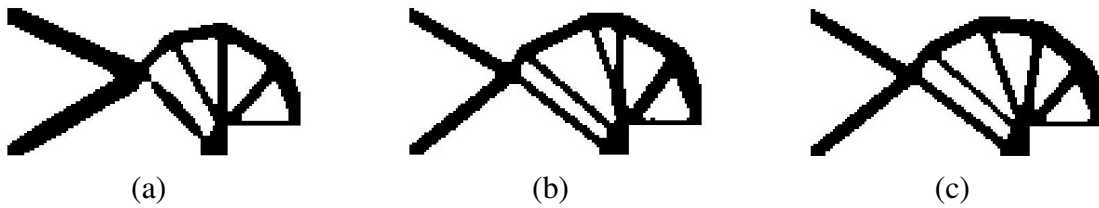


Figure 4.23: Optimal topologies for example 3 (inverse gripper case) with different constant stiffness: (a)  $k_{out} = 0$  N/m; (b)  $k_{out} = 5 \times 10^4$  N/m; (c)  $k_{out} = 1 \times 10^8$  N/m.

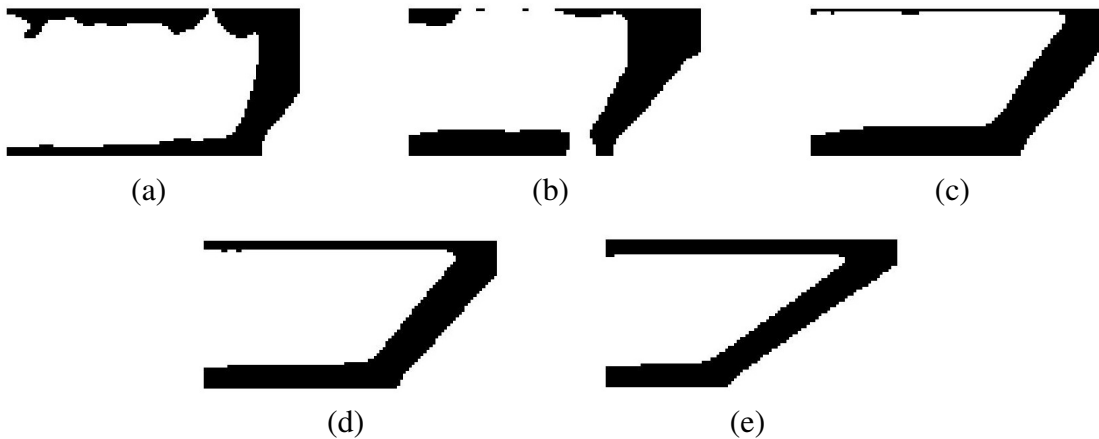


Figure 4.24: Optimal topologies for example 4 (crunching mechanism) with different constant stiffness: (a)  $k_{out} = 0$  N/m; (b)  $k_{out} = 1 \times 10^5$  N/m; (c)  $k_{out} = 1.5 \times 10^5$  N/m; (d)  $2 \times 10^6$  N/m; (e)  $k_{out} = 2 \times 10^{10}$  N/m.

The boundary conditions seen in Figure 4.11 for example 3 was also tested with different values of  $k_{out}$ . This topologies can be seen in Figures 4.23a, 4.23b and 4.23c with  $k_{out} = 0$  N/m,  $k_{out} = 5 \times 10^4$  N/m and  $k_{out} = 1 \times 10^8$  N/m respectively, showing some small variations, but essentially presenting the same topology. However, it is important to mention that the topology obtained for the lowest value corresponding to  $k_{out} = 0$  N/m shows one node connections problems which imply that for this particular example it is not convenient to set this variable to be zero, given that could lead to structural problems. In this case, the inclusion of the objective functions  $SE$  is not enough to ensure the stiffness condition for any  $k_{out}$  value and avoid the problem relative of flexible hinge formation. This will also depend on the material elastic modulus  $E$ , to lower values, the variable  $k_{out}$  will have an increasing influence.

The last examples 4 and 5 showed a noticeable behavior as can be seen in Figures 4.24 and 4.25, where the influence of the variable  $k_{out}$  is also representative. In the case of the cruncher mechanism in example 4, the results for values below to  $k_{out} = 1.5 \times 10^5$  N/m threw out dis-

connected topologies (see Figure 4.24), showing once again that depending on the optimization problem this variable could or not have an important influence. After this value, the topology suffers small changes, simply to readjust to the increase in the workpiece restriction, represented by the increment in  $k_{out}$ .

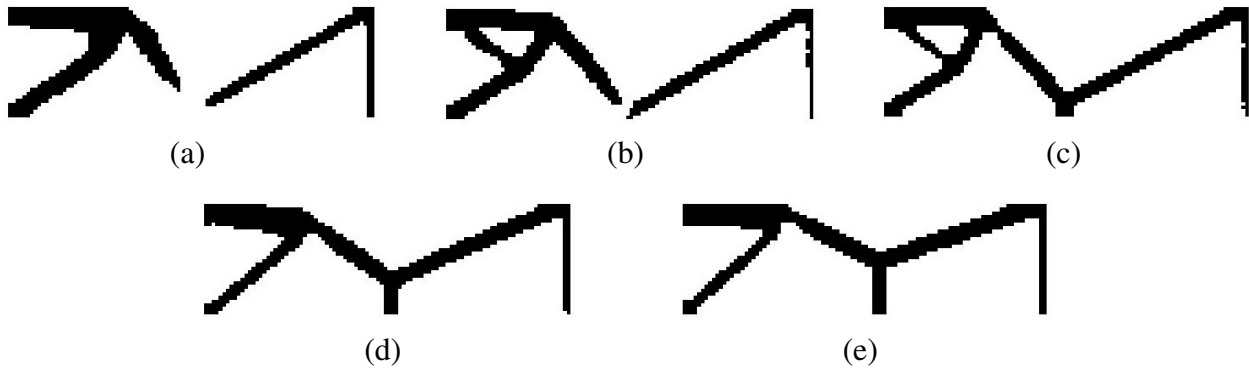
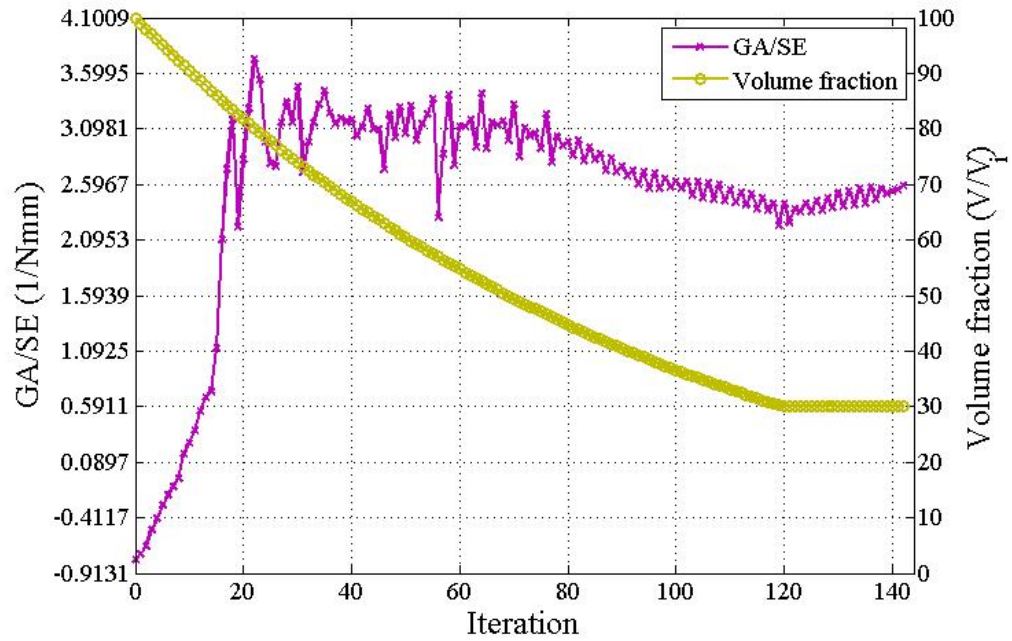


Figure 4.25: Optimal topologies for example 5 (inverter with two output ports) with different constant stiffness: (a)  $k_{out} = 0$ ; (b)  $k_{out} = 100$ ; (c)  $k_{out} = 150$ ; (d)  $2 \times 10^3$ ; (e)  $k_{out} = 2 \times 10^7$ .

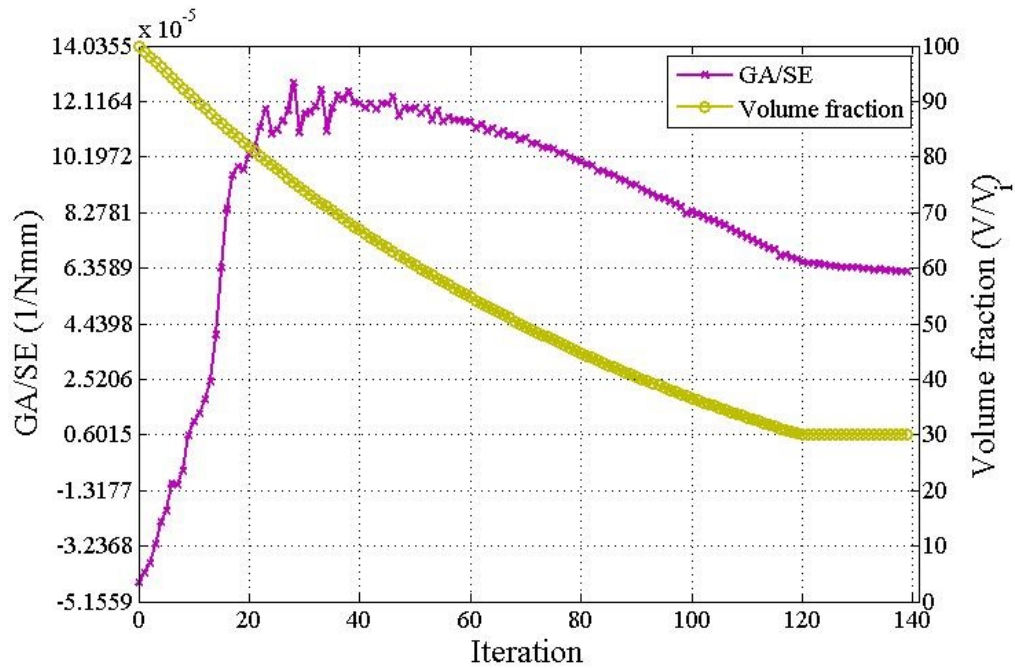
Figure 4.25 shows the final topologies obtained by varying the workpiece restriction  $k_{out}$  for example 5 (inverter with two output ports). In this case, if  $k_{out}$  is below  $1.5 \times 10^5$  N/mm the final topologies turn out disconnected (see Figure 4.25c) which implies that the influence of  $k_{out}$  could be really significant depending on the optimization problem under consideration and in some cases a necessary condition to ensure the algorithm convergence.

Is important to mention that the increment of the workpiece restriction  $k_{out}$  also improves the objective function convergence, a phenomenon observed for the 5 examples under consideration. Figure 4.26 shows this behavior using example 3, one of the cases that showed a major improvement in the objective function evolution. The case with  $k_{out} = 0$  (Figure 4.26a) shows abrupt changes in the objective function almost for the entire optimization process. This could be explained because this particular case showed some difficulties to equilibrate flexibility and stiffness in the objective function. The objective function evolution for  $k_{out} = 1 \times 10^5$  in Figure 4.26b showed a different behavior with a more smooth evolution and with a few small jumps between iterations. This shows once again the dominance of the objective function  $SE$ , given that when the requirements are set to obtain a stiffer structure, this characteristic predominates over the flexibility condition.

Finally, it can be concluded that increasing the  $k_{out}$  value could lead to significant changes in the final topology depending on the optimization problem and in the loading and boundary conditions. It also affects the structure stress distribution and is recommendable not to increase its



(a)



(b)

Figure 4.26: Gripper stress distribution for the optimal topologies for  $k_{out}$  extreme values: (a)  $k_{out} = 0$ ; (b)  $k_{out} = 2 \times 10^7$ .

value close to the maximum, not only to avoid exceeding the material elastic limit but also because the resultant structure will be too stiff to fulfill the flexibility requirements.

#### 4.4 Mesh-independence study

The topology optimization results should not depend on the mesh discretization. To examine with more detail the behavior of both objective functions, the topology of the two first examples the inverter and gripper, are analyzed for different mesh sizes. The inverter final results can be seen in Figure 4.27.

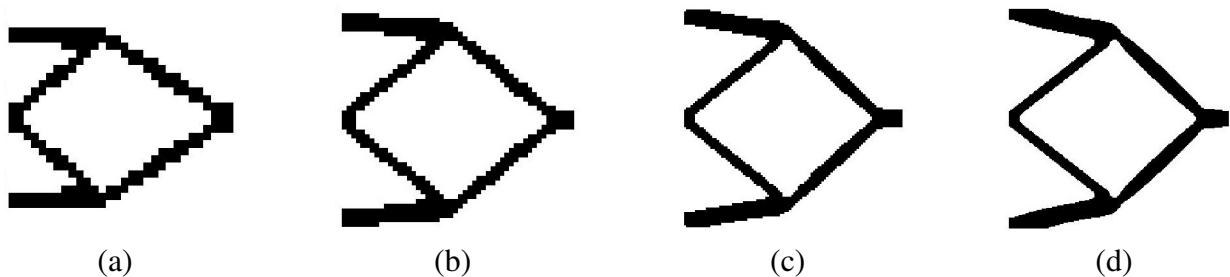


Figure 4.27: Inverter optimal topologies for different mesh sizes: (a)  $30 \times 30$  mesh; (b)  $50 \times 50$  mesh; (c)  $100 \times 100$  mesh; (d)  $200 \times 200$  mesh.

Four mesh sizes were chosen for these two first examples. For the inverter case, a  $30 \times 30$  elements mesh was the first discretization to render a representative result. As for the most detailed mesh, a  $200 \times 200$  quadrilateral elements arrangement was chosen, considering that beyond this value, finest meshes do not turn out into better topologies. The results from Figure 4.27 show that the final results are basically the same for any discretization, showing for this case that BESO algorithm for compliant mechanism design is independent of the discretization and the algorithm can obtain accurate topologies even for a  $50 \times 50$  finite elements mesh. It is noteworthy that the topology with  $200 \times 200$  element mesh shows in detail the flexible hinges in the inverter final topology, which can be favorable for more complex or detailed applications.

In the gripper case, the meshes size was chosen between  $40 \times 40$  and a  $200 \times 200$  finite elements, and the results from Figure 4.28 exhibit a similar behavior to the inverter. The topologies found for each discretization were also identical, which validates the mesh-independency assumption. The conclusion for this case is that the problem of compliant mechanism design is independent of the mesh size and a  $100 \times 100$  discretization can be used to estimate the mechanism topology without a high computational cost.

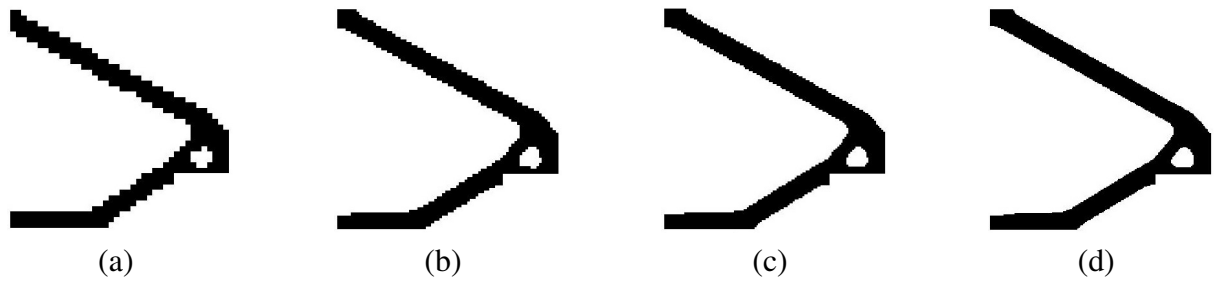


Figure 4.28: Gripper optimal topologies for different mesh sizes: (a)  $40 \times 40$  mesh; (b)  $80 \times 80$  mesh; (c)  $120 \times 120$  mesh; (d)  $200 \times 200$  mesh.

#### 4.5 Stress Analysis of compliant mechanisms

To explore the topology performance under different  $k_{out}$  values, a stress analysis is carried out for the inverter and gripper final results for a final volume of  $V_f = 40\%$  and  $V_f = 20\%$  as can be seen in Figures 4.29, 4.30, 4.31 and 4.32. The presence of hinges into the final topologies is an undesirable characteristic in compliant mechanism design and such hinge zones cause high stress concentration (Li *et al.*, 2013), hence the importance of analyzing the final topologies stress distribution. Additionally, the constant stiffness  $k_{out}$  could affect this distribution, whereby the analysis is made for the workpiece restriction extreme conditions.

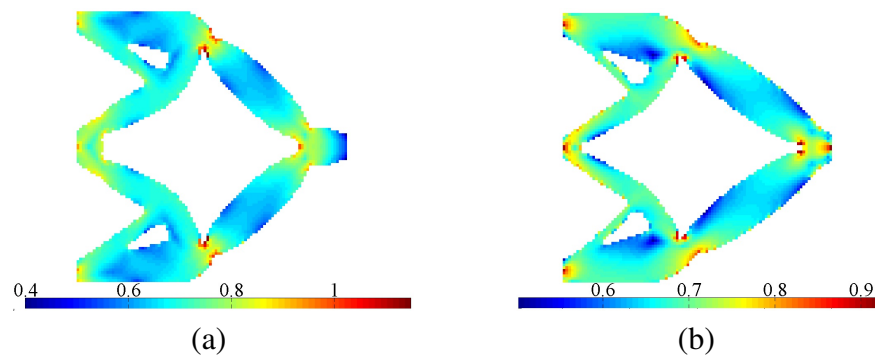


Figure 4.29: Inverter stress distribution for the optimal topologies with  $V_f = 40\%$  and for  $k_{out}$  extreme values: (a)  $k_{out} = 0$ ; (b)  $k_{out} = 4.9 \times 10^5$ .

The topologies seen in Figure 4.29 correspond to the inverter result in example 1, using a final volume of  $V_f = 40\%$ . This characteristic is chosen because the hinges are more visible for the topologies with  $V_f = 40\%$ . The stress distribution for this first case with  $k_{out} = 0$  and  $k_{out} = 4.9 \times 10^5$  can be seen in Figures 4.29a and 4.29b respectively. The Von Mises criterion was used to calculate the structure stress distribution, showing a stress concentration around the hinges

for the first example with  $k_{out} = 0$ . However, the concentration was not severe considering that the highest stress value was 4.7301 MPa, very far from even overcoming the material yield strength ( $\sigma_y = 250\text{MPa}$ ). The inverter second example with  $k_{out} = 4.9 \times 10^5$  shows a stress increment near to the structure supports and to the output and input ports, but once again, the highest stress value is below the material yield strength.

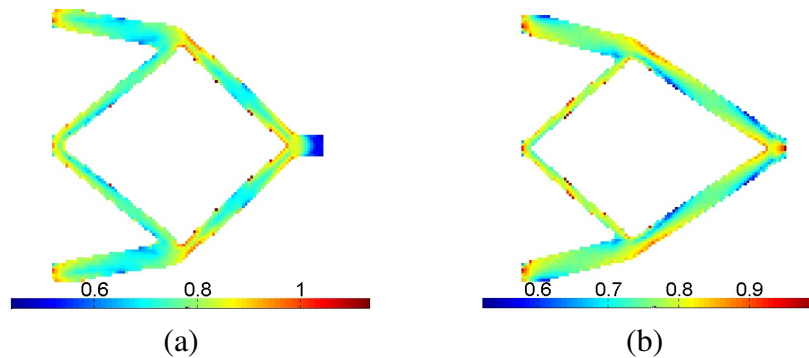


Figure 4.30: Inverter stress distribution for the optimal topologies with  $V_f = 20\%$  and for  $k_{out}$  extreme values: (a)  $k_{out} = 0$ ; (b)  $k_{out} = 4.9 \times 10^5$ .

Figure 4.30a and 4.30b also shows the results for the inverter case in example 1, using a final volume  $V_f = 20\%$ . In this case, it was also observed a stress concentration around the hinges in both  $k_{out}$  extreme conditions, especially when  $k_{out} = 0$ . For  $k_{out} = k_{max}$  it was also observed an increase in the stress concentration close to the input and output node, which can be easily explained by the workpiece resistance high value. Once again the maximum stress value is below the material yield strength, with 8.0047 MPa for the highest value with  $k_{out} = 0$  and 2.2791 MPa for  $k_{out} = 4.9 \times 10^5$ .

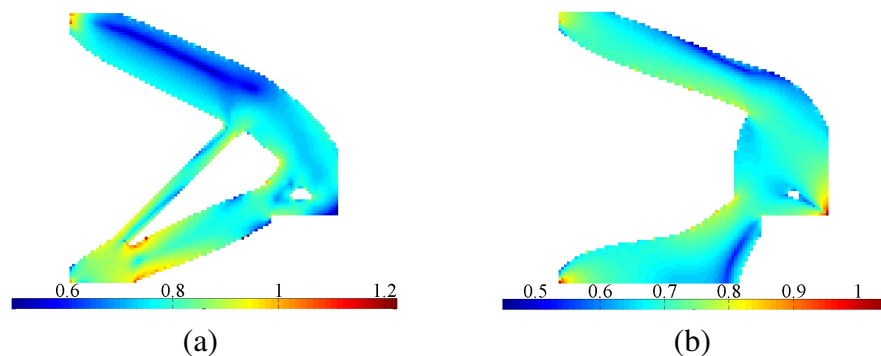


Figure 4.31: Gripper stress distribution for the optimal topologies with  $V_f = 40\%$  and for  $k_{out}$  extreme values: (a)  $k_{out} = 0$ ; (b)  $k_{out} = 2 \times 10^7$ .

Figure 4.31 resumes the results for the gripper case under the workpiece constraint extreme

conditions with a  $V_f = 40\%$ . The first example was for  $k_{out} = 0$  which also shows higher stress values around the structure hinges just as was expected from the inverter results. A maximum stress value of  $\sigma_{max} = 50.08\text{MPa}$  evidence that the structure is far from suffering any mechanical failure. The second gripper case with  $k_{out} = 2 \times 10^7$  presented a very different topology in comparison with the result found for  $k_{out} = 0$  as observed in Figure 4.31b, without hinges and with stress concentrations in the structures supports and the input and output ports.

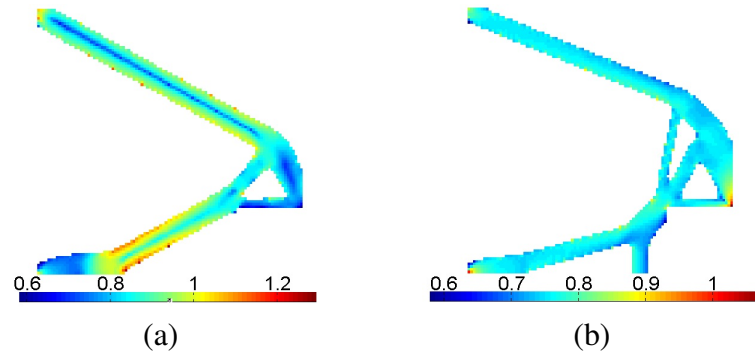


Figure 4.32: Gripper stress distribution for the optimal topologies with  $V_f = 20\%$  and for  $k_{out}$  extreme values: (a)  $k_{out} = 0$ ; (b)  $k_{out} = 2 \times 10^7$ .

Figure 4.32 shows the results for the gripper case in example 2 with a final volume  $V_f = 20\%$ . The first case shows a stress concentration around the hinges for  $k_{out} = 0$  as was also observed for the inverter example (Figure 4.32a). With the increase in  $k_{out}$ , as can be seen in Figure 4.32b the stress concentration changes, increasing close to the input and output nodes when  $k_{out} = k_{max}$  given the workpiece high resistance. The maximum stress values for this case are 167.28 MPa for  $k_{out} = 0$  and 2.78 MPa for  $k_{out} = 2 \times 10^7$ .

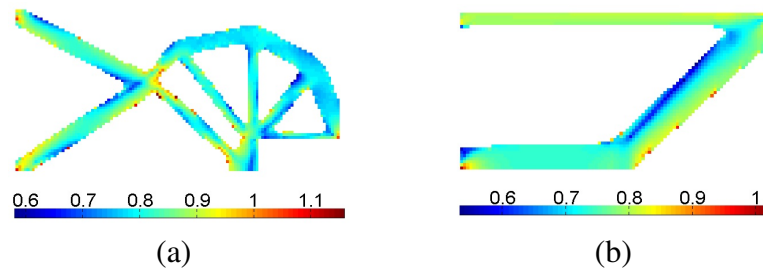


Figure 4.33: Stress distribution for the optimal topologies: (a) Example 3: inverse gripper; (b) Example 4: crunch mechanism.

Finally, the same behavior was observed for the other examples, especially the results found for cases 3 and 4 as can be seen in Figure 4.33. In any of this cases the stress value was superior

to the material yield strength, which shows the benefits of reducing the appearance of hinges in the final topologies, a common problem in compliant mechanism design. This reduction was observed by using the multicriteria approach to defining the objective function and the hinges reduction was observed for all the numerical examples considered in this work.

#### 4.6 Examples of compliant mechanisms from initial guess design

One desired feature for the BESO method is to start the optimization process with an initial guess design different from the full domain. Using this condition, the BESO method for compliance minimization leads to a convergent solution, even if the guess design is different from the initial topology (Huang and Xie, 2010). The same assumption will be tested for the BESO method for compliant mechanism design, using once again the inverter and gripper examples. This section aims to a better understanding of the optimization problem, especially for the iterations where the topology suffers the most dramatic changes.

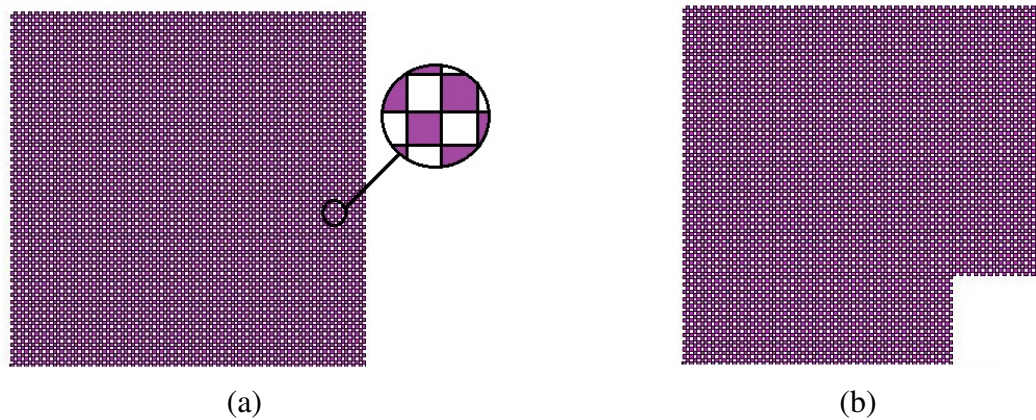


Figure 4.34: Checkerboard initial guess design domain: (a) Inverter; (b) Gripper.

The two examples will have a checkerboard initial design domain as can be seen in Figure 4.34 with a  $V = 50\%$  initial volume. The method was also tested for two different final volume fractions:  $V_f = 20\%$  and  $50\%$ .

### 4.6.1 Inverter case

Figure 4.35 exhibit the inverter topology behavior with a  $V_f = 20\%$  final volume fraction, objective function evolution and volume convergence. The BESO parameters used for the inverter usign a checkerboard initial design domain can be seen in Table 4.5.

Table 4.5: BESO parameters for the example 1 with a checkerboard initial design domain

Variable	Description	Value
$V$	Initial volume	50%
$k_{out}$	Workpiece resistance	$2 \times 10^7$ N/m
$ER$	Evolutionary volume ratio	2%
$AR_{max}$	Maximum addition ratio	1%
$r_{min}$	Filter ratio	6 mm
$\tau$	Stopping criteria tolerance	$1 \times 10^{-3}$
$N$	Stopping criteria parameter	5

The topologies in the first iterations are not symmetrical, however, this condition improves gradually with every new iteration, until finally reaches symmetry and evolves to the topology already found in Section 4.1. for a full initial design domain.

It is important to notice that the objective function convergence in Figure 4.35 evolves more smoothly than the result found in Figure 4.2 for a full initial design domain. A possible explanation is that given the checkerboard initial guess, only a portion of elements are involved in the analysis, allowing the topology to converge more quickly and with lowest oscillations between consecutive iterations.

Some BESO parameters were altered to allow convergence with respect to the example in Figure 4.35, such as the maximum addition ratio  $AR_{max}$  and the constant stiffness  $k_{out}$ . In the inverter case to reach a satisfactory result, the  $k_{out}$  need to be increased to a value close to the material Young modulus  $E$  for a better-restricted problem. Otherwise, the topology will end up to be disconnected or nonconvergent, which can be caused by the artificial stiffness introduced by the checkerboard initial topology assumed in this case. The second parameter  $AR_{max}$  also needed to be reduced to avoid radical changes in the first iterations that will end up deviating the topology from the optimal result already found in Figure 4.3d, ending in a different final topology. The chosen values were  $AR_{max} = 2\%$  and  $k_{out} = 2 \times 10^4$ .

The second example for the inverter was carried for a  $V_f = 50\%$  final volume fraction and

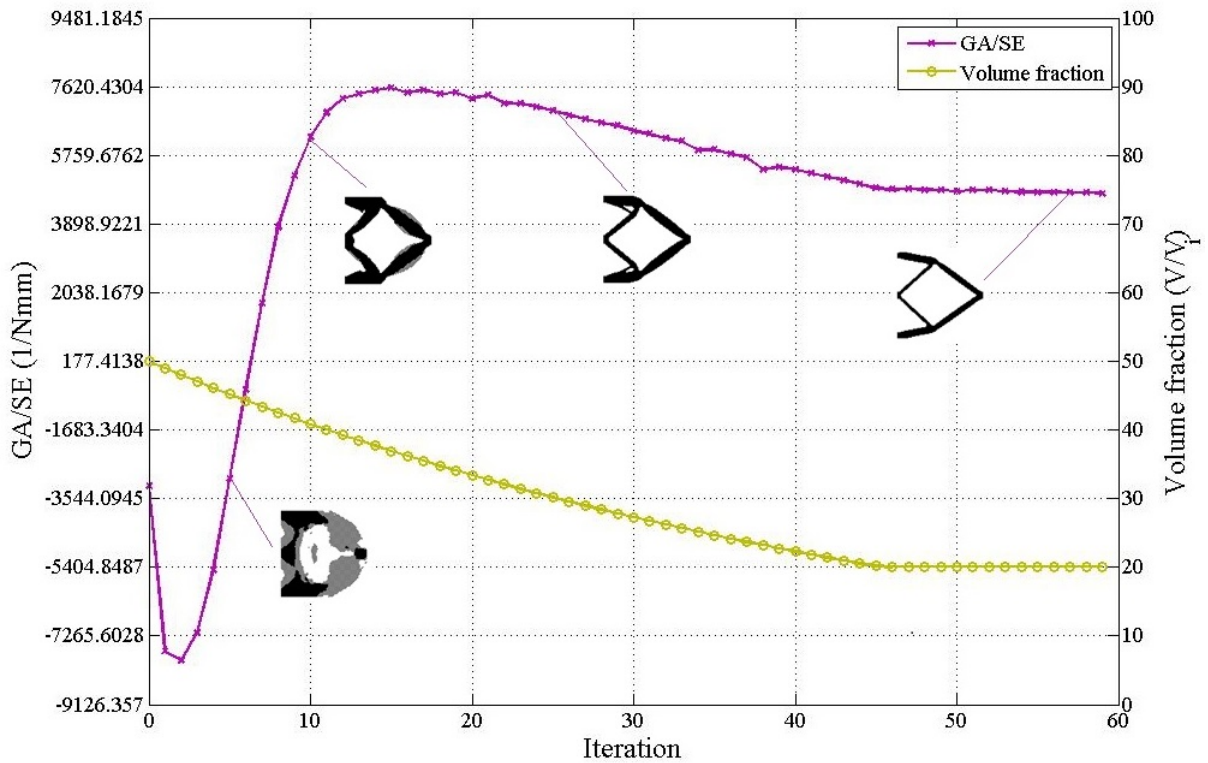


Figure 4.35: Evolution of the volume fraction and objective function for the inverter mechanism with  $V = 50\%$  and  $V_f = 20\%$ .

the topology and convergence results are resumed in Figure 4.36. In this case, the initial and final volume fractions have the same value and the topology reorganizes throughout the iterations to meet the objective function requirements. Figure 4.36 evidences a fluctuating behavior after the 12<sup>th</sup> iteration and this point coincides with the moment in the topology evolution where the checkerboard pattern set as the initial guess design disappears. The result is similar to the final topology already found for a  $V_f = 40\%$  in Figure 4.3c with a full initial design domain. The objective function variations were related to the topology lack of symmetry after the 12<sup>th</sup> iteration, remaining almost until the 50<sup>th</sup> iteration, difficulting the convergence.

#### 4.6.2 Gripper case

Figure 4.37 shows the objective function and volume evolution for the gripper case in example 2 with a 50% initial volume. The BESO parameters for the gripper example using the checkerboard initial design domain are resumed in Table 4.6 and the algorithm converged for both

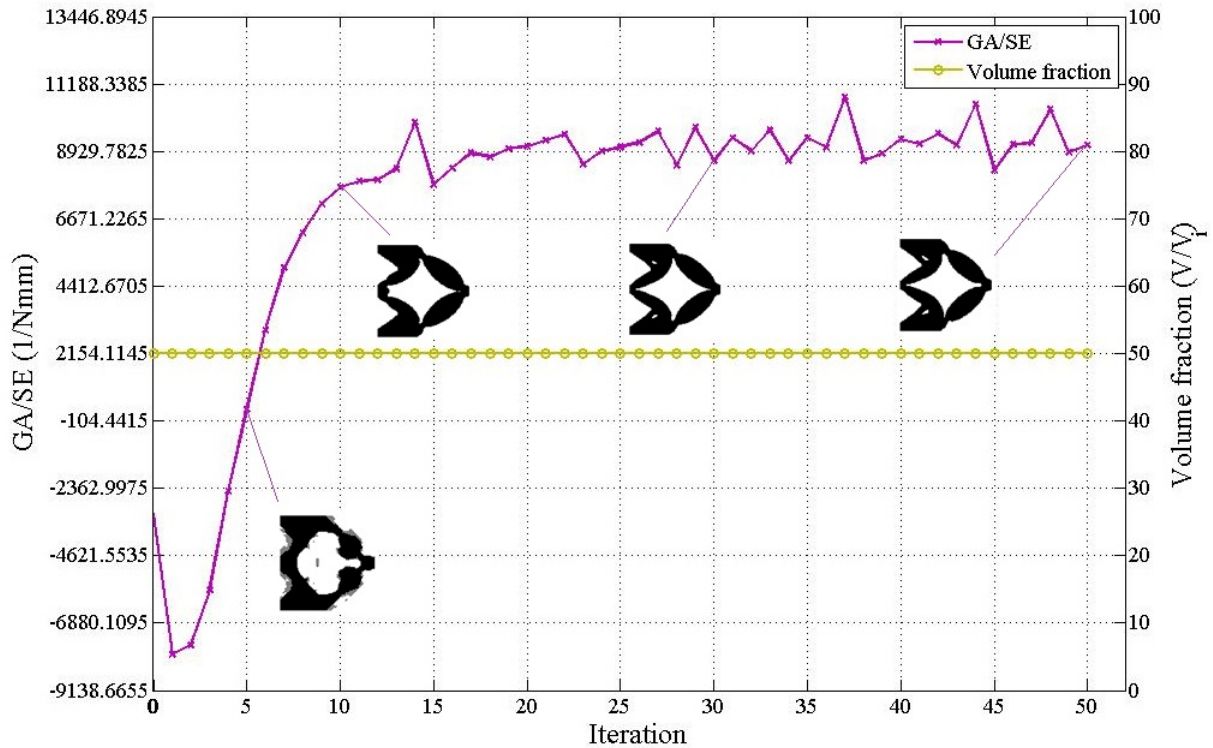


Figure 4.36: Evolution of the volume fraction and objective function for the inverter mechanism with  $V = 50\%$  and  $V_f = 50\%$ .

$V_f = 50\%$  and  $V_f = 20\%$  final volume fractions.

Table 4.6: BESO parameters for the example 2 with a checkerboard initial design domain

Variable	Description	Value
$V$	Initial volume	50%
$k_{out}$	Workpiece resistance	0 N/m
$ER$	Evolutionary volume ratio	2%
$AR_{max}$	Maximum addition ratio	100%
$r_{min}$	Filter ratio	6 mm
$\tau$	Stopping criteria tolerance	$1 \times 10^{-3}$
$N$	Stopping criteria parameter	5

The topology development from Figure 4.37 illustrate that previous to the 15<sup>th</sup> iteration there is not a very clear evolution path, even showing disconnected topologies. However, the algorithm recovers and reach the expected topology after 50 iterations approximately. The result is similar to the one found in Figure 4.7d, except for the presence of an additional bar close to the output port. This happens because the BESO method could converge to a local optimum when starts with

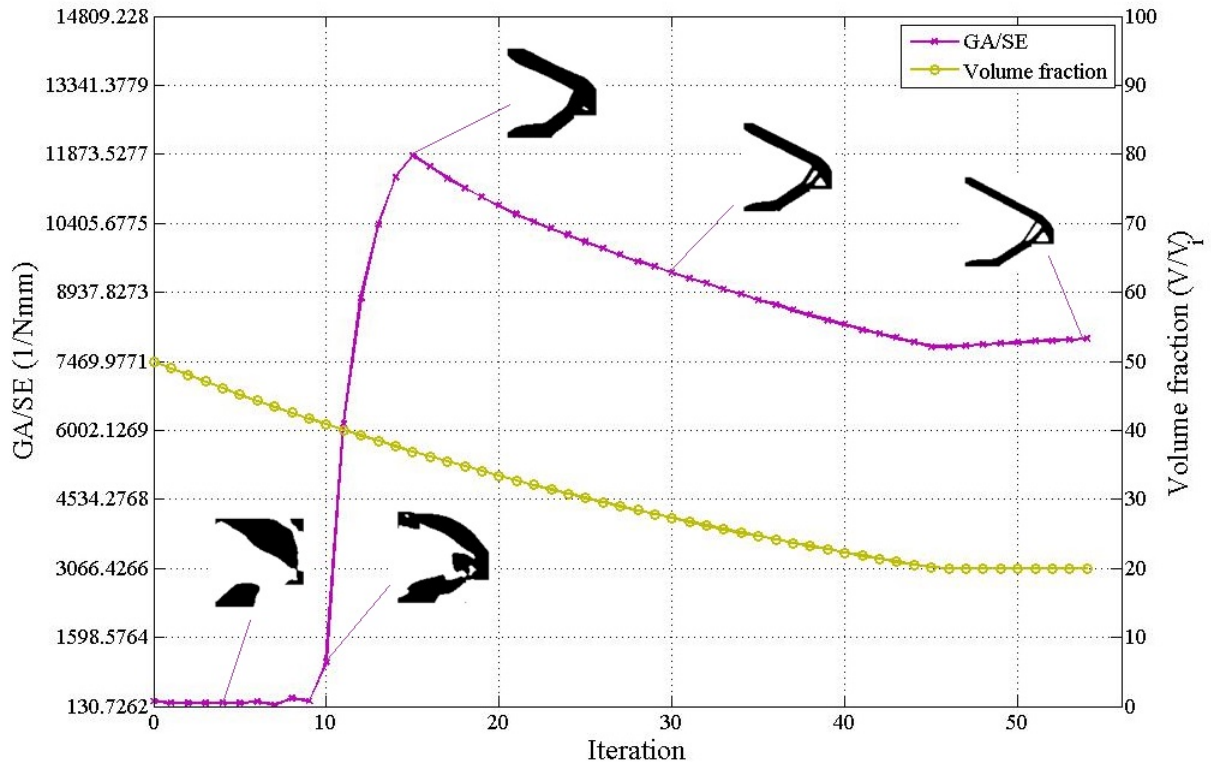


Figure 4.37: Evolution of the volume fraction and objective function for the gripper mechanism with  $V = 50\%$  and  $V_f = 20\%$ .

an initial guess different than a full design domain because some soft elements in the initial guess design may never be included in the finite element analysis during the whole optimization process (Huang and Xie, 2010).

The last example corresponds to the gripper with a final and initial volume fraction of 50%. The results are resumed in Figure 4.38, showing a similar behavior to the inverter example in Figure 4.36. The topology starts on the wrong path but recovers close to the 10<sup>th</sup> iteration. Beyond this point, the topology rapidly reorganizes, converging after 32 iterations. From the previous results is undeniable that the initial design domain affects the optimization process for compliant mechanism design. The problem is also dependent on the loading conditions, showing very different behaviors from one problem to another.

The maximum addition ratio  $AR_{max}$  also exhibited an important influence over the topology optimization, where the material addition should increase gradually to ensure convergence. This influence was observed for the inverter but did not appear for any problem with a  $V = 100\%$  initial

volume. Considering a full initial design domain for the first iteration ensures that every element in the design domain is included into the finite element analysis which can minimize the  $AR_{max}$  influence over the optimization process.

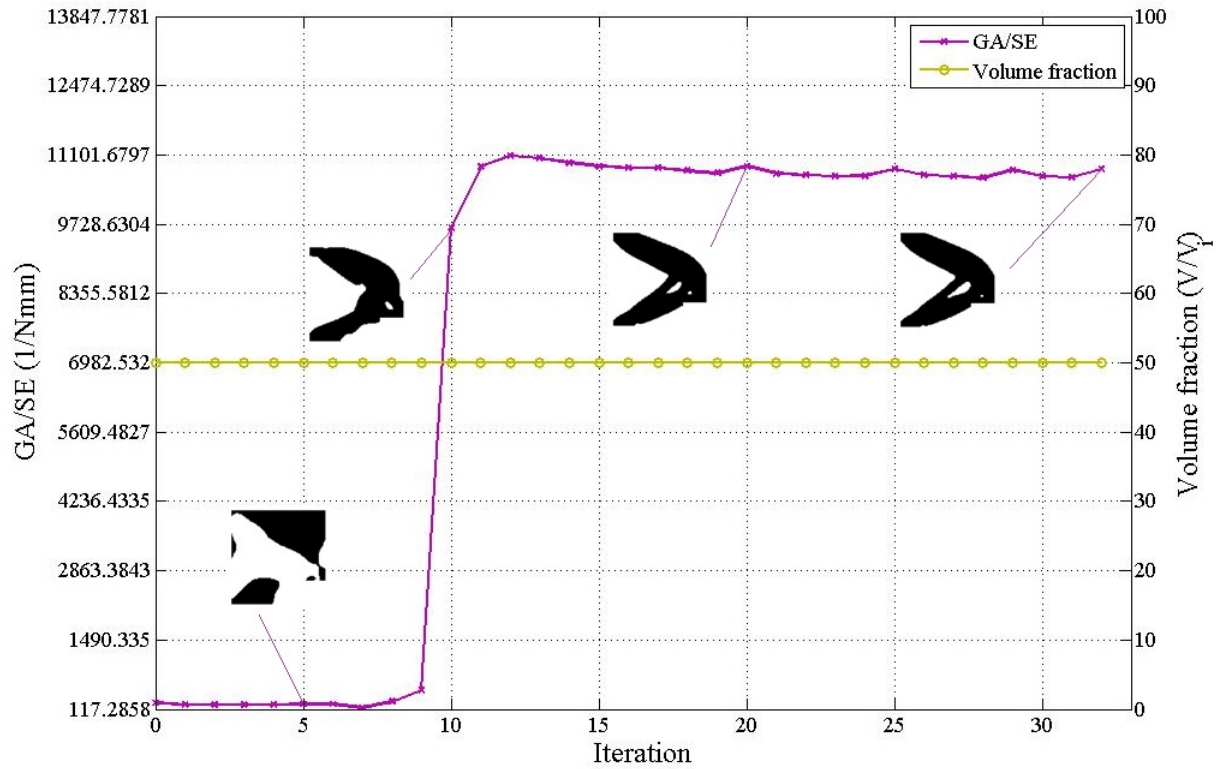


Figure 4.38: Evolution of the volume fraction and objective function for the gripper mechanism with  $V = 50\%$  and  $V_f = 50\%$ .

## 5 CONCLUSIONS AND SUGGESTED FUTURE WORKS

This chapter presents the analysis and conclusions related to the development of this investigation, which had as its main objective the numerical implementation of an algorithm for compliant mechanism design using the bi-directional evolutionary topology optimization. Additionally, some suggestions for future research are made at the end of this chapter, in order to enrich the investigation.

### 5.1 Summery and Conclusions

This investigation explored the design of compliant mechanism using topology optimization, specifically the Bi-directional Evolutionary Topology Optimization (BESO) method. This procedure gradually removes inefficient material from the design domain, constantly evolving until the topology reaches an optimum. The general concepts related to the BESO method were analyzed, and the problem of compliance maximization was successfully solved in Chapter 2 to implement the traditional BESO method.

The first step of this investigation was directed to only maximize the output displacement of the compliant mechanism without further considerations, but the results end up in disconnected topologies and convergence problems. To solve this issue it was essential not only to consider the mechanism flexibility to maximize the output displacement but also the stiffness of the system which is necessary to withstand external loads. In this way, two objective functions with different loading conditions are included into the problem formulation, a "mechanism design" that takes account of kinematic requirements and a "structure design" for structural requirements. The importance of including a structural condition is that guarantees the objective function convergence and also avoid the presence of flexible hinges.

The objective function was defined as a combination between maximizing the output displacement and minimizing the structure compliance. The BESO method was implemented and validated using typical examples of compliant mechanisms. A new strategy to calculate the two objective functions was also implemented to simplify the sensitivity analysis and in consequence, simplify the numerical implementation. This new approach adds the workpiece restriction  $k_{out}$  directly to the global stiffness matrix instead of using the linear combination method to simulate the mechanism behavior as proposed by Li *et al.* (2013). The new strategy also uses virtual load vectors

to express the output and input displacement values, which is the key to simplifying the number of equations necessary to solve the structural analysis problem.

The final results from example 1 and 2 were compared with the Li *et al.* (2013) investigation who already used the BESO method for compliant mechanism design and with topologies found in the literature for other topology optimization methods. The final topologies were the same as the ones found in previous works, including the results that used a different optimization method. In particular, the intermediate topologies and the objective function curve convergence were very similar with the results already found by Li *et al.* (2013). This accuracy shows that the algorithm manages to predict the compliant mechanism behavior and therefore represents a useful design tool.

The influence of some BESO parameters over the final topologies was studied, starting with the impact of the workpiece constraint  $k_{out}$ . Results from the different numerical examples showed that  $k_{out}$  variations do not change dramatically the mechanism topology, although that influence will also depend on the particular optimization problem. The low influence could be related to the inclusion of the structure compliance into the problem formulation, establishing structures already stiff enough to take into account the workpiece constraint. This structural requirement avoids dramatic changes in the final topology when  $k_{out}$  increases and only for high  $k_{out}$  values, the final topologies will show important variations. However, the workpiece constraint could be important to ensure the stiffness condition depending on the particular optimization problem. For examples 1 and 2, this variable was not essential to ensure convergence and could be equal to zero. Examples 3, 4 and 5 showed a different behavior, presenting disconnected topologies and one node connection problems for  $k_{out}$  low values.

A mesh-dependency analysis was also considered to establish if the presented results from the BESO method for compliant mechanism design showed any mesh dependency. In both cases, the results remain invariable with mesh size variations, showing the same behavior observed for the typical BESO methods for compliance minimization.

Finally, the initial guess design influence over the final topologies was also analyzed. Once again, the algorithm was carried out for two different cases, examples 1 and 2 using a checkerboard initial design domain of  $V = 50\%$  and for different final fraction volumes ( $V = 50\%$  and  $V = 20\%$ ). The results showed that by using a different initial design domain, the final topologies could suffer important variations. It was also observed that some optimization variables such as  $AR_{max}$  take an important role to ensure the method convergence, and that its value could influence the final

results. These algorithm dependency is not desirable and it is recommendable to maintain a full initial design domain in all cases. More research must be done in this aspect to find the effective strategies to avoid this problem.

In general, the adopted method showed several advantages for compliant mechanisms design that make this approach especially attractive for applications including design-dependent loads or fluid-structure interaction problems where the structure frontier needs to be well defined. This method overcomes the checkerboard and grayscale problems that could be present in other topology optimization methods and the presence of hinges, which is a typical problem in designing compliant mechanisms.

## 5.2 Suggestions for future research

Some important suggestions for future works to continue the investigation already presented are summarized in the list below:

- Study the dynamic response for compliant mechanisms in order to use the BESO method for its design.
- Algorithm implementation for tridimensional compliant mechanisms using the BESO method.
- Analyze the different possibilities to reformulate the optimization problem for compliant mechanisms to control the influence of the initial design domain on the final topologies.
- Extend the algorithm to consider the design of pressure-actuated compliant mechanisms by including the design-dependent loads into the optimization problem formulation.
- Include the fluid-structure interaction into compliant mechanisms design.
- Addressed new type of multi-physical problems related to the compliant mechanism using the BESO optimization, such as heat transfer, acoustic absorption, piezoelectric actuators, etc.
- Include the effect of geometric nonlinearities into the compliant mechanism problem formulation.

## References

- ALLAIRE, G.; JOUVE, F. and TOADER, A.M. Structural optimization using sensitivity analysis and a level-set method. **Journal of Computational Physics**, v. 194, n. 1, 363–393, February 2004.
- ANANTASURESH, G. **Optimal synthesis methods for MEMS**. Springer, 2003.
- ANANTASURESH, G. and KOTA, S. Designing compliant mechanisms. **Mechanical Engineering**, v. 117, n. 11, 93–96, November 1995.
- ANANTASURESH, G.K. **A new design paradigm for micro-electro-mechanical systems and investigations on the compliant mechanism synthesis**. 1994. PhD Thesis. University of Michigan.
- ANSOLA, R.; VEGUERÍA, E.; CANALES, J. and TÁRRAGO, J.A. A simple evolutionary topology optimization procedure for compliant mechanism design. **Finite elements in Analysis and Design**, , n. 44, 53–62, 2007.
- BATHE, K.J. **Finite Element Procedures**. Prentice Hall, 1996.
- BENDSOE, M. Optimal shape design as a material distribution problem. **Structural Optimization**, v. 1, 192–202, 1989.
- BENDSOE, M. and KIKUCHI, N. Generating optimal topologies in structural design using a homogenization method. **Computer Methods in Applied Mechanics and Engineering**, v. 71, n. 2, 197–224, November 1988.
- BENDSOE, M.P. and SIGMUND, O. **Topology Optimization: Theory, Methods and applications**. Springer, 2 ed., 2003.

BUHL, T.; PEDERSEN, C.B.W. and SIGMUND, O. Stiffness design of geometrically nonlinear structures using topology optimization. **Structural and Multidisciplinary Optimization**, v. 19, 93–104, 2000.

CALIXTO, T.K.L.; MADRID, C.M.P.; V., F.J. and PAVANELLO, R. Manufacturing procedure of multi-scale structures obtained using basis of cellular materials. In **CILAMCE 2015 - XXXVI Iberian Latin-American Congress on Computational Methods in Engineering**. 2015.

CANFIELD, S. and FRECKER, M. Topology optimization of compliant mechanical amplifiers for piezoelectric actuators. **Structural and Multidisciplinary Optimization**, v. 20, n. 4, 269–279, December 2000.

CARBONARI, R.C.; SILVA, E.C.N. and NISHIWAKI, S. Design of piezoelectric multi-actuated microtools using topology optimization. **Smart Materials and Structures**, v. 14, n. 6, 1431–1447, 2005.

CARDOSO, E.L.; SÉRGIO, J. and FONSECA, J.S.O. Strain energy maximization approach to the design of fully compliant mechanisms using topology optimization. **Latin American Journal of Solids and Structures**, pp. 263–275, 2003.

CARDOSO, E.L. and FONSECA, J.S.O. Topology optimization of piezoelectric actuators considering geometric nonlinearities. In **IUTAM Symposium on Topological Design Optimization of Structures, Machines and Materials**, pp. 391–400. 2006.

CHEN, S. and WANG, M.Y. Conceptual design of compliant mechanisms using level set method. **Frontiers of Mechanical Engineering**, v. 2, 131–145, 2006.

CHU, D.; XIE, Y.M.; HIRA, A. and STEVEN, G.P. On various aspects of evolutionary structural optimization for problems with stiffness constraints. **Finite Elements in Analysis and Design**, v. 24, 197–212, 1997.

CHU, D.N.; XIE, Y.M.; HIRA, A. and STEVEN, G.P. Evolutionary Structural Optimization for problems with stiffness constraints. **Finite Elements in Analysis and Design**, v. 21, 239–251,

1996.

DORN, W.; GOMORY, R. and GREENBERG, H. Automatic design of optimal structures. **Journal de Mecanique**, v. 3, n. 25-52, 1964.

FRECKER, M.; ANANTHASURESH, G.K.; NISHIWAKI, S.; KIKUCHI, N. and KOTA, S. Topological synthesis of compliant mechanisms using multi-criteria optimization. **Journal of Mechanical Design**, v. 119, 238–245, June 1997.

HOWELL, L. **Compliant Mechanisms**. WILEY-Interscience, 2002.

HOWELL, L. **2st Century Kinematics**, chapter Compliant Mechanism, pp. 189–216. Springer London, 2013.

HOWELL, L.; MAGLEBY, S.P. and OLSEN, B. **Handbook of Compliant Mechanisms**. Wiley, 2013.

HUANG, X. and XIE, Y.M. Convergent and mesh-independent solutions for the bi-directional evolutionary structural optimization method. **Finite Elements in Analysis and Design**, v. 43, n. 14, 1039–1049, 2007.

HUANG, X. and XIE, Y.M. Bi-directional evolutionary topology optimization of continuum structures with one or multiple materials. **Computational Mechanics**, pp. 393–401, 2009.

HUANG, X. and XIE, Y.M. **Evolutionary Topology Optimization of Continuum Structures: Methods and Applications**. Wiley, 2010.

JOG, C.S. and HABER, R.B. Stability of finite element models for distributed-parameter optimization and topology design. **Computational Mechanics**, v. 130, 203–226, 1996.

JOUBE, F. and MECHKOUR, H. Level set based method for design of compliant mechanisms. **REM - 17/2008. GIENS2007**, pp. 957–971, 2008.

LAZAROV, B.; SCHEVENELS, M. and SIGMUND, O. Robust design of large-displacement compliant mechanisms. **Mechanical Sciences**, v. 2, 175–182, 2011.

LI, Q.; STEVEN, G. and XIE, Y. Thermoelastic topology optimization for problems with varying temperature fields. **Journal of Thermal Stresses**, v. 24, 347–366, 2001.

LI, Y. **Topology Optimization of Compliant Mechanics Based on the BESO Method**. 2014. PhD Thesis. School of Civil - Environmental and Chemical Engineering - RMIT University.

LI, Y.; HUANG, X.; XIE, Y. and ZHOU, S. Evolutionary topology optimization of hinge-free compliant mechanisms. **International Journal of Mechanical Sciences**, pp. 69–75, 2013.

LIN, J.; LUO, Z. and L., T. A new multi-objective programming scheme for topology optimization of compliant mechanisms. **Structural and Multidisciplinary Optimization**, , n. 40, 241–255, January 2010.

LOBONTIU, N. **Compliant Mechanisms - Design of Flexure Hinges**. CRC PRESS, 2003.

LOPES, C.G. and NOVOTNY, A.A. Síntese de mecanismos flexíveis com restrição em tensão utilizando o conceito de derivada topológica. In **XXXI Ibero-Latin American Congress on Computational Methods in Engineering - CILAMCE**. 2015.

LUO, Z.; CHEN, L.; YANG, J.; ZHANG, K. and ABDEL-MALEK, K. Compliant mechanism design using multi-objective topology optimization scheme of continuum structures. **Structural and Multidisciplinary Optimization**, v. 30, n. 2, 142–154, 2005.

LUO, Z.; TONG, L.; WANG, M.Y. and WANG, S. Shape and topology optimization of compliant mechanisms using parametrization level set method. **Journal of Compliant Physics**, , n. 227, 680–705, 2007.

LUO, Z. and WANG, Y. Design of compliant mechanisms of distributed compliance using a level-set based topology optimization method. **Applied Mechanics and Materials**, v. 110-116, 2319–2323, 2011.

MANICKARAJAH, D.; XIE, Y. and STEVEN, G. An evolutionary method for optimization of plate buckling resistance. **Finite Elements in Analysis and Design**, v. 29, n. 3-4, 205–230, June 1998.

MIDHA, A.; W., N.T. and L., H.L. On the nomenclature, classification, and abstractions of compliant mechanisms. **Journal of Mechanical Design**, v. 116, n. 1, 270–279, 1994.

NISHIWAKI, S.; FRECKER, M.I.; MIN, S. and KIKUCHI, N. Topology optimization of compliant mechanisms using the homogenization method. **International journal for numerical methods in engineering**, v. 42, 535–559, 1998.

OSHER, S. and SETHIAN, J.A. Fronts propagating with curvature-dependent speed: Algorithms based on hamilton-jacobi formulations. **Journal of Computational Physics**, v. 79, 12–49, 1988.

PANGANIBAN, H.; JANG, G. and CHUNG, T.J. Topology optimization of pressure-actuated compliant mechanisms. **Finite Elements in Analysis and Design**, v. 46, n. 3, 238–246, March 2010.

PEDERSEN, C.B.W.; BUHL, T. and SIGMUND, O. Topology optimization of large-displacement compliant mechanisms. **Numerical Methods in Engineering**, v. 50, n. 12, 2683–2705, 2001.

PICELLI, R. **Otimização Estrutural Evolucionária usando malhas hexagonais**. 2011. Master Thesis. Universidade Estadual de Campinas.

PICELLI, R. **Evolutionary Topology Optimization of Fluid-structure Interaction Problems**. 2015. PhD Thesis. Universidade Estadual de Campinas.

PICELLI, R.; VICENTE, W. and PAVANELLO, R. Bi-directional evolutionary structural optimization for design-dependent fluid pressure loading problems. **Engineering Optimization**, pp. 1–19, 2014.

ROZVANY, G.I.N. A critical review of established methods of structural topology optimization. **Structural and Multidisciplinary Optimization**, v. 37, n. 3, 217–237, 2009.

RUBIO, W.M.; SILVA, E.C.N.; BORDATCHEV, E. and ZEMAN, M. Topology optimized design, microfabrication and characterization of electro-thermally driven microgripper. **Journal of Intelligent Material Systems and Structures**, v. 20, n. 6, 669–681, 2009.

SAXENA, A. and ANANTASURESH, G. On an optimal property of compliant topologies. **Saxena, A. and Anantasuresh G.K.**, v. 19, 36–49, 2000.

SAXENA, A. and ANANTHASURESH, K. Topology optimization of compliant mechanisms with strength considerations. **Mechanics of Structures and Machines**, v. 29, n. 2, 199–221, 2001.

SCHEVENELS, M.; LAZAROV, B. and SIGMUND, O. Robust topology optimization accounting for varying manufacturing errors. **Computer Methods in Applied Mechanics and Engineering**, v. 200, n. 49-52, 3613–3627, December 2011.

SIGMUND, O. On the design of compliant mechanisms using topology optimization. **Mechanics of Structures and Machines: An International Journal**, , n. 25, 493–524, 1997.

SIGMUND, O. Design of multiphysics actuators using topology optimization - part i: One-material structures. **Computer methods in applied mechanics and engineering**, v. 190, 6577–6604, 2001.

SILVA, E.C.N.; CARBONARI, R.C. and G.H., P. On graded element for multiphysics applications. **Smart Materials and Structures**, v. 16, n. 6, 2408–2428, 2007.

SILVA, F.I. and PAVANELLO, R. Synthesis of porous-acoustic absorbing systems by an evolutionary optimization method. **Engineering Optimization**, v. 42, n. 10, 887–905, 2010.

SOLEHUDDIN, S.; RIDZWAN, M. and KADARMAN, A. Methodology of compliant mechanisms and its current developments in applications: A review. **American Journal of Applied Sciences**, pp. 160–167, 2007.

VICENTE, W.; PICELLI, R.; PAVANELLO, R. and XIE, Y.M. Topology optimization of frequency responses of fluid-structure interaction systems. **Finite Elements in Analysis and Design**, v. 98, 1–13, January 2015.

WANG, M. and CHEN, S. Design of multimaterial compliant mechanisms using level-set methods. **Journal of Mechanical Design**, v. 127, 941–956, September 2005.

WANG, M.; WANG, X. and GUO, D. A level set method for structural topology optimization. **Computer Methods in Applied Mechanics and Engineering**, v. 192, n. 1-2, 227–246, January 2003.

WANG, N. and ZHANG, X. Multi-material topology optimization of compliant mechanism using ground structure approach. In **2014 International conference on manipulation, manufacturing and measurement on the nanoscale**. 2014.

XIE, Y.M. and STEVEN, G.P. A simple evolutionary procedure for structural optimization. **Computer and Structures**, v. 49, 885–896, 1993.

XIE, Y.M. and STEVEN, G.P. Evolutionary structural optimization for dynamic problems. **Computers and Structures**, v. 58, 1067–1073, 1996.

YANG, X. and XIE, Y.M. **Bi-directional Evolutionary Method for Stiffness and Displacement Optimization**. 1999a. Master Thesis. School of the Built Environment - Victoria University of Technology.

YANG, X. and XIE, Y.M. Bidirectional evolutionary method for stiffness optimization. **AIAA Journal**, v. 37, n. 11, 1483–1488, November 1999b.

YOON, G. Topology optimization of compliant mechanism design with stationary fluid-structure interaction. **Blucher Mechanical Engineering Proceedings**, v. 1, n. 1, 2014.

ZHAN, J. and ZHANG, X. Topology optimization of multiple inputs and multiple outputs compliant mechanisms using the ground approach. In **2nd International Conference on Industrial Mechatronics and Automation**. 2010.

ZHOU, M. and ROZVANY, G.I.N. The coc algorithm, part ii: Topological, geometrical and generalized shape optimization. **Computer Methods in Applied Mechanics and Engineering**, v.

89(1-3), 309–336, 1991.

ZHU, B.; ZHANG, X. and FATIKOW, S. Level set-based topology optimization of hinge-free compliant mechanisms using a two-step elastic modeling method. **Journal of Mechanical Design**, v. 136, n. 3, 2014.